Determination of spatial and temporal water relations in single leaves and canopies based on thermographic measurements

Dissertation

zur

Erlangung des Doktorgrades (Dr. rer. nat.)

der

Mathematisch-Naturwissenschaftlichen Fakultät

der

Rheinischen Friedrich-Wilhelms Universität Bonn

vorgelegt von:

Hendrik Albrecht

aus

Gelsenkirchen

Bonn, 9. Mai 2016

Angefertigt mit Genehmigung der Mathematisch-Naturwissenschaftlichen Fakultät

der Rheinischen Friedrich-Wilhelms-Universität Bonn

Erster Gutachter: Prof. Dr. Uwe Rascher

Zweiter Gutachter: Prof. Dr. Lukas Schreiber

Tag der mündlichen Prüfung: 16. September 2016

Erscheinungsjahr: 2016

"Water is not a commercial product like any other but, rather, a heritage which must be protected, defended and treated as such"

Directive 200/60/EC of the European Parliament and of the Council of 23. October 2000 establishing a framework for Community action in the field of water policy

Summary

Water is the elixir of life for all living organisms on earth. Land plants are exposed to an exceptional challenge, because they need to take up CO_2 from a dry atmosphere, which induces water loss while incorporating CO_2 into photosynthesis. To adapt to water loss and in parallel maximize CO_2 uptake, plants have evolved a complex system to optimize water transport and transpiration ration. Water is absorbed from the soil and transported through the xylem into the leaves, where it is finally released through the stomata. As the leaf water content (LWC) is a result of an equilibrium between water uptake and water loss through transpiration, it is an important parameter in the overall plant-water relation. Water loss, and thus LWC, is mainly affected by transpiration, which in turn is regulated by stomata. Furthermore, water vapor released through the stomata is restricted by the leaf boundary layer, a thin air layer surrounding the leaf and acting as a heat barrier. Convection that is the heat transfer from the leaf surface into the ambient air via air movement further influences the boundary layer. Both, stomata and convection respond to a wide range of environmental factors, such as light, air temperature (T_a), and wind.

The relationships between LWC, transpiration, convection, and the leaf boundary layer, are summarized in the leaf energy balance model that relates all these parameters to the leaf temperature (T_L). Therefore, thermography, non-invasive and spatial T_L measurements is a convenient method to derive information about the plant-water relations. A commonly used parameter is the crop water stress index (CWSI), which empirically relates passively measured T_L to rates of transpiration.

This work introduces the active thermography as a valuable method for plant science to estimate LWC and the plant-water relations. In active thermography, T_L is manipulated by exposure to short heat pulses inducing a transient shift in T_L. Resulting cooling curves are measured and quantified with the time constant (τ). In theory, τ is the product of the leaf heat capacity per unit area, which is proportional to LWC, and the inverse of the leaf heat transfer coefficient (h_{leaf}). h_{leaf} describes the boundary layer conductance to heat and is the sum of heat transfer coefficients for transpiration, convection, and thermal radiation.

Using two plant species, spring barley (*Hordeum vulgare*) and common bean (*Phaseolus vulgaris*), it was extensively tested whether and under which conditions the parameter τ can be used to derive LWC. Finally, the active thermography was transferred from the laboratory into the greenhouse were the applicability to detect mild drought stress on the canopy scale was tested.

In the laboratory under well-defined ambient conditions, τ of dark-adapted leaves was proportional to LWC. This relationship was valid for the both plants species and under varying wind-speed. By using this relationship, τ of whole leaves could be mapped, providing LWC maps that illustrated high water containing leaf parts, such as the vascular tissues. Furthermore, τ tracked dehydration in response to water loss through transpiration. Active thermography measurements were compared with active temperature measurements using a thermocouple within a leaf gas exchange cuvette. The comparison revealed a strong relationship between τ and h_{leaf} and thus boundary layer. In the well ventilated gas exchange cuvette, τ dynamics were mainly driven by changes in LWC. In contrast, leaves which were measured under wind-free conditions showed different τ-dynamics, which were primarily related to boundary layer conditions. Under wind-free conditions, the boundary layer is highly affected by the gradient between T_L and T_a, which is also affected by transpiration. Thus, under these conditions τ is related to both, LWC and h_{leaf}.

Forward modeling of h_{leaf}, showed a strong impact of h_{leaf} on τ, which significantly differed with wind and illumination. Thus, the relative contribution of the single heat transfer coefficients for the single components (transpiration, convection, and thermal radiation) greatly depended on the environmental conditions. While the heat transfer coefficient for thermal radiation was nearly negligible, the heat transfer for convection and transpiration showed a much stronger impact on h_{leaf}, respectively. Irrespectively of wind-speed and illumination, the heat transfer coefficient for convection contributed most to the overall h_{leaf}. In the dark, the heat transfer coefficient for transpiration had no impact on h_{leaf}, but upon illumination the impact became significant. With increasing wind-speed the contribution of transpiration became less important, while the impact of convection became stronger.

Finally, the active thermography approach was transferred from the laboratory into the greenhouse, where the applicability for mild drought stress detection on the canopy scale was tested. Four different barley varieties were exposed to a deficit irrigation (DI) treatment providing water-limiting conditions. Diurnal and seasonal dynamics of τ were observed and compared to the commonly used CWSI. Both parameters showed diurnal trends, where the lowest values occurred at midday and the highest values were measured during the night. The CWSI mainly responded to changes in h_{leaf}, while τ responded to changes in LWC and h_{leaf}. Consideration of both parameters in parallel revealed an overall insight in the plant-water relations, which could

be related to canopy water loss rates and biomass production. Therefore, combining τ and the CWSI in one single index would be advantageous.
A first attempt to develop such an index was made, and the empirical dehydration index (DHI) was suggested as basis for future development of an index combining passive and active thermography.

This work demonstrates, that the active thermography is a valuable tool for a wide range of applications in plant science. The measurement of τ can be used to detect dynamics in the plant-water relations, when regarding the environmental conditions properly. Additionally, τ may be used in modeling studies, e.g. to model leaf and canopy heat transfer processes or to model water-relations of plants with respect to hydrological cycles of whole ecosystems.

Content

1. Introduction

Water is the elixir of life for all living organisms on earth. Land plants are exposed to an exceptional challenge, because they need to take up gaseous CO_2 from the atmosphere to drive photosynthesis and incorporate carbon in organic molecules for growth and maintenance processes. However, the exchange of gases at the leaf surface occurs through the regulation of stomata, which not only mediate CO_2 uptake but also water loss and thus expose the plants to risk of dehydration. For every gram organic matter produced by the plant, the plant has to transport approximately 500 grams of water extracted by the roots from the soil through the plant vascular system into the leaves, where it is eventually lost to the atmosphere (Taiz and Zeiger, 2006). Water is not only important for metabolic processes, such as photosynthesis, it also functions as transport medium for nutrients and it is required to maintain the cell turgor pressure, which is required for cell expansion and growth (Lockhart, 1967; Schopfer, 2006; Nobel, 2009). To adapt to water loss and in parallel to maximize CO_2 uptake, plants have evolved a complex water transport system from the soil to the leaves. Additionally, a complex control system avoids lethal dehydration of the plants.

1.1 The soil-plant-atmosphere continuum

Water is transported from the soil, where it is taken up by the roots, through the vascular system and is finally released at leaf level via transpiration. The water transport into, through, and out of the plant is maintained by pressure gradients between the different plant organs and between the plant and the ambient environment.

Water availability in the soil principally depends on the environmental conditions and on the soil properties (Hillel, 1980). The most obvious parameter is the amount and frequency of precipitation, which determines the amount of water that reaches the soil. Soil structure, texture, and mechanical properties and their depth distribution in the profile determine water retention capacity and hydraulic conductivity which, in turn, determine available water for root uptake. Usually, the soil is not water saturated (Bodner *et al.*, 2015), but, depending on the soil, heavy rainfalls can result in oversaturation and thus water logging, which in turn results in a stress situation for plants not adapted to these conditions. Water logging results in a lack of dissolved oxygen in water for aerobic respiration and, additionally, results in a nutrient deficiency, both of which inhibit plant performance and finally plant growth (Steffens *et al.*, 2005). The other extreme is drought, where the stress source is the lack of water. Drought can be defined as a

period of dry weather, where the lack of precipitation causes considerable hydrological imbalances (Bodner *et al.*, 2015). Hot and dry weather conditions force evaporation of water from the soil, which can reach up to 35% of the total water loss in agro-ecosystems (Wallace, 2000). Roots are the plant organs which are in direct contact with soil and water. Therefore, root-system structure and architecture, such as root thickness, deepness, and density of the root-system affect the efficiency of water uptake (Subbarao *et al.*, 1995; Nguyen *et al.*, 1997; Rodriguez-Iturbe *et al.*, 1999; Watt *et al.*, 2006; Bodner *et al.*, 2007). Furthermore, roots act as sensors and transmit signals to the leaves to induce stress responses. Drying soil induces a cascade of phytohormone transduction pathways. For example, the release of abscisic acid (ABA) induces stomatal closure in order to reduce the water loss (Gollan *et al.*, 1992; Schurr *et al.*, 1992; Schwartz *et al.*, 1994; Allan *et al.*, 1994; Wilkinson and Davies, 2002; Langer *et al.*, 2004; Levchenko *et al.*, 2005).

The water transport from the soil into the roots mainly occurs via bulk flow in response to a pressure gradient. Once the water has entered the root xylem, it is transported through the stem into the leaves. Water flux in the stem xylem over a long distance is described by the cohesion-tension theory (Tyree and Sperry, 1989; Tyree *et al.*, 1997). The length and the structure of the xylem is species-specific and determines the overall hydraulic conductance, which affects the velocity of water replacement in the leaves.

A well-hydrated leaf is nearly water-saturated, so that the relative water content can reach levels up to 0.95. Additionally, the internal pressure results in the vaporization of water, so that the air space inside leaves is nearly saturated with water vapor (Nobel, 2009). In order to maintain the pressure difference between the leaves and the roots, and thus to maintain the water transport through the whole plant, water has to be released from the leaves to induce a suction pressure. However, as water may be limited periodically, the water loss has to be controlled. The cuticle, a waxy surface covering the leaf epidermis acts as a barrier for water (e.g. Riederer and Schreiber, 2001), so that only about 5% of the water is lost via the epidermis. However, control of the water loss mainly occurs by controlling the leaf transpiration, which is the whole process of water vapor transport from the leaf inner tissues into the atmosphere. The driving force for transpiration are differences in water potentials that occur between leaf and atmosphere. Usually, leaves have a higher concentration of water vapor resulting in a higher water potential compared to the ambient air. The water vapor pressure difference (VPD) is the driving force for water vapor movement form the leaf surface into the atmosphere. As this water vapor flux would occur obeying to physics as long as the gradient was present, this mechanism needs regulation. Regulation of water loss through transpiration occurs via stomatal complexes,

whose opening and closure is affected by plant internal and external processes (e.g. Roelfsema and Hedrich, 2005).

1.2 Leaf water content, transpiration, and stomata

The water loss via transpiration is determined by the stomatal conductance (g_s), which determines how much water is released per area and second (mol m^{-2} s^{-1}). As the leaf water content (LWC) decreases in response to increased g_s, LWC and g_s are coupled (Schmidhalter *et al.*, 1998; Tardieu and Simonneau, 1998). It was observed that g_s and LWC oscillate during the day, where LWC and g_s showed time-shifted amplitudes (Cowan, 1972; Hennessey and Field, 1991). LWC was found to decrease after stomata have opened and to increase again after stomata have closed. Although, this behavior is generally valid for a wide range of plant species, there are two different strategies of isohydric and anisohydric plants (Stocker, 1956). Isohydric plants, such as maize, show a reduction in the leaf water potential, and thus in LWC, in response to increased transpiration, but LWC does not drop below a certain level. Additionally, maize is a C_4-plant, in which the CO_2-fixation is spatially separated from the Calvin cycle. Particularly, at hot and dry conditions, this mechanism provides a more efficient carbon use, which results in lower transpiration rates and finally reduces water loss. In isohydric plants, the water uptake is balanced to the water loss so that a plateau is maintained. Often this behavior is referred to as a conservative or water saving strategy (Levitt, 1972). In contrast, anisohydric plants, such as barley or bean, are risk-taking plants (Sade *et al.*, 2012) which allow a stronger dehydration in order to keep photosynthesis rate high. Often, those plants show a stronger oscillation in LWC and g_s. However, in both cases, isohydric and anisohydric, a too strong drop in LWC may cause embolism and cavitation (Sack and Holbrook, 2006), which would result in a disruption of the overall water transport system and eventually be lethal. Therefore, the water loss has to be equilibrated with the water uptake by the roots, which requires a fine regulation of stomatal closure in response to internal and external factors (Mott *et al.*, 1997; Roelfsema and Hedrich, 2005).

Stomata respond to decreasing LWC with closure that can achieve water saving, because further water loss through transpiration is limited (Cowan, 1972; Syvertsen, 1982; Martin and Ruiz-Torres, 1992; Tardieu and Simonneau, 1998). As transpiration is the water loss from the inner leaf tissue into the surrounding atmosphere, external parameters that increase the evaporative demand also affect the behavior of stomata. Changes in the VPD gradient from leaf to air cause stomatal opening or closure (Hall and Kaufmann, 1975; Mott *et al.*, 1997). For example, dry air that has a rather low water vapor concentration increases the VPD, which in turn increases

evaporative demand of the surrounding ambient air. To prevent severe dehydration, stomata have to close in order to reduce the water vapor flux. Additionally, stomata are sensitive to light (Mott *et al.*, 1997; Roelfsema and Hedrich, 2005; Pieruschka *et al.*, 2010). Light is the driving factor for the electron transport chain of the photosynthesis, generating reduction equivalents that are used in the Calvin cycle, where CO_2 is fixed (Schulze and Caldwell, 1995). To satisfy the CO_2-demand, the stomata have to induce opening, enabling an increased CO_2 diffusion into the leaf, which in parallel increases water loss. Additionally, light is converted into heat upon absorption by the leaf, which increases the leaf temperature (T_L) and finally increases the vaporization rate of water. Comparable to the heat originating from light absorption, increases in air temperature (T_a) also increases the internal heat, increasing T_L, and thus accelerating the water evaporation (Jones, 1992; Monteith and Unsworth, 2008). If stomata are opened, high T_a will result in an increased water loss. Resulting changes in leaf water potential and LWC, upon light absorption and exposure to high T_a, can then again affect stomatal aperture, which provides a feed-back control mechanism. Next to transpiration a further physical process influences the removal of produced heat. Convection is heat transported by air movements and occurs at the leaf surface. It is strongly coupled to transpiration and thus, indirectly, affects the plant-water relation. Convection and transpiration are both restricted by the leaf boundary layer.

1.3 Leaf boundary layer

Although the leaf boundary layer is not a plant organ, it is of fundamental importance for plant productivity and functionality (Shibuya *et al.*, 2006; Schymanski and Or, 2015). The boundary layer is a thin layer of air of a few millimeters that surrounds the leaf and acts as heat barrier between the leaf surface and the ambient air. Within the boundary layer, gradients of temperatures, gas concentrations, and air velocities are present, providing a complex microclimate on the leaf surface (Raschke, 1960; Schreuder *et al.*, 2001). The thickness and the compositions of the boundary layer determines how fast heat can be released from the leaf surface into the ambient air, which is defined as boundary layer conductance. Convection strongly affects the leaf boundary layer, as convection is the heat transport via air movement. There are two main forms of convection that also determine the boundary layer conductance. The first form is the free convection, where no wind is present and the transfer of heat mainly depends on the T_L-T_a difference that provides a heat gradient (Dixon and Grace, 1983). The steeper the heat gradient, the larger is the convective heat flux. The second form is the forced convection, which occurs in conditions where wind is present (Vogel, 2009). In forced convection, T_L-T_a plays a second-

ary role, as the air is transported away with the wind. The convection rate increases with increasing wind speed. Transpiration is inevitably coupled with convection and thus also strongly depends on the boundary layer conductance. Water vapor that is released from the leaf inner tissues through the stomata have to pass the boundary layer before it is finally released into the ambient air. Consequently, transpiration is also affected by free and forced convection. In a wind-free environment water vapor accumulates in the boundary layer. This decreases the VPD between the leaf and the boundary layer, which may result in and increased g_s (Bunce, 1985). As soon as wind is present the boundary layer thickness is progressively removed reducing the boundary layer thickness and increasing boundary layer conductance. With the removal of the boundary layer, the water vapor accumulated within it is removed resulting in an increased VPD and ultimately in stomatal closure (Grace, 1974; Dixon and Grace, 1983; Bunce, 1985). Next to wind and temperature several other parameters affect the boundary layer and boundary layer conductance, such as leaf size and leaf shape (Parkhurst, 1976; Schreuder *et al.*, 2001). Narrow leaves have a higher boundary layer conductance compared to broader leaves, because the boundary layer thickness increases with the distance from the leaf edge (Gates, 1965; Sinclair, 1970; Vogel, 2009). Additionally, lobes and serration of leaves also reduce the boundary layer thickness, because leaf area is reduced and leaf edges are closer together (Schuepp, 1993). Thus, these parameters also affect convection, transpiration and consequently plant-water relations.

1.4 Leaf energy balance

LWC, transpiration, convection, and the boundary layer are coupled to each other. LWC decreases with increasing transpiration, because the leaf loses water, but in the other direction stomata are also controlled by LWC so that LWC provides a restriction for transpiration. Furthermore, transpiration is affected by convection, which is a main parameter determining the boundary layer conductance. This interaction is summarized in the leaf energy balance model (e.g. Linacre, 1972; Jones, 1992; Monteith and Unsworth, 2008). In general, the leaf energy balance model describes energy flux densities across the leaf surface (Equation 1.4.1, and Fig. 1.4.1, see Chapter 2.2).

$$S = \Phi_{in} - (LW + H + \lambda E) \qquad \text{Equation 1.4.1}$$

Where S is the physically stored heat in the leaf, Φ_{in} is the incoming heat deriving from solar and thermal irradiation, LW is the long-wave, or thermal radiative, heat flux density, H is the convective heat flux density, and λE is the latent heat flux related to transpiration.

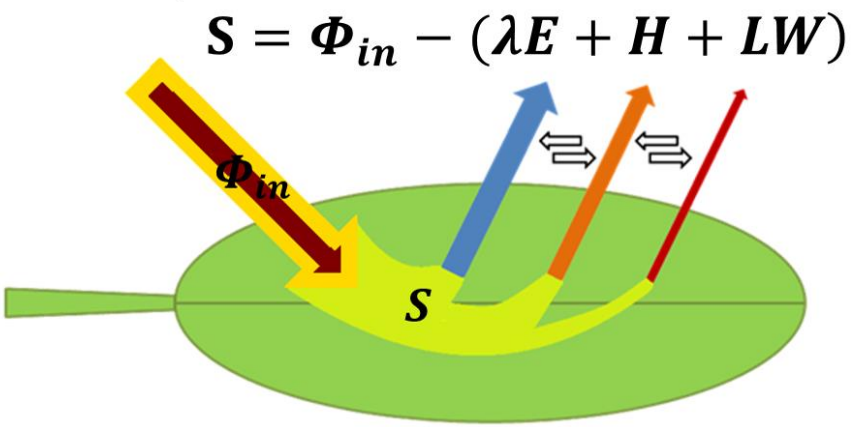

Figure 1.4.1: Leaf energy balance model. Incoming energy (Φ_{in}) is absorbed (S) and released via transpiration (LE), convection (H), and thermal radiation (LW).

Incoming heat is first absorbed by the leaf and then released in three forms of heat. The long-wave radiative heat flux density is heat which is released as thermal radiation, thus as electro-magnetic energy. Convective heat flux density is the heat transport via air movement, and the latent heat flux density is the heat associated with water vapor. How much energy can be stored (S in Fig.1.4.1) depends on the leaf heat capacity. Because water is the main component of leaves and has a very high specific heat capacity, the leaf heat capacity depends to a great extent on LWC. At steady state conditions, the leaf energy balance is assumed to be at equilibrium, meaning that all incoming energy is released by the respective heat fluxes (e.g. Jones, 1992). In this case, S equals zero. All energy flux densities are driven by a heat gradient, which is determined by T_L-T_a. Additionally, all fluxes are restricted by the boundary layer. However, as described in the previous section, LWC, transpiration, and convection are affected by a wide range of environmental factors. Additionally, the leaf energy balance reveals a relationship of all these parameters to T_L. Therefore, the measurement of T_L to assess the plant-water-relations and plant-environment-interactions is a useful method and has been widely used in previous research in this field.

1.5 Leaf temperature measurement to assess the plant-water relations

As T_L-T_a is linearly related to evapotranspiration under stable conditions (Monteith, 1981), the measurement of T_L and T_L-T_a provides an attractive method to estimate plant transpiration. Based on the assumption that a plant transpiring at a relatively high rate shows a lower T_L (Araus *et al.*, 2003), both parameter, T_L and T_L-T_a, have been often used to detect drought stress in plants, for instance in studies directed to assess the breeding value of traits linked to drought tolerance (Ehrler, 1972; Sánchez *et al.*, 2001; Baker *et al.*, 2007; Khan *et al.*, 2007; Nautiyal *et*

al., 2008; Reynolds *et al.*, 2009). Particularly in terms of water use efficiency, which refers to the ratio of water used in the plant metabolism and water loss through transpiration, these parameters are used to evaluate plant performance in response to variable water irrigation regimes (García-Tejero *et al.*, 2011). Although it is clear that T_L shows a high variation as a function of variable environmental factors (Jones, 1999*b*) these measurements are still widely spread and used. Under stable environmental conditions and if measurements are performed at the same time point, the single assessment of T_L is argued to be sufficient (Araus *et al.*, 2003). However, even within in a short time period the repetition of T_L measurements can result in largely different values (Maes and Steppe, 2012). Therefore, T_L or T_L-T_a measurements do not seem to be adequate to assess diurnal or seasonal variation of plant-water relations. Early on, first efforts were done to create indices, which can overcome the issue of variable meteorological parameters. One idea was to simply use the variability of T_L within a canopy as an indicator for drought stress (Aston and van Baverl, 1971; Fuchs, 1990). Indeed, severely stressed vegetation was found to show a higher standard deviation of T_L compared to non-stressed vegetation (González-Dugo *et al.*, 2006). But at the single leaf or single plant level these observations could not be confirmed (Grant *et al.*, 2007; Maes *et al.*, 2011). Further ideas like the stress degree day, where T_L-T_a is summed up and referred to stress (Jackson *et al.*, 1977) did not really overcome the problem of a varying environment, although this approach seemed to be more robust compared to T_L measurements.

An important step was achieved by Idso *et al.* (1981) and Jackson *et al.* (1981) who developed the crop water stress index (CWSI). The CWSI related the measured T_L of a canopy to a theoretically non-transpiring and a fully transpiring canopy, respectively. The actual and the theoretical canopy are assumed to have an identical structure, so that heat transfer properties do not differ, except for transpiration. To obtain T_L-T_a for a fully transpiring canopy, a so-called non-stressed baseline has to be established. T_L-T_a, which is proportional to evapotranspiration under stable conditions, is also linearly related to VPD. Under water-limiting conditions T_L approaches or exceeds T_a and the linear relationship breaks down, which provides the stressed-baseline. Referring T_L to the two boundary conditions, the CWSI normalizes relative changes in the leaf heat fluxes to a range between zero and one, where zero refers to non-stressed conditions and one refers to stressed conditions. The basic CWSI was based on theoretical considerations and requires the establishment of the mentioned baselines before it could be applied (Costa *et al.*, 2013). Because these baselines are different for different plant species and different environmental conditions a more practical approach of the CWSI was developed by using

artificial references, which represent a fully transpiring leaf or canopy (T_{wet}) and a non-transpiring leaf or canopy (T_{dry}). Using such references, the CWSI can be expressed as a simple ratio:

$$CWSI = \frac{T_{wet} - T_L}{T_{wet} - T_{dry}} \qquad \text{Equation 1.5.1}$$

Reference surfaces are for example leaves which are covered with Vaseline, providing a dry reference, and leaves which are sprayed with water, providing a wet reference (Jones, 1999*b*). Other practical reference surfaces are wetted and dry cotton cloths, which are connected to water reservoirs and are protected against drying (Möller *et al.*, 2007; Alchanatis *et al.*, 2009). Such reference can be positioned near the measured plants or, when thermal cameras are used, placed within the field of view of the camera. This enables to measure the references at the same time point as the actual plants. Additionally, the references are exposed to the same environmental conditions, eliminating the necessity of the theoretical baselines. Jones (1999*a*) has demonstrated that these boundary conditions are related to different heat transfer states and thus the CWSI is a measure of the relative change in the heat transfer state. Additionally, Jones (1999*a*) developed another index, the I_G, which is a reformulation of the CWSI. It was demonstrated that the I_G was positively related to g_s (Grant *et al.*, 2007). However, for measuring and computing both indices, LWC which is an important parameter affecting leaf-water-relations is not considered. In few studies, the CWSI was found to be correlated with the leaf water potential (e.g. Cohen *et al.*, 2005). Leaf water potential and LWC are related to g_s and to water loss through transpiration. Additionally, the CWSI, in theory, reflects changes in the leaf heat flux. This relationship may not be reproducible under all circumstances. Transpiration results in dehydration of the plant inducing stomatal closure, which may result in a high CWSI. However, mild dehydration of a plant does not necessarily induce stomatal closure, which in in turn would not result in a high CWSI. Under these conditions, dehydration and CWSI were not positively related.

1.6 Active thermography

The above mentioned methods usually use the passive thermography approach, where temperature measurements are performed with the assumption that the leaf energy balance is in an equilibrium and the sum of incoming and lost heat is zero. As it can be concluded from Equation 1.4.1, LWC theoretically plays any role in the leaf energy balance, if the latter is zero. However, a relationship between the CWSI and LWC was found indicating that T_L can be related to LWC

(Cohen *et al.*, 2005). It can be argued that this relationship is not valid under all circumstances, because the CWSI reflects the actual heat transfer state, whereas the leaf water potential represents a delayed response and additionally, it is a parameter which is affected by long-term water loss through transpiration (Cowan, 1972; Hennessey and Field, 1991). LWC becomes more relevant when the leaf energy balance is in a non-equilibrium, for instance due to an additional heat flux, which would result in warming of the leaf surface. The rate of leaf warming or of leaf cooling, after a transient T_L change, depends on the leaf heat capacity that in turn depends to a great extent on LWC. Kümmerlen *et al.* (1999) and Garbe *et al.* (2002) made first attempts to establish active temperature measurements to derive LWC. Leaves were enclosed in a large gas exchange cuvette to record leaf heat fluxes, particularly transpiration, and T_L was observed with a thermal camera. Then the leaf was exposed to an additional heat flux resulting in a transient leaf warming. Leaf warming and leaf cooling kinetics follow Newton's law of cooling resulting in an exponential function, which can be characterized by a time constant (τ). This τ is the product of the leaf heat capacity per unit area ($C\ A^{-1}_{leaf}$) and a leaf resistance to heat, the inverse of the leaf heat transfer coefficient (h_{leaf}), characterizing leaf boundary layer conductance

$$\tau = \frac{C}{A_{leaf}} \frac{1}{h_{leaf}} \qquad \text{Equation 1.6.1}$$

These pioneering studies, using the active thermography method, have demonstrated that the combination of passive and active temperature measurements can be used to assess LWC and suggested that these approaches can be of great value in quantitative measurements of heat exchange processes at the leaf surface.

1.7 Objectives and goals

The overall goal of this work was to determine the water status, particularly LWC, of single leaves and whole canopies by using a further developed active thermography approach. For this purposes experiments were performed in two different environments. In the laboratory, which provides a well-defined and stable environment, measurements on the leaf level were performed. Here two plant species were chosen, spring barley (*Hordeum vulgare*) and common bean (*Phaseolus vulgaris*). Both plant species are anisohydric, so that the water status can easily be manipulated by changing the transpiration experimentally. Additionally, in these two species plant architecture and leaf surface are different, so that both plant species show different leaf heat transfer properties. As barley has narrower leaves compared to bean, barley is generally assumed to have a thinner boundary layer and thus a higher boundary layer conductance. The second experimental environment was the greenhouse, where measurements were performed

on barley canopies. Four different varieties were used and older varieties were compared with newer ones. It was assumed, that the older varieties were more drought susceptible compared to the newer varieties.

The work was divided into two main parts with two key questions:

1. Validation of the active thermography approach
    a) How is the measured τ related to LWC?
    b) How is the measured τ affected by a varying boundary layer conductance?
2. Use of the active thermography on canopy scale
    a) How is the measured τ on canopy scale related to water-limiting conditions?
    b) How is τ related to the CWSI and can both parameters together reveal overall insights in the plant water relations?

2. Theoretical background[1]

2.1 The principle of non-invasive thermal-infrared radiation measurements

All bodies, which have a temperature above 0 K or -273.15 °C (absolute zero) emit electromagnetic radiation. Electromagnetic radiation is characterized by electromagnetic fields, propagated as waves, which differ in their frequency and wavelength. The higher the frequency, the lower the wavelength and the higher is the energy of the radiation. The spectral region which is of primary concern for plant physiological processes is located in between 0.3 and 100 µm (Jones, 1992; Monteith and Unsworth, 2008). This region can be separated into further subregions: i) 0.3 to 0.4 µm refers to ultra-violet (UV) radiation, ii) 0.4 to 0.7 µm refers to the photosynthetically photon flux density (PPFD) and covers nearly the whole visible light region in the spectrum (0.38 to 0.78 µm), and iii) 0.7 to 100 µm, which is the infrared (IR) radiation. The IR spectrum is divided into further regions: i) near infrared (NIR), covering the wavelengths from 0.75 to 1.4 µm; ii) short-wave infrared (SWIR) in the region between 1.4 to 3 µm; iii) middle wave IR (MWIR) in the region in between 3 to 8µm; iv) long wave IR (LWIR) from 8 to 15 µm, and v) the far-infrared (FIR), which is located between 15 and 1000 µm. The LWIR region is often referred to as thermal IR (TIR) radiation, which is of primary interest for non-invasive temperature measurements.

According to laws of thermodynamics, temperature is a measure of the inner energy of a body, which arises from the movement of molecular particles, like molecules, atoms, and electrons. Occasionally, particles emit energy as electromagnetic radiation and photons to reach a lower energy level. Within a body, this energy is re-absorbed by other particles, which then reach a higher energy level. At any surfaces of a body, energy exchange between the body and the environment occurs. If the environment is cooler than the body, the body will lose energy as heat, whereas it will absorb energy, if the environment is warmer compared to the body.

2.1.1 Physical description of thermal infrared radiation

To describe the physics of TIR radiation, the model of the black-body is used. A black-body is a perfect radiator, which means that this object always emits radiation at the highest possible intensity compared to any other object with the same temperature. The distribution of electromagnetic energy of radiation (Φ) as a function of wavelength and frequency for black bodies is described by Planck's law (Fig. 2.1.1). In short, Planck's law shows that the warmer an object, the higher is the electromagnetic energy and the lower is the wavelength, where the maximum

[1] Abbreviation list in Appendix – Chapter 2

emission occurs. For objects with a temperature above 500 °C parts of the emitted radiation are already located within visible region of the electromagnetic spectrum, whereas objects below 500 °C do not emit any radiation in the visible spectrum region. Derived from Planck's law, two further laws are of importance, the Stefan Boltzmann law and Wien's displacement law.

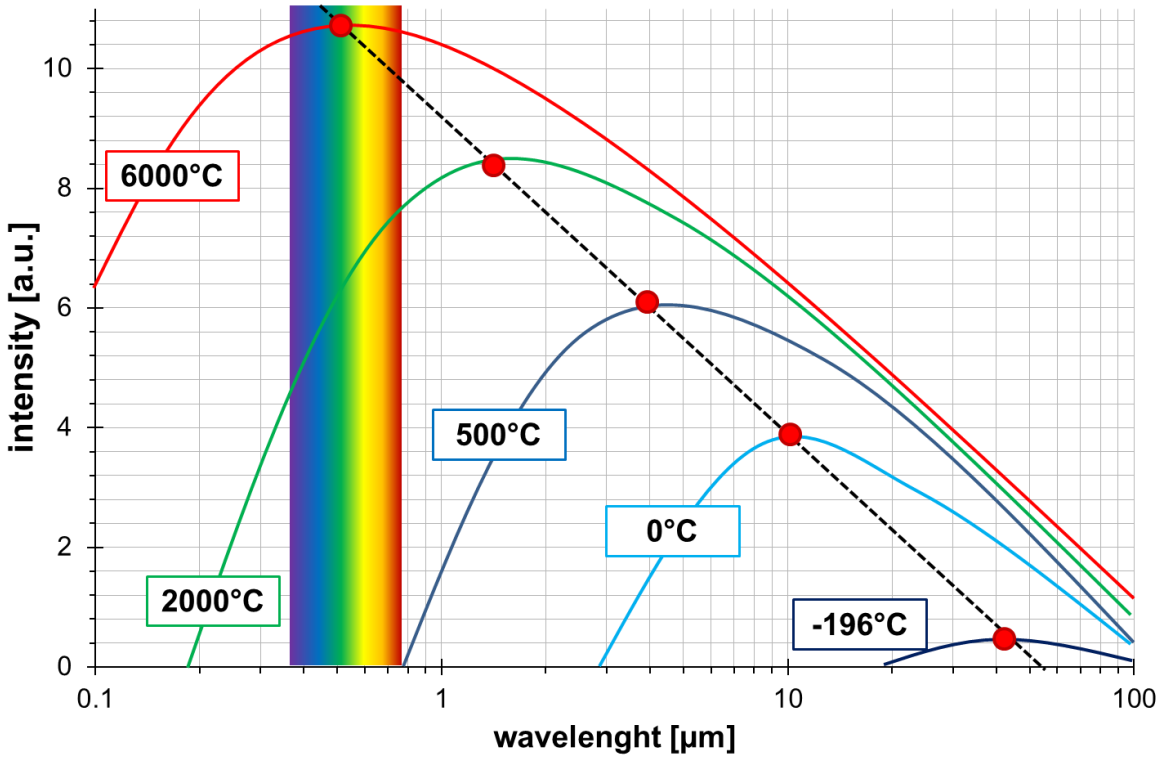

Figure 2.1.1: Schematic illustration of Planck's law. Electromagnetic radiation emitted by a black-body, which is in thermal equilibrium. Five representative temperatures are shown: 6000 °C, red line, 2000 °C green line, 500 °C blue line, 0 °C light blue line, and -196 °C dark blue line. Emission maxima are highlighted by red points. Dotted line emphasizes Wien's displacement law: The higher the temperature of a black body the higher the emitted radiation intensity and the shorter the peak wavelength, where maximum emission occurs. Figure is based on Glückert (1992).

The Stefan-Boltzmann law states that radiation emitted by an object is proportional to the fourth power of its temperature.

$$\Phi_M = \varepsilon\sigma T^4 \qquad \text{Equation 2.1.1}$$

where Φ_M is the measured electromagnetic radiation in W m^{-2}, ε is the emissivity, σ the Stefan Boltzmann constant (5.670373 ×10^{-8} W m^{-2} K^{-4}), and T the object's temperature in K.

Wien's displacement law describes the effect that objects with comparatively higher temperatures, which then emit more electromagnetic energy, emit radiation at lower wavelengths.

$$\lambda_{max} = \frac{b_W}{T}$$ Equation 2.1.2

where λ_{max} is the peak wavelength at which maximum emission occurs, and b_W is the Wien's displacement constant (≈ 2900 µm K).

Generally, TIR radiation behaves like any other type of radiation, meaning that it propagates in all directions with light speed, and all optical laws are valid. There are three fates for radiation, when it is intercepted by an object. It can be absorbed, reflected or transmitted. According to the law of energy conservation, the sum of the relative contribution of all three processes is always 1.

$$\alpha_\Phi + \rho_\Phi + \tau_\Phi = 1$$ Equation 2.1.3

where $\alpha_\Phi$is the absorptance, ρ_Φ the reflectance and $\tau_\Phi$the transmittance. Absorptance, reflectance and transmittance are the portions of incident electromagnetic energy, which are absorbed, reflected, or transmitted, respectively.

Particularly for temperature measurements, a further important law is Kirchhoff's law. Kirchhoff's law states, that the ability to absorb radiation of a certain wavelength equals the ability to emit radiation of a certain wavelength. Thus, the absorptance (α) equals emissivity (ε).

$$\alpha = \varepsilon$$ Equation 2.1.4

As α is the portion of incident radiation, which is absorbed, ε is the portion of incident radiation, which is emitted. Black bodies, objects which emit radiation at the highest possible intensity, have an ε value of 1, which also implies that all absorbed radiation is emitted. Usually, any objects other than a black-body are not perfect radiators and thus have an ε value that is below 1.

2.1.2 Theory of thermography

All the above mentioned laws describe the basics for thermography. Because thermography is a non-invasive method and temperature is measured from a certain distance, further factors have to be considered for accurate temperature measurements. In any measuring set-up, radiation has to travel through the measurement path from the measured object to the sensor (Fig. 2.1.2). For thermal measurements there are two interfering factors arising from this measuring path: i) transmittance of the measuring path medium (τ_Φ), which describes the relative amount of radiation passing the measuring path and ii) the temperature of the measuring path. Usually, the transmission medium in the measuring path is air.

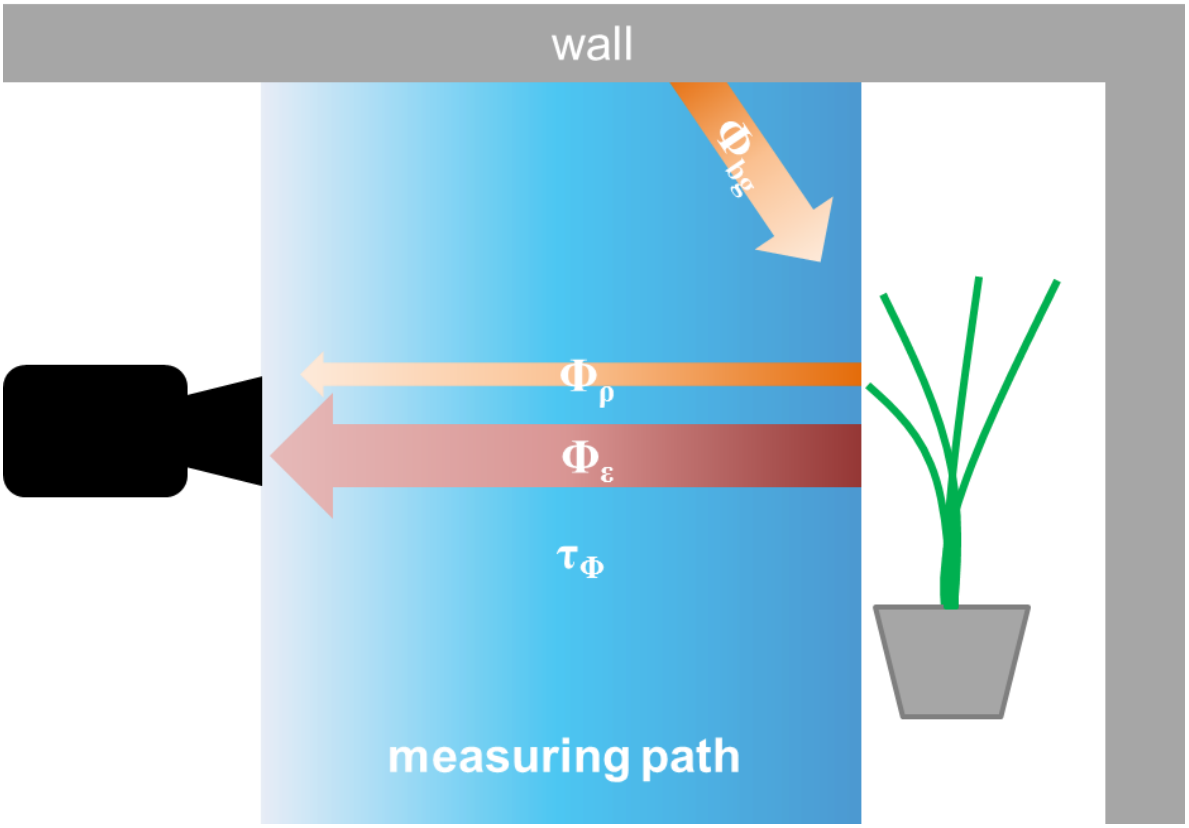

Figure 2.1.2: Schematic illustration of common measurement set-up. The measured object emits radiation (Φ_{ε}), which has to penetrate a measurement path with a certain transmittance (τ_{Φ}). Additionally, objects in the vicinity of the measured object emit background radiation (Φ_{bg}), which is reflected by the measured object (Φ_{ρ}). Finally, the camera captures the sum of radiation, which is emitted and reflected by the measured object minus the radiation which is absorbed along the measurement path.

Therefore, for non-invasive measurements it is convenient to use wavelength regions where the air transmittance for TIR radiation is high (Fig. 2.1.3). There are two atmospheric windows, located in between 3 to 5 µm and in between 8 to 14 µm, which are suitable for non-invasive thermal measurements. Because in the region between 8 and 14 µm the transmittance for thermal radiation is high and reasonably uniform over large distances, it is the most suitable spectral range for thermography and the interfering factors are negligible, particularly for short distances. For relatively short distances, e.g. 10 m, the transmittance reaches 1, which means, that 100% of TIR can pass the air in this particular wavelength region.

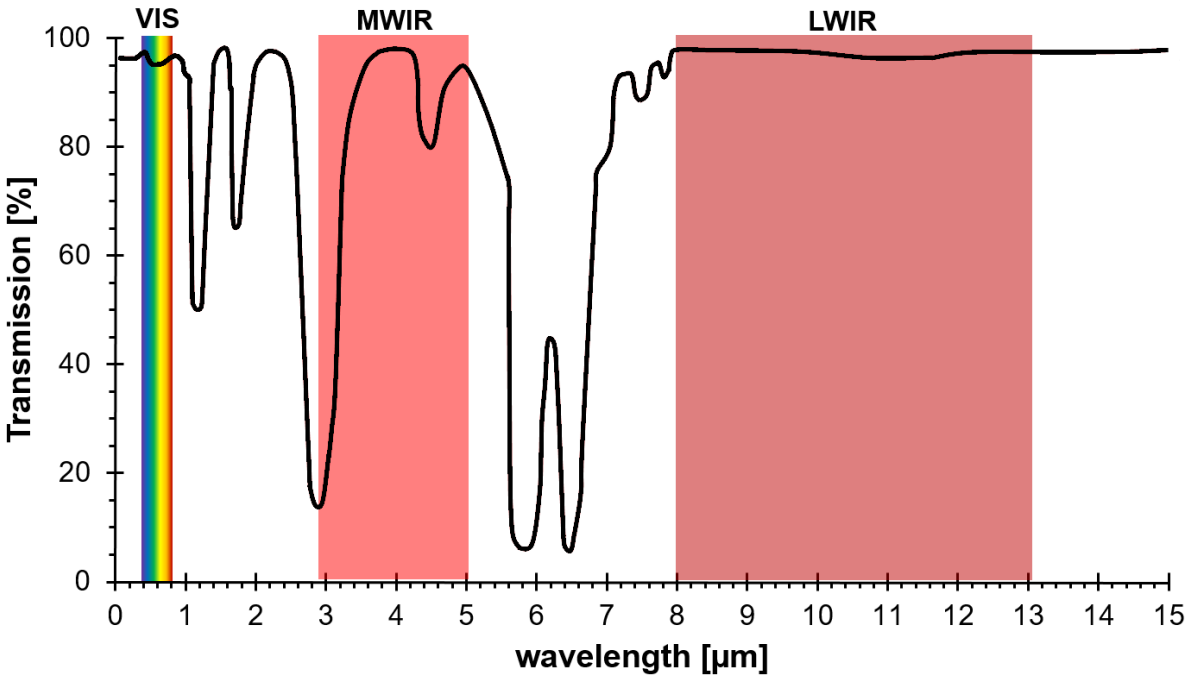

Figure 2.1.3: Relative transmission of the atmosphere in the wavelength range between 0 to 15 µm, measured over a distance of 1 m at 32 °C air temperature and air humidity of 75%. Relative transmission is given in %. Spectral region for visible light (VIS), mid wave infrared radiation (MWIR), and long wave infrared radiation (LWIR) are highlighted by colored areas. Figure is based on Gaussorgues (1994).

Another interfering factor is the background radiation (Φ_{bg}), which originates from any object in the vicinity of the measured object. As the measured object itself, any ambient object has an ε above 0, so that these objects emit TIR. If the measured object has an ε value lower than 1, the object will reflect Φ_{bg} (Φ_{ρ}). For example, an object that does not transmit any radiation and has an ε value of 0.9, has, according to Equation 2.1.3, a reflectance (ρ) of 0.1. This means that 10% of the measured signal originate from reflected Φ_{bg} and thus, the measured signal is a mixture of both, the object's temperature and the temperature reflected by the object. Therefore, for adequate measurements, it is crucial to know ε and to determine Φ_{bg}. Both parameters can easily be measured. For example, to obtain ε for any object, this object is measured with a thermal camera and the obtained temperature is compared to the temperature which is measured by a common thermometer. Usually, currently available software for thermographic measurement allow to adapt ε-values, so that ε has simply to be varied until the measured temperatures are similar. Another possibility to obtain ε, is to compare an object with a black-body at the same temperature. Again, ε has to be adapted until the temperatures are equal. Additionally, there are tables available to obtain an appropriate ε-value for different materials. The Φ_{bg} can be assessed either by direct measurements of the background or by objects which are highly reflective, such as mirrors or aluminum foil, which can be placed within the measured scene. A

convenient method is to use crumbled aluminum foil, which due to its surface reflects all incoming radiation. As for ε, today's software used in thermography usually provide a correction function for the measured temperature by introducing Φ_{bg}. Detailed correction formulas are presented, for example, in the extensive review about thermography by Maes and Steppe (2012).

2.1.3 Thermographic measuring systems

There are several thermographic systems available. Photon detectors usually measure in the spectral region between 3 to 5 µm and are suitable for the measurements of very small temperature differences and very fast processes. Disadvantageous is that these systems have to be cooled and therefore are expensive and bulky. The most commonly used thermal cameras are focal-plane-array (FPA) cameras because they are usually much smaller and much cheaper. Additionally, in present days those cameras have a high thermal sensitivity, which provide a wide applicability, including plant science research. In FPAs, thermal detectors which react on heating or cooling by thermal infrared radiation are arranged in an array. Examples for such thermal detectors are thermopile detectors, which are based on a voltage change induced by thermal radiation, or microbolometer, which are thermal resistors. If thermal radiation hits such a thermal resistance it will be absorbed and results in a change of the electrical resistance. This change in the electrical resistance is measured and converted into temperature. Typical materials for microbolometers are vanadium oxide or amorphous silicon.

In contrast to detectors used for the MWIR range, microbolometers itself usually do not have a specific spectral sensitivity. However, optics that are coated with germanium are used to restrict the incoming spectral range in between 8 and 14 µm, because the transmittance of air for TIR radiation is reasonably high in this region (Fig. 2.1.3). Consequently, interfering signals that arise from the emissivity of air in other spectral regions are eliminated.

2.2 Leaf temperature and the leaf energy balance model

Plants are always exposed to energy coming from the environment. The incoming energy (Φ_{in}), which mainly derives from solar radiation in the wavelength range 250 to 2500 nm, may be stored by leaves (S) or used for physiological processes (M). All the energy, which is not used for S or M has to be dissipated by heat loss processes (Fig. 2.2.1). These heat loss processes are:

i) Heat loss by longwave radiation (LW), which is TIR radiation. This is the energy which is emitted as electromagnetic radiation in the longwave thermal region above 2500 nm.

ii) Heat loss by convection, often referred to as sensible heat loss (H), is the transport of molecules (mainly air) through liquids or gases by diffusion and the Brownian molecular movement. Convection combines conductive and convective heat losses.

iii) Heat loss by evapotranspiration (λE), which is the heat loss by water vapor. λE describes both, water vapor evaporated from surfaces, like the leaf surface, and transpiration. As water accumulation on the leaf surface occurs only under certain circumstances, for example after rain, it can be usually neglected. Transpiration is mainly dependent on stomatal closure and opening in response to environmental parameter, such as water availability, irradiance, and temperature.

In plant research, the physical storage of heat is often neglected and assumed to be zero, providing a leaf energy balance, which is an equilibrium, meaning that all incoming energy is dissipated by the respective heat loss processes (Monteith and Unsworth, 2008).
If the leaf is in full equilibrium with the environment and all incoming energy were dissipated by the above mentioned heat fluxes, the net energy flux density (Φ_{net}) is zero. A simplified formulation of the leaf energy balance is:

$$0 = \Phi_{in} - (LW + H + \lambda E) \qquad \text{Equation 2.2.1}$$

Generally, all quantities are described as net energy flux densities in W m^{-2}.

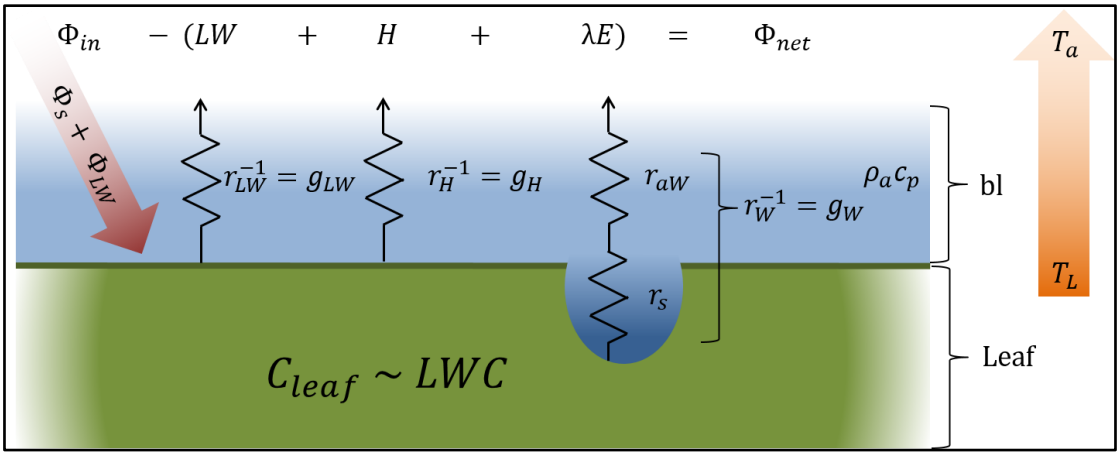

Figure 2.2.1: Schematic illustration of leaf energy balance. The net heat flux of the leaf (Φ_{net}) is the difference between absorbed incoming energy (Φ_{in}), composed of solar radiation (Φ_s) and long-wave thermal radiation (Φ_{LW}) and re-emitted heat as long-wave radiative heat (LW), convective heat (H) and evapotranspiration (λE). Heat fluxes are driven by the difference between leaf temperature (T_L) and ambient air temperature (T_a) providing a heat gradient. T_L changes due to absorbed Φ_{in} depend on leaf heat capacity (C_{leaf}), which is proportional to leaf water content (LWC). Velocity of heat fluxes further depend on boundary layer (bl) composition. This is defined by the energy density of the bl as the product of air density and specific heat capacity of air (ρ_a c_p) and the respective conductances (g) for the respective heat fluxes: g for LW (g_{LW}), g for H (g_H) and g for λE (g_w). The reciprocals of g are the respective resistances (r). g_W is the reciprocal of r_w, which in turn is the sum of the bl resistance to water vapor (r_{aW}) and stomatal resistance (r_s).

2.2.1 Net energy flux density

The net energy flux density is the energy that potentially can be used for physical storage of heat (S) or for metabolic processes (M) like photosynthesis. Because, M is quite small (less than 5%) it can be neglected in the overall leaf energy balance (Jones, 1992). In contrast, S may have significant influence on the leaf energy balance and should not be neglected (Leigh *et al.*, 2012). In principle, S describes how much energy can be stored and to what extent this energy changes the leaf temperature (T_L) over time. The heat capacity (C), which per definition is the energy (Q) that is required to heat up an object by one degree of temperature, is an important component of S.

$$C = \frac{Q}{T} \qquad \text{Equation 2.2.2}$$

where C is expressed in J K^{-1}.

Generally, energy flux densities are described as energy fluxes (j) in J s^{-1} across a certain area (A), which gives the unit W m^{-2}. So the general Equation form for S is:

$$S = \frac{j}{A} \qquad \text{Equation 2.2.3}$$

Considering, that C is the limiting factor for the energy uptake, the net energy flux density can be written as:

$$S = \frac{C}{A}\frac{\Delta T_L}{\Delta t} \qquad \text{Equation 2.2.4}$$

where ΔT_L describes the change in T_L and Δt the time difference. To what extent T_L may change, depends on C A^{-1}, whereas the rate of this change in the time interval (Δt) is highly affected by the heat loss processes of a leaf.

In conclusion, T_L may depend on the leaf heat capacity (C_{leaf}). It is convenient to express the leaf heat capacity per unit area (C $A^{-1}{}_{leaf}$) to relate C_{leaf} to the energy flux densities, which are generally normalized to (leaf) area. The specific heat capacity of properly hydrated leaves is usually close to that of water (~4.2 kJ kg^{-1} K^{-1}), which varies according to parameters such as hydration state of cellular structure of the leaves. According to Jones (1992), the specific heat capacity of leaves ranges between 3.5 and 4.0 kJ kg^{-1} K^{-1}.

2.2.2 Incoming heat and radiative heat flux density

The source of the incoming heat derives from shortwave (solar) and longwave (thermal) radiation (Fig. 2.2.1). The net radiative heat flux density (Φ_{net}) is defined as the sum of the absorbed fraction (α) of solar irradiance (I_s) and longwave irradiance (I_{LW}) minus the longwave radiative heat loss, which is described by the Stefan-Boltzmann law.

$$\Phi_{net} = \alpha I_s + \alpha\, I_{LW} - \varepsilon\sigma T_L^4 \qquad \text{Equation 2.2.5}$$

The emissivity (ε) of plants is typically between 0.95 and 0.98 (e.g. Nobel, 2009). For simplification, the term $\alpha\, I_s + \alpha\, I_{LW}$ is replaced by Φ_{in}, which describes the overall absorbed energy.

For predictive studies, the concept of the net isothermal radiation (Φ_{ni}) was developed (Jones, 1992; Monteith and Unsworth, 2008). This concept assumes, that the surface, which receives the radiation is at air temperature (T_a). Thus, Φ_{ni} describes the maximum possible radiation which may be absorbed by an object in the respective environment.

$$\Phi_{ni} = \Phi_{in} - \varepsilon\sigma T_a^4 \qquad \text{Equation 2.2.6}$$

By substituting Equation 2.2.5 from Equation 2.2.6 and using the approximation $\varepsilon\sigma(T_L^4 - T_a^4) \approx 4\varepsilon\sigma T_a^3(T_L - T_a)$, which is valid for small temperature differences (Monteith and Unsworth, 2008), the net radiative heat flux density finally becomes:

$$\Phi_{net} = \Phi_{ni} - 4\varepsilon\sigma T_a^3(T_L - T_a) \qquad \text{Equation 2.2.7}$$

For further simplification of the overall leaf energy balance Equation, one can define a conductance to radiative heat loss (g_{LW}):

$$g_{LW} = \frac{4\varepsilon\sigma T_a^3}{\rho_a c_p} \qquad \text{Equation 2.2.8}$$

where ρ_a is the density of air and c_p the specific heat capacity of air. The product of ρ_a and c_p is the energy density of air in dependency of temperature. With g_{LW}, the radiative heat flux density becomes:

$$\Phi_{net} = \Phi_{ni} - \rho_a c_p \left(\frac{4\varepsilon\sigma T_a^3}{\rho_a c_p}\right)(T_L - T_a) \qquad \text{Equation 2.2.9}$$

2.2.3 Convective heat

Heat or mass exchanges between leaves and ambient air described best by Fick's law that states that heat fluxes occur along a heat gradient, which is given by T_L-T_a (Fig. 2.2.1). Heat, which is transported away from a leaf surface, has to penetrate a boundary layer (bl), a thin layer of air between the leaf and the ambient air. This bl determines the velocity of heat fluxes. Thus, the thickness and composition of the bl determines the conductance (velocity of heat transfer) to convective heat (g_H). The transported heat is described by the product of the ρ_a and c_p, both of which depend on T_a. Relating this temperature dependent energy density of air to g_H and to the heat gradient T_L-T_a finally gives a formulation of the convective heat loss.

$$H = \rho_a c_p g_H(T_L - T_a) \qquad \text{Equation 2.2.10}$$

The bl and thus g_H highly depend on the prevailing environmental conditions, particularly whether wind occurs or not. Under wind-still conditions the dominant form of convection is the free convection, where the bl is mainly affected by buoyancy forces of air. In conditions, where wind occurs, the bl becomes a function of wind speed and the dominant form of convection is the forced convection.

There are several approaches available to estimate g_H with respect to free and forced convection (Jones, 1992; Monteith and Unsworth, 2008; Nobel, 2009). A frequently used approach is the

application of dimensionless numbers, which relates the leaf geometry (d) to the bl thickness. This ratio is known as the Nusselt number (Nu). Because, g_H is a function of leaf diameter and bl thickness, Nu can be used for calculations of g_H with respect to leaf properties, such as size and shape. Using Nu, g_H may be calculated as follows:

$$g_H = \frac{Nu\ k}{\rho_a c_p d} \qquad \text{Equation 2.2.11}$$

where k is the thermal conductivity of air (≈ 0.026 W $m^{-1}K^{-1}$) and d, the characteristic dimension of a leaf. The definition of Nu depends on whether the prevailing conditions are free or forced convection.

In free convection, the heat transfer depends on upwelling air movement from the leaf surface into the ambient air, which is maintained by T_L-T_a. Under these conditions, Nu is the function of another dimensionless number, the Grashof number (Gr). Using Gr, bl is mainly characterized by T_L-T_a, the leaf dimension, and buoyancy forces of air. The detailed calculation of Gr is as follows:

$$Gr = \frac{g\ \beta d^3 (T_L - T_a)}{\nu^2} \qquad \text{Equation 2.2.12}$$

where g is the gravitational acceleration, β the thermal expansion coefficient of air and ν the kinematic viscosity of air.
With Gr, Nu becomes

$$Nu = aGr^b \qquad \text{Equation 2.2.13}$$

where a and b are numerical constants describing the geometry of a leaf. Typical numbers are for instance given by Dixon and Grace (1983), Schuepp (1993), and Monteith and Unsworth (2008).
For forced convection, i.e. conditions where wind occurs, Nu becomes a function of the Reynold's number (Re). Re relates the bl composition to the wind speed (u) and the characteristic leaf dimension.

$$Re = \frac{u\ d}{\nu} \qquad \text{Equation 2.2.14}$$

Similar to the formulation for free convection, in forced convection Nu becomes

$$Nu = aRe^b \qquad \text{Equation 2.2.15}$$

However, the ambient conditions are rarely that stable, as it is assumed for the above calculations. For instance, in greenhouses air circulation maybe low; or in canopies, free convection from one leaf disturbs the bl of another leaf, so that under both conditions wind is not completely still. Under conditions, where slight wind movements are present, the usage of mixed convection is preferable. This means that both free and forced convection contributes to leaf heat transfer. As for free and forced convection, there are several formulations available for mixed convection (Schuepp, 1993; Bird *et al.*, 2002; Monteith and Unsworth, 2008). In the present study, the following formulation adapted from Bailey (1993) is used:

$$Nu = a(Gr + 1.4Re^2)^b \qquad \text{Equation 2.2.16}$$

2.2.4 Transpiration

The transpiration, often referred to as latent heat flux density, describes the heat loss by transpiration, which is heat loss by water vapor (Fig. 2.2.1.). Because a certain amount of energy is required to transfer liquid water into vapor, the latent heat flux is the product of the latent heat of vaporization (λ) and the transpiration rate (E). According to the form of Fick's law, as already used for convective heat, the heat has to travel through a bl, that is characterized by its conductance to water vapor (g_W), and flows along a heat gradient given by the difference of the water vapor concentration between the leaf and the ambient air (c_W).

$$\lambda E = \lambda \, \Delta g_W \, c_w \qquad \text{Equation 2.2.17}$$

To express λE in a form analogically with the convective heat, which depends on T_L and T_a, c_w is defined as the product of a water vapor related energy density of air, and the vapor pressure deficit (Δe) between leaf and ambient air.

$$\Delta c = \frac{\rho_a c_p}{\gamma} \, \Delta e \qquad \text{Equation 2.2.18}$$

The psychrometric constant (γ) relates T_a to actual air pressure and contains the heat of vaporization of water (λ).

As already mentioned, the water vapor pressure deficit (Δe) is the difference between the water vapor pressure at the leaf surface and the partial water vapor pressure of the ambient air (e_a). Usually, it is assumed, that the partial vapor pressure of leaves corresponds to the saturation vapor pressure at T_L ($e_{s(T_L)}$).

$$\Delta e = e_{s(T_L)} - e_a \qquad \text{Equation 2.2.19}$$

To relate the above term to T_L-T_a it is made use of an approximation suggested by Penman (1948), which replaces the surface to air vapor pressure deficit by the vapor pressure deficit of ambient air (δe), and adds a term, which relates it to T_L-T_a:

$$\Delta e = \delta e + s\,(T_L - T_a) \qquad \text{Equation 2.2.20}$$

where *s* is the slope relating saturation vapor pressure to temperature and is valid for small temperature differences (Penman, 1948; Jones, 1992; Monteith and Unsworth, 2008).
Substituting these reformulations and approximations into Equation 2.2.17., λE finally becomes:

$$\lambda E = \frac{\rho_a c_p}{\gamma r_w}\,[\delta e + s\,(T_L - T_a)] \qquad \text{Equation 2.2.21}$$

In Equation 2.2.21 r_W is a resistance and thus the reciprocal value of g_W. r_W is a series of resistances, composed of the resistance to water vapor of the bl (r_{aW}), and the stomatal resistance (r_S).

$$r_W = d_s\, r_{aW} + r_s = g_W^{-1} \qquad \text{Equation 2.2.22}$$

The parameter d_s refers to the stomatal distribution of leaves. If leaves are amphistomatous as for example barley leaves, d_s will equal 1. For hypostomatous leaves, as for example bean leaves are, d_s equals 2, because r_{aW} has to be taken into account for two leaf sides, whereas (r_S) applies only for one leaf side.

2.2.5 Leaf energy balance Equation

By now, all heat flux densities were described in detail. Substituting all heat flux densities into Equation 2.2.1. and 2.2.4., the leaf energy balance Equation becomes:

$$\frac{C}{A_{leaf}}\frac{\Delta T_L}{\Delta t} = \Phi_{ni} - \rho_a c_p (T_L - T_a)(g_{LW} + g_H) - \frac{\rho_a c_p}{\gamma r_W}[\delta e + s(T_L - T_a)] \qquad \text{Equation 2.2.23}$$

which for later purposes can be rearranged to:

$$\frac{C}{A_{leaf}}\frac{\Delta T_L}{\Delta t} = \Phi_{ni} - \rho_a c_p (T_L - T_a)\left[g_{LW} + g_H + \left(\frac{s}{\gamma r_W}\right)\right] - \rho_a c_p \frac{\delta e}{\gamma r_W} \qquad \text{Equation 2.2.24}$$

Note that this formulation of the leaf energy balance describes the overall energy balance of two leaf sides. For leaves, which are not amphistomatous, this formulation differs, particularly in the formulation of λE (see Equation 2.2.22).

2.2.6 Non-equilibrium of the leaf energy balance

As the environmental parameters are highly variable and frequently change within minutes and seconds, the leaf energy balance is seldom in equilibrium. If the incoming energy changes (Φ_{ni}'), the leaf approaches a new steady state T_L (T_L') and how much and how fast T_L changes depends on the heat capacity of the leaf (C A_{leaf}^{-1}). The leaf energy balance Equation then becomes:

$$\frac{C}{A_{leaf}}\frac{\Delta T_L}{\Delta t} = \Phi'_{ni} - \rho_a c_p (T'_L - T_a)\left[g_{LW} + g_H + \left(\frac{s}{\gamma r_W}\right)\right] - \rho_a c_p \frac{\delta e}{\gamma r_W} \quad \text{Equation 2.2.25}$$

If T_a and δe were unchanged, the leaf adaptation to the changed environment would be simply the difference between Equation 2.2.24 and Equation 2.2.25.

$$\frac{C}{A_{leaf}}\frac{\Delta T_L}{\Delta t} = (\Phi'_{ni} - \Phi_{ni}) - \rho_a c_p (T'_L - T_L)\left[g_{LW} + g_H + \left(\frac{s}{\gamma r_W}\right)\right] \quad \text{Equation 2.2.26}$$

If environmental change is only a transient change, and Φ_{ni} is the same for Equation 2.2.24 and Equation 2.2.25, the term Φ_{ni}' - Φ_{ni} can be cancelled, so that Equation 2.2.26. becomes:

$$\frac{C}{A_{leaf}}\frac{\Delta T_L}{\Delta t} = \rho_a c_p (T'_L - T_L)\left[g_{LW} + g_H + \left(\frac{s}{\gamma r_W}\right)\right] \quad \text{Equation 2.2.27}$$

Because, the product of ρ_a, c_p, and g is known as the heat transfer coefficient (h), given in W m^{-2} K^{-1}, Equation 2.2.27 can be written as:

$$\frac{C}{A_{leaf}}\frac{\Delta T_L}{\Delta t} = (T'_L - T_L) h_{leaf} \quad \text{Equation 2.2.28}$$

Where h_{leaf} is the total leaf heat transfer coefficient and is the sum of the heat transfer coefficient for long-wave radiative heat (h_{LW}), the heat transfer coefficient for convective heat (h_H), and the heat transfer coefficient for transpiration ($h_{\lambda E}$).

$$h_{leaf} = h_{LW} + h_H + h_{\lambda E} \quad \text{Equation 2.2.29a}$$

$$h_{LW} = \rho_a c_p g_{LW} = \rho_a c_p \frac{4\varepsilon\sigma T_a^3}{\rho_a c_p} = 4\varepsilon\sigma T_a^3 \quad \text{Equation 2.2.29b}$$

$$h_H = \rho_a c_p g_H \quad \text{Equation 2.2.29c}$$

$$h_{\lambda E} = \rho_a c_p \left(\frac{s}{\gamma r_W}\right) \quad \text{Equation 2.2.29d}$$

2.2.7 The principle of active thermography

In active thermography, T_L is manipulated in a controlled way, for example with near-infrared radiation (Fig. 2.2.2). Short heat pulses, single pulses or repeated pulses, are applied to the leaf,

inducing a transient increase in T_L. After the additional heat source is switched off, T_L returns to its former steady T_L as described by Equations 2.2.27 to 2.2.29. Here it is of importance that the leaf is exposed to the same environment directly before and after the transient heat pulse and during the whole cooling process.

According to Newton's law of cooling Equation 2.2.28 can be solved with a first-order differential Equation:

$$dT_L(t) = \frac{1}{\frac{C}{A_{leaf}} h_{leaf}} (T_L' - T_L) \qquad \text{Equation 2.2.30}$$

which has the following boundary conditions:

$$dT_L(0) = T_L' \qquad \text{Equation 2.2.30a}$$

$$dT_L(\infty) = T_L \qquad \text{Equation 2.2.30b}$$

Using these boundary conditions, the decline of the leaf temperature is limited and can be solved with the following exponential function:

$$dT_L^* = T_L - (T_L - T_L')e^{-\frac{t}{\tau}} \qquad \text{Equation 2.2.31}$$

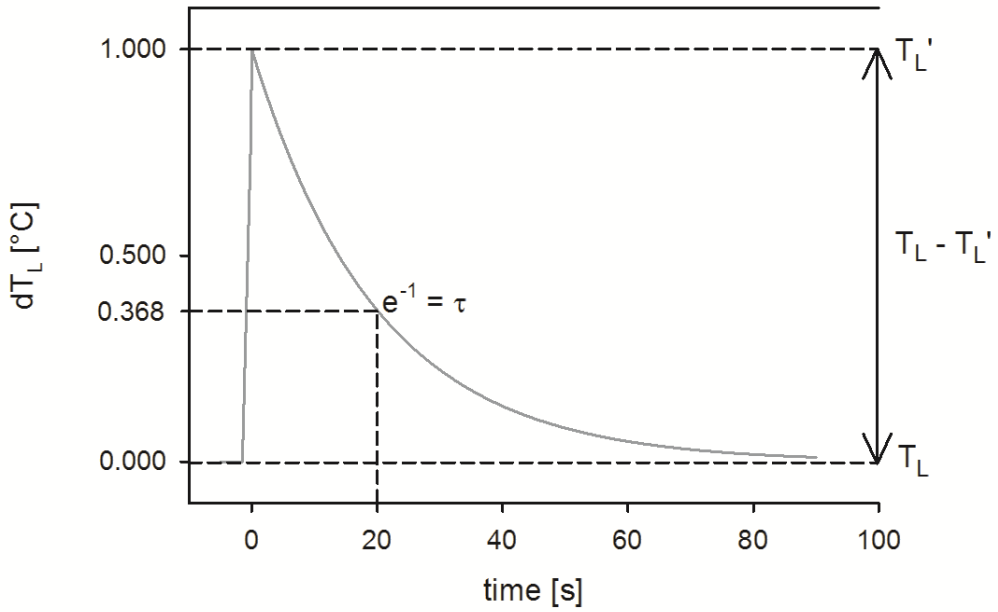

Figure 2.2.2: Principle of active thermography. A heat pulse is applied to a leaf inducing a shift from steady state leaf temperature (T_L) to a transient T_L (T_L'). Leaf cooling kinetic is characterized by an exponential decay constant (e^{-1}), which is the time constant (τ) and is the time that is required to reach about 36.8% of T_L-T_L'.

Where T_L^* is any T_L during leaf cooling and τ the time constant in s, which is according Equation 2.2.28 the product of leaf heat capacity and the inverse of the leaf heat transfer coefficient:

$$\tau = \frac{C}{A_{leaf}} h_{leaf}^{-1} \qquad \text{Equation 2.2.32}$$

As described in section 2.1., C A^{-1}_{leaf} mainly depends on leaf thickness and leaf water content per unit area (LWC) and thus these parameters are proportional to each other.

Under conditions, where the leaf boundary layer is kept constant, for example with constant wind speeds, h_{leaf} is a constant, so that τ mainly depends on LWC (Fig. 2.2.3) and τ increases with increasing LWC. If LWC were unchanged and bl were allowed to change, τ would mainly depend on h_{leaf}, while C A^{-1}_{leaf} remained constant. In this scenario τ would increase with decreasing h_{leaf}. However, under natural conditions the reality is a mixture of both scenarios, where both parameters are highly variable and contribute accordingly.

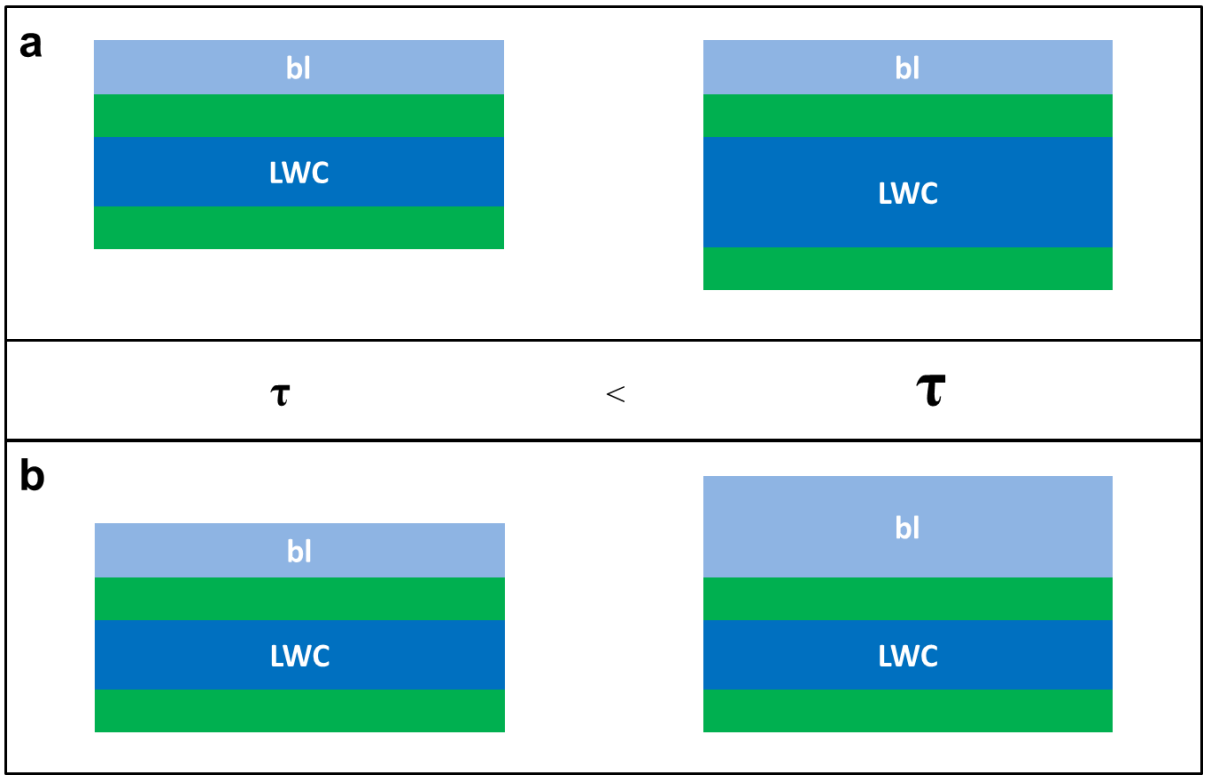

Figure 2.2.3: Schematic illustration of relationships between time constant (τ) and leaf water content per unit area (LWC) and leaf boundary layer (bl). **a**, increasing LWC increases τ, while bl remains constant. **b**, increasing bl increases the leaf heat transfer resistance and thus decreases the leaf heat transfer coefficient, which results in an increased τ.

3. Methodologies

In order to evaluate the leaf heat capacity per unit area ($C\ A^{-1}_{leaf}$), which is proportional to leaf water content (LWC) and the leaf heat transfer coefficient (h_{leaf}), which is related to the boundary layer conductance, these parameters and their dynamic changes were assessed using different methodologies:

i. Passive thermography, to estimate leaf heat flux densities and the corresponding leaf conductance to heat, by using the leaf temperature (T_L) to ambient air temperature (T_a) difference (T_L-T_a) and the crop water stress index (CWSI) (Chapter 3.2)
ii. Active thermography, to derive $C\ A_{leaf}^{-1}$ and h_{leaf} (Chapter 3.3)
iii. Gas exchange measurements combined with active thermometry, to measure dynamic changes in $C\ A_{leaf}^{-1}$ and h_{leaf}, in response to leaf dehydration due to transpiration (Chapter 3.5)

3.1 Thermography

For all thermographic measurements a VarioCAM ® hr head thermal camera (InfraTec, Germany) was used. This camera is equipped with a microbolometer focal plane array (FPA) that captures and integrates thermal infrared radiation in the spectral range between 7.5 µm and 14 µm. It has a field of view (FOV) of 30° by 23°, with a geometric resolution of 640 by 480 pixels. The measuring accuracy is ± 1K with a thermal sensitivity, <30 mK. For thermal image recording the IRBIS® 3 software was used (InfraTec, Germany), that allows real-time tracking of the measurements and correction of the temperature by setting parameters, such as emissivity (ε) and background radiation, often referred to as background temperature (T_{bg}). Additionally, the software allows to export point data or pixel data as table files (e.g. ASCII), which can be later on used in a more common software like Microsoft Excel (Microsoft Corp., USA) or in MATLAB (Mathworks, Inc., USA)

Because in thermography the surface temperature is derived from thermal infrared radiation, the application of thermography requires a few correction factors, before the "real" surface temperature can be obtained.

3.1.1 Correction factors: Ambient air temperature, background temperature, and emissivity

Usually, T_a is measured by common thermometers, or thermocouples. However, these measurements are based on a completely different method compared to thermographic measurements. While in thermography the temperature is derived from electromagnetic radiation in the

thermal infrared range of the spectrum, thermometers directly measure the "mass" of heat in the air. Therefore, there may be an offset in the measured temperatures, when comparing these measurements directly with each other. To account for this possible offset, a simple protocol to adapt measured T_a to thermographically obtained temperatures was developed.

T_a was measured with a nickel-chrome thermocouple (Type K, Newport Omega, Germany). In order to compare the measured temperature by the thermal camera with the temperature measured by the thermocouple, reference measurements were performed with a 2 x 2 x 15 cm box made of black construction cardboard. This box was thermally isolated from the surrounding with a 0.5 cm thick Styrofoam layer, to avoid strong fluctuations of temperature. The inner side of the box was covered with aluminum foil, which was crumbled and painted with emissivity paint that has an emissivity of >0.95 (TETENAL Europe GmbH, Germany). In theory, all incoming radiation is several times reflected and absorbed by all sides of the box, so that the overall emissivity of the inner box is as close as possible to 1. The upper side of the box, always facing to the camera, had a 1-cm-diameter hole. Due to the dimension of the box and the coating of the inner box, this construction provides a radiation trap, where all incoming radiation is absorbed and emitted through the small hole. Within the box a thermo-couple was placed which is identically constructed to the one that measures T_a. To adapt the measured T_a to temperatures obtained by thermography, the difference between the thermo-couple within the box and the temperature measured by thermography within the hole was calculated. In preliminary trials, T_L-T_a obtained with the thermal camera was compared to T_L-T_a obtained by thermocouples. It was found that the difference between the temperature obtained by the thermocouple within the box and the temperature of the hole in the upper side of the box obtained with the thermal camera could be used as a correction factor for T_a.

Additionally, a sheet of crumbled aluminum foil was placed within the field of view. This sheet provides T_{bg}, which is required to correct temperatures when objects have an emissivity lower than 1. ε for leaves was set at 0.95 (Nobel, 2009), whereas the ε of a whole canopy was set at 0.98, because the thermal radiation is assumed to be emitted by leaves and then re-absorbed by other leaves within the canopy, so that total ε is higher than compared to single leaves. The parameters, T_{bg} and ε, were supplied to the IRBIS® 3 software, which then automatically corrects temperature measurements according the theory introduced in Chapter 2.1.

3.2 Passive thermography

According to Equation 2.2.25, if the leaf energy balance is in equilibrium it is zero and T_L-T_a is an approximation of the occurring heat flux densities. Particularly in the greenhouse where

the measurements were performed several times a day, the environmental conditions were highly variable. Under these conditions, the comparison and interpretation of T_L-T_a is difficult. To overcome this problem, the CWSI was used, which corrects for variable environmental conditions (Idso *et al.*, 1981; Jackson and Idso, 1981). The CWSI normalizes the leaf heat flux densities to a range in between 0 and 1, where 0 represents the maximum possible heat flux densities and 1 represents the minimum possible heat flux densities.

$$CWSI = \frac{T_L - T_{wet}}{T_{dry} - T_{wet}} \qquad \text{Equation 3.2.1}$$

T_L is the measured leaf temperature, T_{wet} is the wet-reference temperature and refers to a fully transpiring surface, and T_{dry} is the dry-reference temperature, which refers to a non-transpiring surface. Because T_L did not exceed T_a at any time point during the greenhouse experiment and, particularly during the night, was at maximum near T_a, T_{dry} was set equal to T_a. To obtain T_{wet} a wet reference was constructed similar to an atmometer (Fig. 3.2.1).

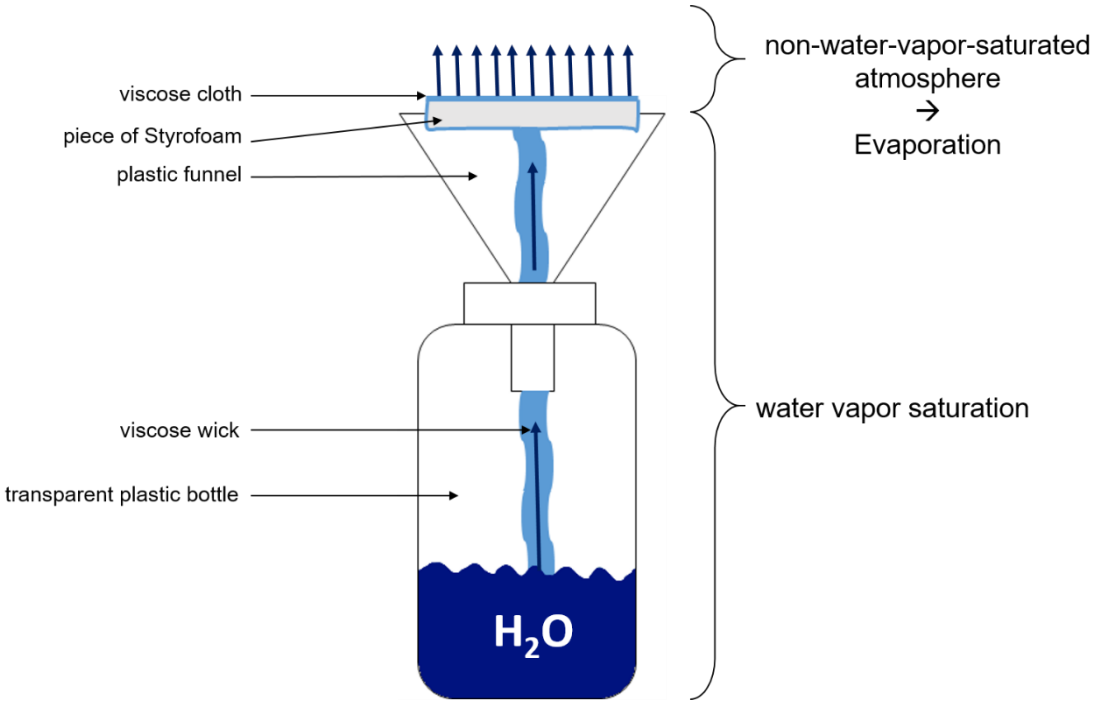

Figure 3.2.1: Constructed atmometer to measure wet-temperature (T_{wet}) for the assessment of the crop water stress index (CWSI). A transparent plastic bottle was filled with water. In the lid a funnel was placed, which was covered with a piece of Styrofoam, which, in turn, was covered by viscose cloths. The viscose cloth was connected to the water stock via a viscose wick and the surface was water vapor saturated providing a thin layer of pure water. As pure water has an emissivity of 0.98, the viscose cloth surface has the same emissivity as assumed for the measured barley canopies. Arrows in the Figure indicate flow direction of water and evaporation at viscose to ambient air boundary.

A transparent plastic bottle was filled with water and in the lid of the bottle a funnel was placed. The upper opening of the funnel was completely covered with a piece of Styrofoam, which,

additionally, was completely covered by several layer of a viscose cloth. The upper viscose cloths surface was in direct contact with the ambient air and was connected to the water stock in the bottle via a viscose wick. Because the bottle was completely closed, the air within the bottle was water vapor saturated as well as the viscose cloths. Usually, the ambient air was not water vapor-saturated, providing a water vapor pressure deficit between the viscose cloth and the ambient air, which drives evaporation. Similar to the leaf energy balance, the rate of evaporation depends on the incident energy, originating from incoming radiation, on water vapor pressure deficit, ambient air temperature, and wind speed. The viscose cloths were always exposed to similar environmental conditions as the plants and therefore represent the maximum possible evapotranspiration rate at the prevailing conditions.

3.3 Active thermography

As described in Chapter 2.2.7, in active thermography a sequence of images is recorded, during which an additional heat source induces a T_L shift. The most straightforward way is to apply a short heat pulse that induces a transient T_L increase and record the following cooling kinetic, which can be analyzed using Equations 2.2.31 and 2.2.32 (Chapter 2.2.7), providing the data series for the calculation of the time constant (τ). The benefit of this approach is that the incoming energy is only transiently changed and at the time point the cooling process starts, the incoming energy is equal to that before and after the heat pulse, so that T_L approaches the former steady state temperature.

3.3.1 Heating unit

To actively and transiently warm up leaves with short heat pulses, two commercial near-infrared (NIR) heating units were used, Heizmeister 1000 IP65 (Infralogic, Germany), equipped with a "long life Helen Goldröhre" light-tube (Infralogic, Germany), which emits radiation with a maximum power of 1000 W m^{-2} in the range between 750 and 2000 nm. This spectral range is suitable for actively heating leaves because plants have strong water absorption bands located at 1450 and 1950 nm (Gausman and Allen, 1973; Asner, 1998; Seelig *et al.*, 2008, 2009). The heating units were connected to an Eurolite® ESX-4 DMX switch pack (Eurolite, Germany), which was controlled via DMX-Configurator software (DMX4ALL GmbH, Germany), allowing the setting of intensity, duration, and interval of NIR heat pulses. Note that for the analysis, the absolute amount of heat applied onto the leaf surface is not relevant because transiently absorbed heat does not affect τ and the transpiration after each heat pulse. This was confirmed by tests, where three subsequent heat pulses were applied onto the leaf surface (Fig. 3.3.1). For

the actual measurements, a single heat pulse was applied onto the leaves and canopies. In laboratory experiments, where single leaves were measured, a 1.15 s heat pulse was applied onto the leaves with approximately half of the maximum power. In the greenhouse, where a whole barley-canopy was measured, a heat pulse of 3.3 s duration with the maximum available power was applied onto the canopy.

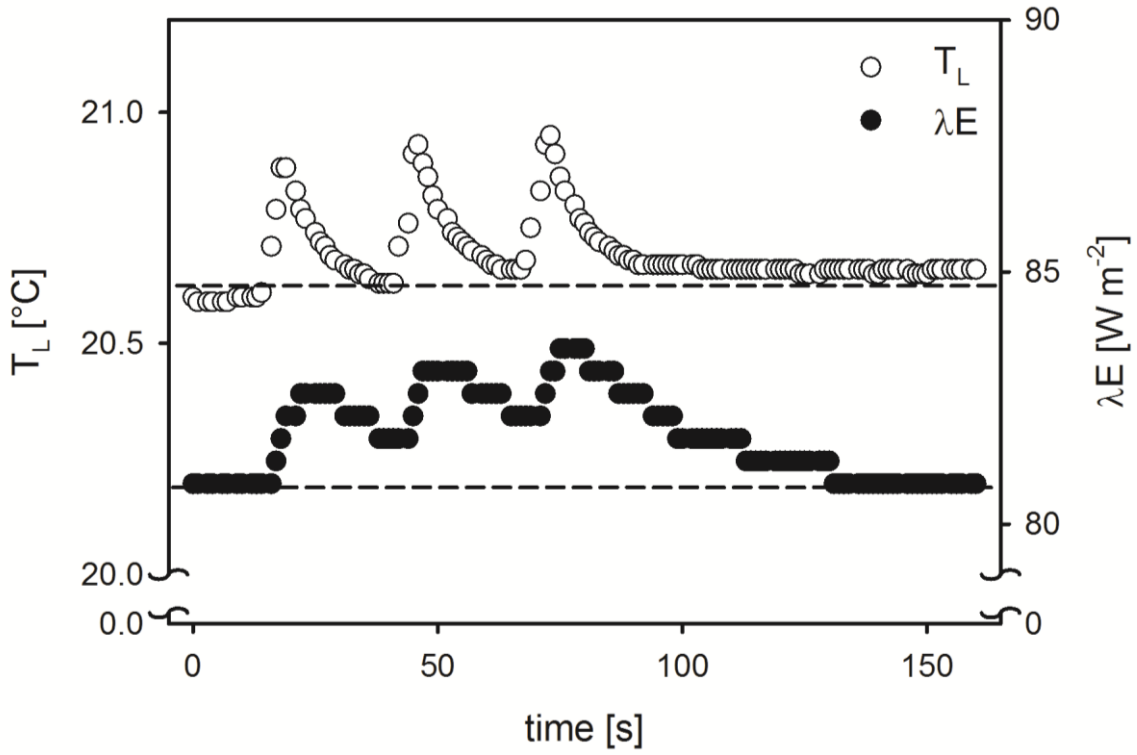

Figure 3.3.1: Effect of repeated heat pulses on leaf temperature (T_L) and transpiration (λE). Tests were performed with barley leaves using the Licor-6400 gas exchange device. Three consecutive heat pulses were applied onto the leaf in order to test whether T_L (open symbols) and λE (transpiration) are affected by successive pulses. For the measurements a single-pulse protocol was used.

3.3.2 Active thermography data processing and analysis

Measured cooling curves were evaluated using two procedures. In a first procedure, the mean T_L values were used, which were obtained by defining an area of interest within the IRBIS® 3 software, which covered the whole leaf. The software automatically integrates all temperature pixels and provides the mean T_L value. Measured cooling curves were then fitted with Equation 2.2.31 to obtain τ from the fitting, using the Origin 8.5 software (OriginLab, USA).

In a second procedure, τ was spatially mapped by calculating τ for each single pixel in the image. For this purpose, an automated analysis routine for the MATLAB Environment was developed. A typical data set consists of *n* images, containing a data matrix with the temperatures T^t at the measured time *t*. The fitting function $T_L(t)_{ij} = T_L(t_\infty)_{ij} - dT_{L_{ij}} e^{-(t\,\tau^{-1})}$ was

computed for each pixel at the position *ij* and is in the form of Equation 2.2.31. The optimization of the curve fitting was done by minimizing the sum of squared residuals using the downhill simplex approach (Nelder and Mead, 1965).

A graphical user interface (GUI) supports the processing of a single image series, or of several image series. The required input data are an Excel-file containing the time points of each recorded image and the corresponding images as a text files (ASCII), which were exported from the IRBIS® 3 software before. For the data import of several image series, a list (Excel-file) referring to the respective file path is required. Images and time data, which are located in the respective file-path, are then automatically loaded. Additionally, the GUI provides functions for post-processing of τ-matrices. Minimum- and maximum-thresholds for τ-values can be used, which generally were set between 0 s and 250 s. Additionally, the r-value of the exponential regression can be used as a further filter-parameter, which was set to r = 0.9487, corresponding to a r^2-value of 0.9. Resulting filtered τ-matrices as well as non-filtered τ-matrices are provided as Excel-tables for further manual post-processing. The thresholds used in the post-processing procedure may result in empty pixels on the imaged leaf, which were filled by using the median-value of the surrounding pixels.

3.4 Experimental set-up

3.4.1 Laboratory set-up

In laboratory experiments, the whole set-up was mounted on a metal profile construction (Fig. 3.4.1). The VarioCAM ® hr head and two NIR-heaters were mounted on a metal profile, which was mounted cross-wise to the upper horizontal bar of the overall construction. While the camera pointed in a 90° angle to the ground, the NIR-heaters were orientated approximately at a 45° angle to the ground (Fig. 3.4.1). The distances of the camera and the heaters to the ground were about the same, i.e., one meter. Additionally, two SL 3500-W-G LED panels (Photon System Instruments, Czech Republic) were installed at the horizontal metal profile in a 45° angle to the ground. At one side, a ventilator, capable to produce wind speeds between 0.2 and 1.6 m s^{-1}, was installed at a vertical metal profile. Wind speeds were measured by a VT 110 thermo-anemometer with hotwire (KIMO Instruments, France). Leaves were fixed by lab-stand clamps horizontally to the ground, providing a 90° angle the camera's FOV (Fig. 3.4.2). T_a was measured with a thermo-couple, which was attached to the lab stand and protected against radiation with aluminum foil. To correct T_a according to Chapter 3.1.1 the reference box was placed in the camera's FOV. Both thermo-couples, the thermo-couple measuring T_a and the one

within the reference box, were connected to a HH506RA data logger (Newport Omega, Germany) which recorded the temperatures every second.

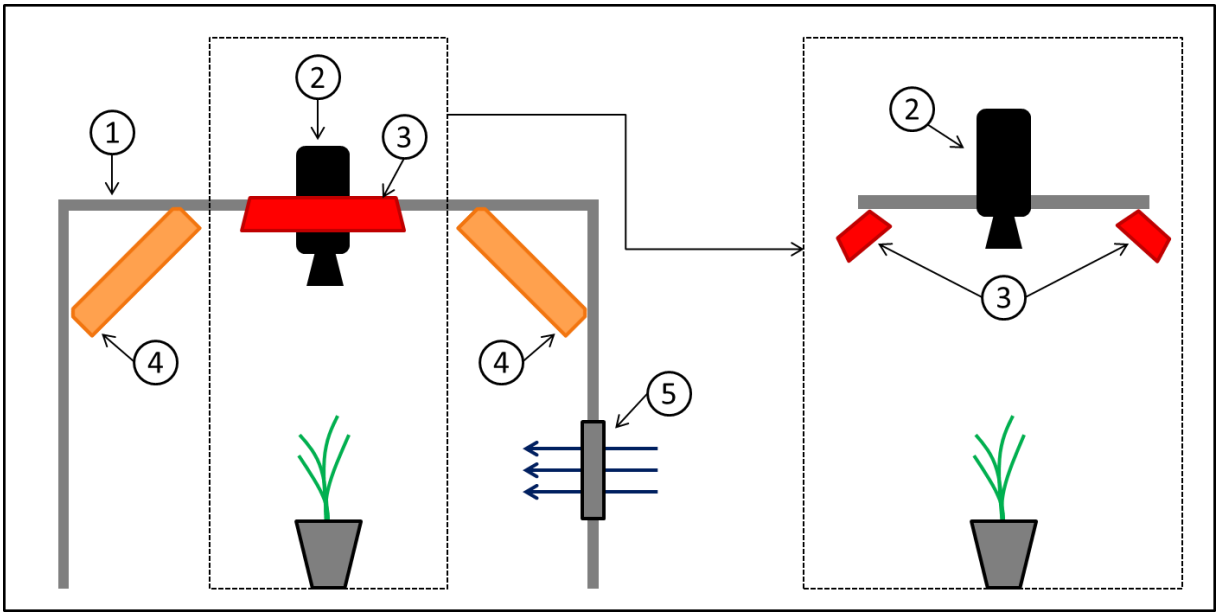

Figure 3.4.1: Schematic illustration of laboratory set-up. The whole set-up was mounted on a metal profile construction (1). Thermal camera (2) and two near-infrared (NIR) heaters (3) were fixed at the upper horizontal bar. Additionally, two LED panels (4) were fixed in the edges of the overall construction. At one side a ventilator (5) was installed. The left scheme shows the front view and the right scheme a section of the side view, showing both NIR-heaters and the thermal camera.

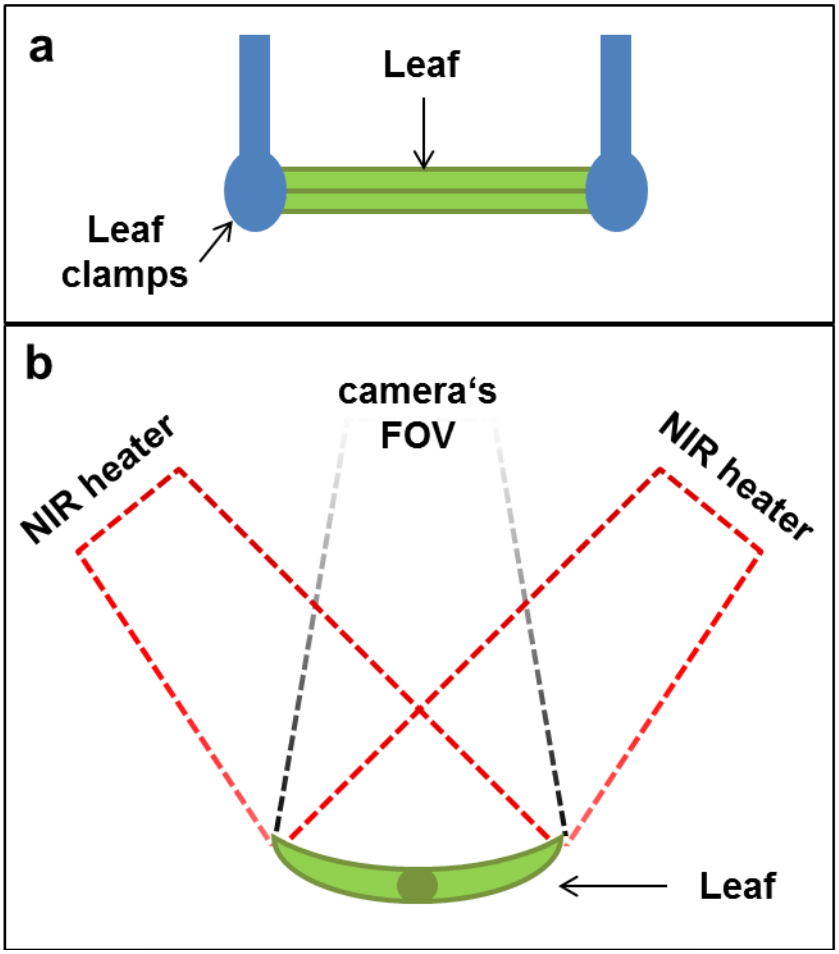

Figure 3.4.2: Schematic illustration of leaf position in relation to the camera and the near-infrared (NIR) heaters. **(a)** Leaf clamps fixed the leaves in a horizontal orientation. **(b)** Leaf to thermal camera's field of view (FOV) angle was 90°, and the leaf to heater angle was about 45°.

3.4.3 Greenhouse set-up

In contrast to the laboratory experiments, whole barley canopies were measured in the greenhouse, which required a modified set-up. Because there were frequently occurring air drafts in the greenhouse that disturbed the measurements, the set-up was installed in an open-top-chamber-like construction. A construction scaffold was covered from four sides with transparent foil. Metal profiles were attached to the scaffold, providing an angular mounting for the thermal camera and two NIR-heaters (Fig. 3.4.3). The camera was approximately at a 45° angle orientated to the canopy so that the angle to the single leaves was about 90°. One heater was installed above the canopy and the second one was installed facing the canopy more from the side. Next to the plant boxes a lab-stand was placed, to which the wet-reference body, the T_a reference construction, and a thermo-couple measuring T_a was attached. For each measurement, a cross with crumbled aluminum-foil was placed into the plant boxes to measure T_{bg}.

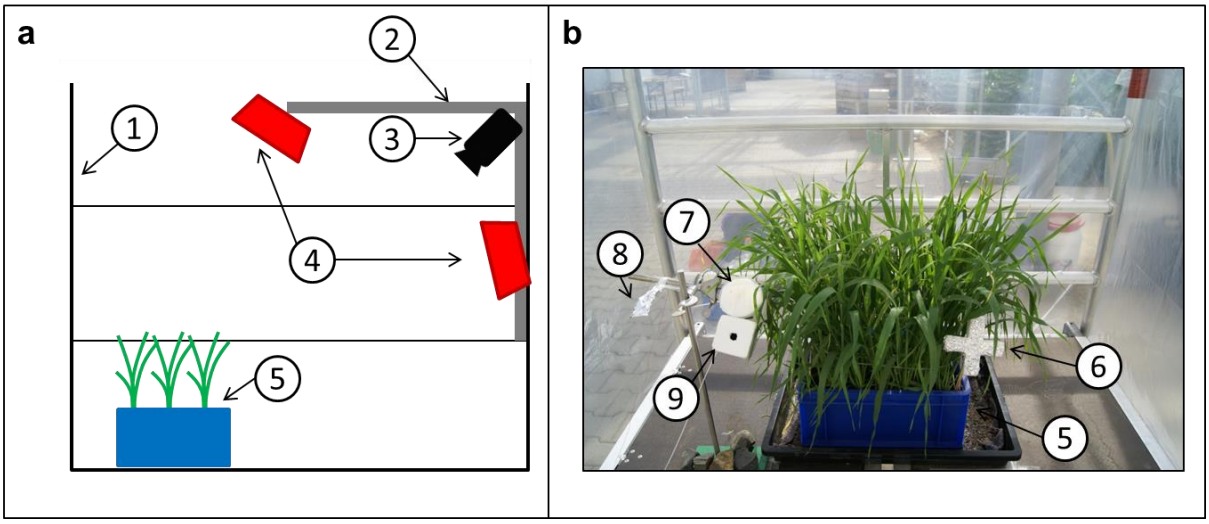

Figure 3.4.3: Schematic illustration of greenhouse set-up. **(a)** measurements took place in an open-top-chamber-like construction (1). For this all four sides of a construction scaffold were covered with transparent foil. To the scaffold a metal profile construction (2) was attached, which was the holding for the thermal camera (3) and two near-infrared (NIR) heaters (4). The camera was in a 45° angle to the barley canopy box (5). One NIR-heater was installed at the horizontal metal profile above the canopy. The second NIR-heater was installed at the vertical metal profile, providing heat from the side. **(b)** Barley canopy (5) in the camera's field of view. To measure background temperature a cross covered with crumbled aluminum foil (6) was placed in the boxes. On a lab-stand, the wet-reference (7), a thermo-couple, protected with aluminum foil (8), and the reference construction for ambient air temperature correction (9) was mounted.

3.5 Leaf gas exchange measurements

To measure dynamic changes in C A^{-1}_{leaf} in response to leaf dehydration due to water loss by transpiration, C A^{-1}_{leaf}, h_{leaf}, and stomatal conductance (g_s) was quantified using the Licor-6400 gas exchange device (LI-COR Biosciences, USA). The Licor-6400 is an open system, measuring photosynthesis and transpiration by differences of H_2O and CO_2 in an air stream, which is flowing through a leaf cuvette. Part of a leaf is enclosed in a cuvette, where air flows through, that has a defined amount of CO_2 and H_2O. In parallel, the air flows through a reference chamber. Both air streams are measured by an infrared gas analyzer (IRGA). The difference in the gas concentration between both chambers, provide the leaf's consumption or release of the respective gas. Because, measurements take less than one minute, the Licor-6400 can be used to measure actual g_s, assuming that stomata do not react within seconds to changed ambient conditions.

In contrast to leaves, which are exposed to laboratory conditions, where no recognizable wind occurs, leaves within a leaf cuvette are exposed to a permanent air stream. This air stream removes nearly the whole boundary layer of a leaf, so that boundary layer conductance is very high. Because, the air flow velocity is kept constant, boundary layer conductance remains stable throughout the measurements.

In order to observe dynamic changes in $C\ A^{-1}_{leaf}$ due to light exposure, the gas exchange measurements were integrated in the laboratory set-up, providing a combined approach of gas exchange measurements and active thermometry, where thermometry refers to single point T_L measurements with the integrated thermo-couple. The Licor-6400 was equipped with a clear topside leaf cuvette, allowing the application of heat pulses with the NIR heaters onto the leaves within the leaf cuvette.

The gas exchange system automatically calculates transpiration rate in mmol $m^{-2}\ s^{-1}$, g_s in mol $m^{-2}\ s^{-1}$, and the total boundary layer conductance to water vapor (g_W) in mmol $m^{-2}\ s^{-1}$ from the measured differences in the gas concentration. Detailed information on the used equations can be found in von Caemmerer and Farquhar (1981). For appropriate calculations of the respective parameters, the system requires a parameter describing the enclosed area of the leaf, where the maximum area is 6 cm^2 which is the area of the gas exchange cuvette, and a parameter describing the stomatal distribution on the two leaf surfaces, where 1 refers to amphistomatous leaves such as barley leaves, and 0 refers to hypostomatous leaves such as bean leaves. For conversion, conductance was multiplied by $m^3\ mol^{-1}$ (0.024 at 20°C) to obtain units of m s^{-1} (Monteith and Unsworth, 2008)

4. Leaf water content and leaf water content dynamics in response to water loss through transpiration

4.1 Background and scope of the experiment

The time constant (τ), obtained from leaf cooling kinetics measured with active thermography, is proportional to both leaf heat capacity per unit area ($C\ A^{-1}_{leaf}$) and the leaf heat transfer coefficient (h_{leaf}) (Equation 2.2.32). Because water has a very high specific heat capacity in comparison to other leaf tissue components, $C\ A^{-1}_{leaf}$ depends mainly on leaf water content per unit area (LWC) (Jones, 1992; Monteith and Unsworth, 2008). Therefore, τ is presumably directly proportional to LWC which makes the active thermography to an interesting approach for non-invasive LWC estimations. In the following experiments the active thermography was tested at the leaf scale under semi-controlled conditions in the laboratory and under strictly controlled conditions using a Licor-6400 gas exchange device, where the leaf is enclosed in a gas exchange cuvette. Additionally, the robustness of τ as an approximation of LWC was tested by actively manipulating h_{leaf} and affecting the convective heat transfer coefficient (h_H) with varying wind speed, and by affecting the heat transfer coefficient for transpiration ($h_{\lambda E}$) with varying light intensity. The main goal of this experiment was to establish τ, measured with the active thermography protocol, as a valuable parameter reflecting leaf water content and in particular dehydration due to water loss by transpiration.

4.2 Material and Methods

4.2.1 Plant material

All plants were grown in the greenhouse facilities at IBG-2, Forschungszentrum Jülich. For these experiments spring barley (*Hordeum vulgare*, variety Victoriana) and a common bean (*Phaseolus vulgaris*, variety fadenlose Shiny) were grown. Barley plants were germinated in 12 x 12 x15 cm pots and bean plants in 15 x 15 x 18 cm pots. Pots were filled with a potting substrate, enriched with 1 g L^{-1} NPK fertilizer and with 2 g L^{-1} of a long-time acting fertilizer (Einheitserde Typ ED73). Pots were placed on water-retentive cloths, which were kept moist constantly.

For gas exchange measurements only barley plants were used and the experiment was performed during the winter of 2013. Plants used for these experiments were grown in a day to night cycle of 16 hours with air humidity around 55% ± 10%. On cloudy days the maximum measured photosynthetic photon flux density (PPFD) in the greenhouse was 85 µmol $m^{-2}\ s^{-1}$ and air temperature (T_a) ranged between 20 °C at night and 24 °C during the day. On sunny days,

light intensities reached on maximum 372 µmol m^{-2} s^{-1}, with maximum T_a up to 31 °C during the day.

Experiments with barley and bean plants were repeated in the spring of 2015. Plants grew in a day to night cycle of 16 hours with air humidity around 55% ± 13%. The mean temperature was 21 °C, and the highest measured temperature during this period was 31 °C, whereas the minimum temperature was 17 °C. On sunny days, light intensities in the greenhouse reached at maximum 1335 µmol m^{-2} s^{-1}, while the minimum illumination was around 85 µmol m^{-2} s^{-1}. For the measurements, bean plants were about 2 weeks old and barley plants were about 6 weeks old. In all experiments, plants were moved from the greenhouse into the laboratory where they were dark-adapted over night for at least 14 hours before measurements.

4.2.2 Leaf water content measurements

For all non-invasive measurements, the active thermography protocol and setup was used as described in the methodology part (see Chapter 3.3 and 3.4). Leaves of different size were chosen to obtain a wide range in LWC by natural differences. While for the measurements with barley leaves of different stages and positions were chosen, measurements with bean were performed on the first pair of leaves. Single leaves were measured under three different ambient conditions. While T_a and air humidity were not changed, the leaves were exposed to varying wind speeds. The relationship between τ and LWC was assessed at wind speeds of 0, 0.5, and 1.0 m s^{-1}, respectively. After leaves were measured by the active thermography approach, they were harvested and analyzed for leaf area and fresh weight. For dry weight determination harvested leaves were dried in an oven at 80°C for 48 hours until reaching a constant weight. Data were used to calculate the LWC.

4.2.3 Gas exchange measurements

Gas exchange measurements were performed with the Licor-6400 (LI-COR Biosciences, USA) in a combined mode of gas exchange measurements and active thermometry as described in the methodology section (Chapter 3.5). The measurements were integrated into the laboratory setup (Chapter 3.4). A part of the measured leaf was enclosed in the leaf cuvette whereas the remaining part outside the cuvette was measured with the active thermography approach. In order to observe de-and rehydration of barley leaves, the leaves were exposed to light at increasing intensities of 0, 50, 100, 200, 400, 600, and 800 µmol m^{-2} s^{-1} and were allowed to adapt to the new ambient conditions within the leaf cuvette for 30 to 40 minutes before applying the next heat pulses. During this time, leaf temperature (T_L) and stomatal conductance (g_s) stabilized

and reached steady state values. After the light phase, leaves were exposed to a dark phase during which leaves reached a maximum hydration. During the dark phase, heat pulses were applied approximately every 20 minutes until g_s reached minimum values. Because stomatal closure occurs at different speeds for different leaves, the number of measurements during the dark phase differed among the measured leaves. The gas exchange parameters were continuously recorded every second during the measurement, including T_L, T_a, g_s, and boundary layer conductance (g_{bl}), required to calculate the heat transfer coefficients (h). The total leaf h (h_{leaf}) as the sum of h for long wave radiative heat (h_{LW}), h for convective heat (h_H), and h for transpirative heat ($h_{\lambda E}$) was calculated according to Equations 2.2.29 (see Chapter 2.2.6). With the calculated h_{leaf} and the measured τ, the specific heat capacity per unit area of the leaves ($C\ A^{-1}_{leaf}$) was calculated.

4.2.4 Data processing and analyses

Measured cooling curves were recorded and fitted according to Equation 2.2.31 to obtain τ from the fitting using the Origin 8.5 software (OriginLab, USA) or, for τ images the automated MATLAB tool was used. Statistical analyses included analyses of variance (ANOVA) and Pearson correlation analyses, both performed using SigmaPlot (Systat Softwarer Inc., USA).

4.3 Results

In order to test the relationship between τ obtained by active thermography and LWC, dark-adapted leaves of spring barley and common bean were measured at different wind speeds. Strong correlations between τ and LWC for both, barley and bean at different wind speeds was found (Fig. 4.3.1). With increasing wind speeds the differences between τ became smaller despite comparable differences in LWC. Therefore, linear regressions of the relationship between τ and LWC, generally, revealed the steepest slope at wind speeds of 1.0 m $s^{-1}$and slopes decreased with decreasing wind speeds. For barley, the strongest correlation was observed in conditions where wind was absent ($p < 0.001$) and the weakest correlation in conditions with a wind speed of 1.0 m s^{-1} ($p < 0.05$) (Fig. 4.3.1a). In contrast, for bean the strongest correlation between τ and LWC was found under conditions with 1.0 m s^{-1} wind ($p < 0.01$) and the weakest correlation under conditions with 0.5 m s^{-1} wind ($p < 0.05$) (Fig. 4.3.1b). In all cases, correlations between τ and LWC were significant for both barley and bean in all conditions ($p < 0.05$).

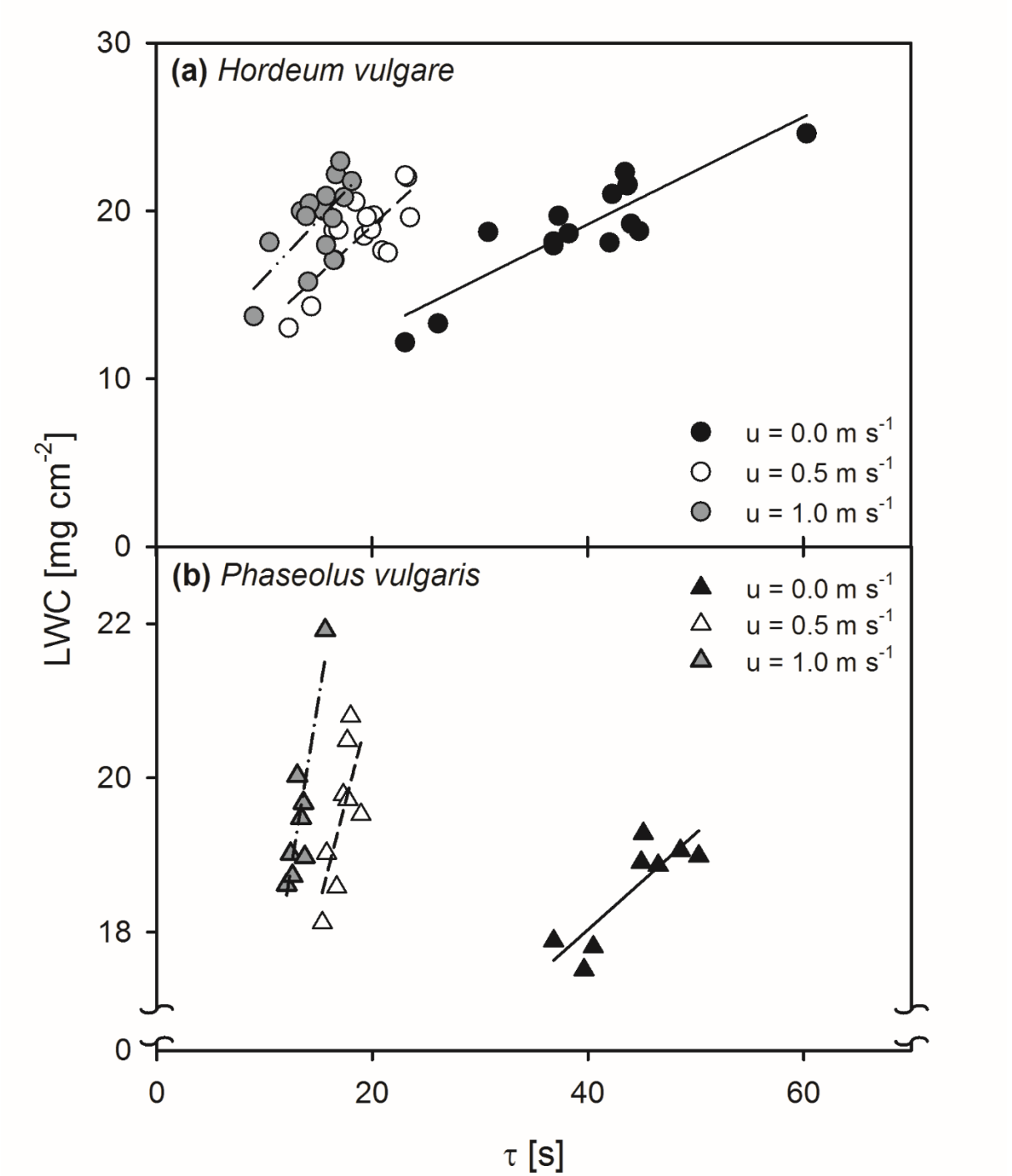

Figure 4.3.1: Relationship between leaf water content per unit area (LWC) and time constant (τ) of dark-adapted leaves. Relationships were assessed at different wind speeds of 0.0 m s^{-1} (closed symbols), 0.5 m s^{-1} (open symbols), and 1.0 m s^{-1} (grey symbols). **(a)** Measurement of single spring barley (*Hordeum vulgare*) leaves. Linear regression for measurements at a wind speed of 0.0 m s^{-1} (solid line): $y = 0.32x + 6.40$, $r^2 = 0.79$, $p < 0.001$, for measurements at wind speeds of 0.5 m s^{-1} (dashed line): $y = 0.59x + 7.29$, $r^2 = 0.63$, $p < 0.001$, and for measurements at wind speeds of 1.0 m s^{-1} (dash-dot-dotted line): $y = 0.68x + 9.18$, $r^2 = 0.48$, $p < 0.05$. **(b)** Measurements of single common bean (*Phaseolus vulgaris*) leaves. Linear regression for measurements at a wind speed of 0.0 m s^{-1} (solid line): $y = 0.12x + 13.04$, $r^2 = 0.72$, $p<0.01$, for measurements at wind speeds of 0.5 m s^{-1} (dashed line): $y = 0.54x + 10.17$, $r^2 = 0.51$, $p < 0.05$, and for measurements at wind speeds of 1.0 m s^{-1} (dash-dot-dotted line): $y = 0.86x + 8.14$, $r^2 = 0.79$, $p < 0.01$. Each point represents an individual leaf that was measured by the active thermography approach and afterwards destructively analyzed for LWC.

By spatially mapping τ and LWC values, obtained from the relationship above, it was possible to attribute pixels to leaf anatomical structures associated with LWC and thus C A^{-1}_{leaf}, such as the leaf veins (Fig. 4.3.2). The given examples show a barley leaf measured at a wind speed of 0.0 m s^{-1}, and a bean leaf measured at a wind speed of 1.0 m s^{-1}. For both plant species, the highest τ values were associated with the mid-veins and decreased from the leaf base to leaf tip, whereas interveinal areas had much lower τ-values and LWC values. For the barley leaf, minor veins were not visible (Fig. 4.3.2a) in contrast to the bean leaf, where minor veins were clearly visible (Fig. 4.3.2b). Moving away from the mid-vein, τ and LWC values decreased towards leaf edges. The median value of the integrated LWC pixels in the barley leaf image was 18.3 (±6.2) mg cm^{-2}, which was similar compared to the actually measured LWC of 18.7 mg cm^{-2}. For the bean leaf, the median of the integrated LWC value was 19.8 (±12.0) mg cm^{-2} whereas the measured value was 17.8 mg cm^{-2}.
Gradients of τ, which could be observed in the spatial maps, were illustrated by transverse sections of the mid-vein and the leaf lamina (see dotted lines in Fig. 4.3.2). Transverse sections showed that τ decreased form the leaf base to leaf tip along the mid-vein (Fig. 4.3.3a and c) and from the mid-vein to the leaf margins (Fig. 4.3.3b and d). For bean leaves, the minor-veins were associated with higher τ values compared to other regions of the leaf lamina and could be observed also in the leaf transverse section (Fig. 4.3.3d).

Leaf dehydration in response to water loss by transpiration was measured with the active thermography and compared to gas exchange measurements. τ values showed comparable pattern between active thermography and gas exchange measurements, while the T_L-T_a measurements showed distinct patterns (Fig. 4.3.4). Namely, for thermographic measurements a permanent decrease in T_L-T_a was observed (Fig. 4.3.4a), whereas T_L-T_a measured by the gas exchange device initially decreased and, when light intensity of 200 µmol m^{-2} s^{-1} and above were reached, it increased to values above zero (Fig. 4.3.4a). During the recovery phase in the dark (Fig. 4.3.4b), thermographically measured T_L-T_a reached values near zero already after about 20 minutes and remained relatively stable throughout the measurements. In contrast, T_L-T_a measured by gas exchange tended towards zero, but showed a high variability among the individual leaves as indicated by the comparatively high standard deviations.

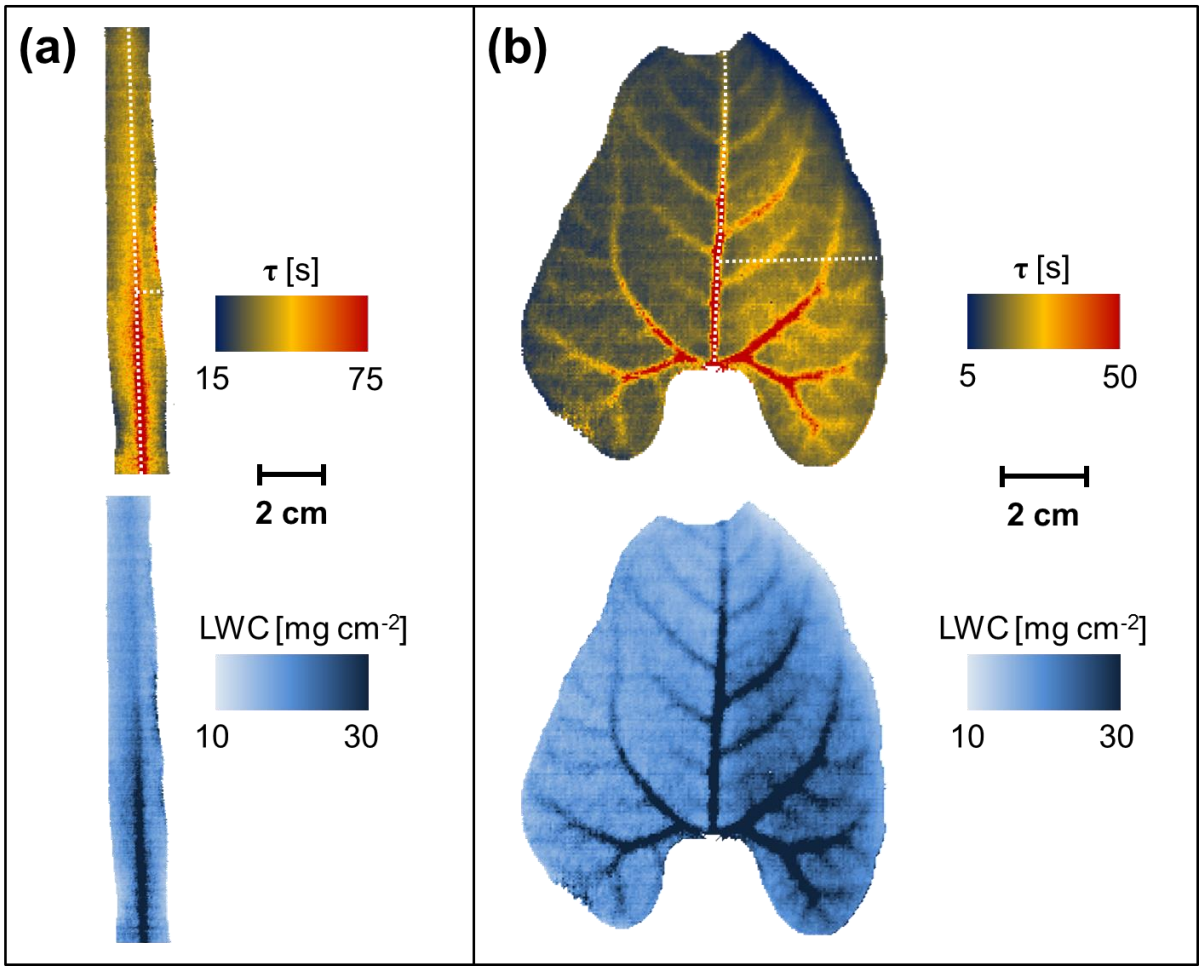

Figure 4.3.2: Spatial map of time constant (τ) and leaf water content per unit area (LWC). **(a)** Spring barley (*Hordeum vulgare*) leaf measured in absence of wind (0.0 m s^{-1}). τ range between 15 and 75 s as indicated by colored scale, blue color indicates low τ-values and red color indicates high τ-values. LWC values range between 10 and 30 mg cm^{-2} as indicated by blue-gradient scale, light-blue represents low LWC and dark-blue indicates high LWC. **(b)** Young primary leaf of common bean (*Phaseolus vulgaris*) measured at wind speeds of 1.0 m s^{-1}. τ range between 5 and 50 s as indicated by colored scale, blue color indicates low τ-values and red color indicates high τ-values. LWC values range between 10 and 30 mg cm^{-2} as indicated by blue-gradient scale, light-blue represents low LWC and dark-blue indicates high LWC. Dotted lines on the leaf mid-vein and across the leaf lamina represent leaf transverse sections presented in Figure 4.3.3.

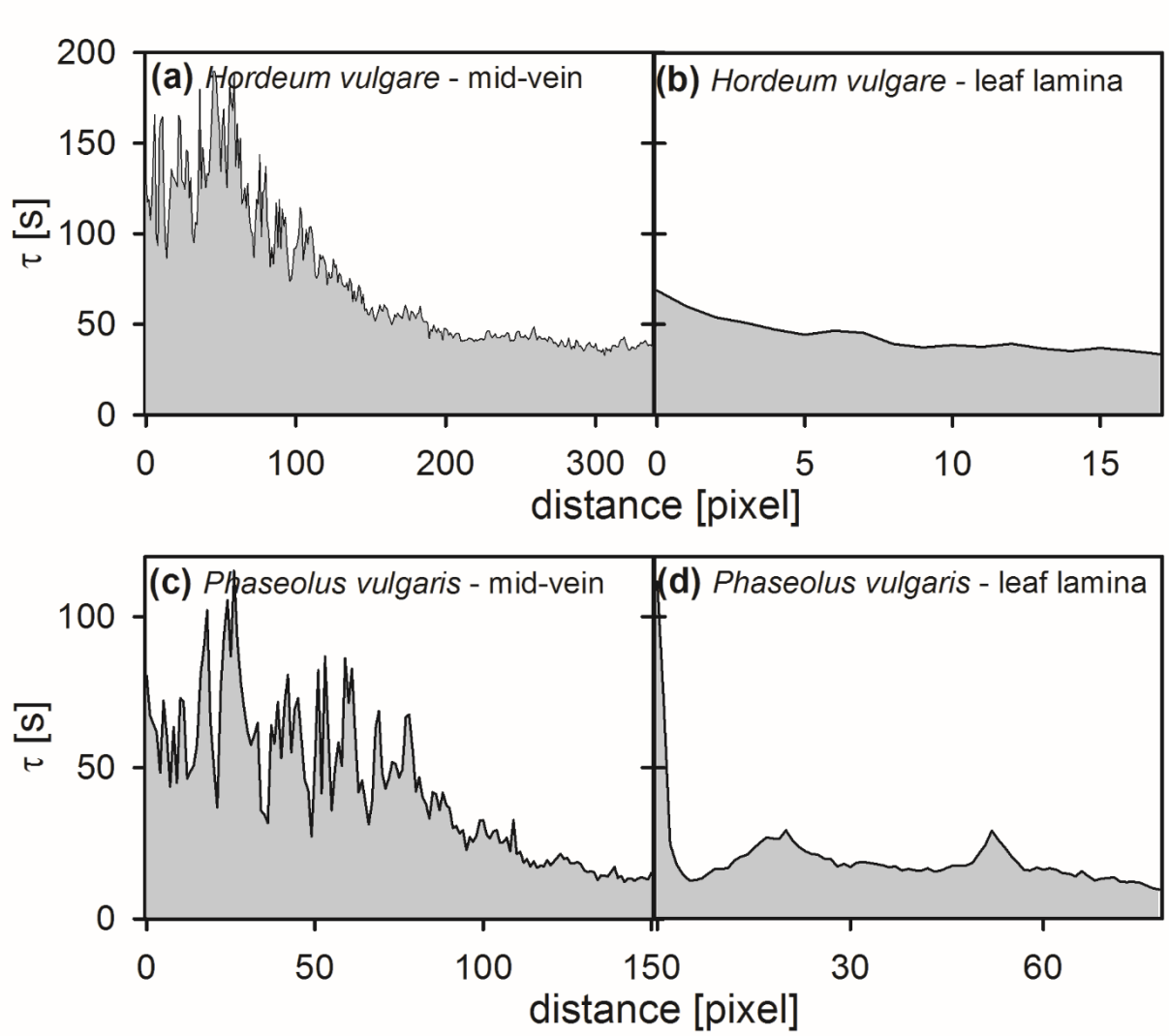

Figure 4.3.3: Time constant (τ) gradients along the mid-vein and across the leaf lamina. Transverse sections refer to dotted lines in Figure 4.3.2. **(a)** τ-gradient along the mid-vein of a spring barley (*Hordeum vulgare*) leaf. **(b)** τ-gradient across the leaf lamina of a barley leaf. **(c)** τ-gradient along the mid-vein of a common bean (*Phaseolus vulgaris*) leaf. **(d)** τ-gradient across the leaf lamina of a bean leaf.

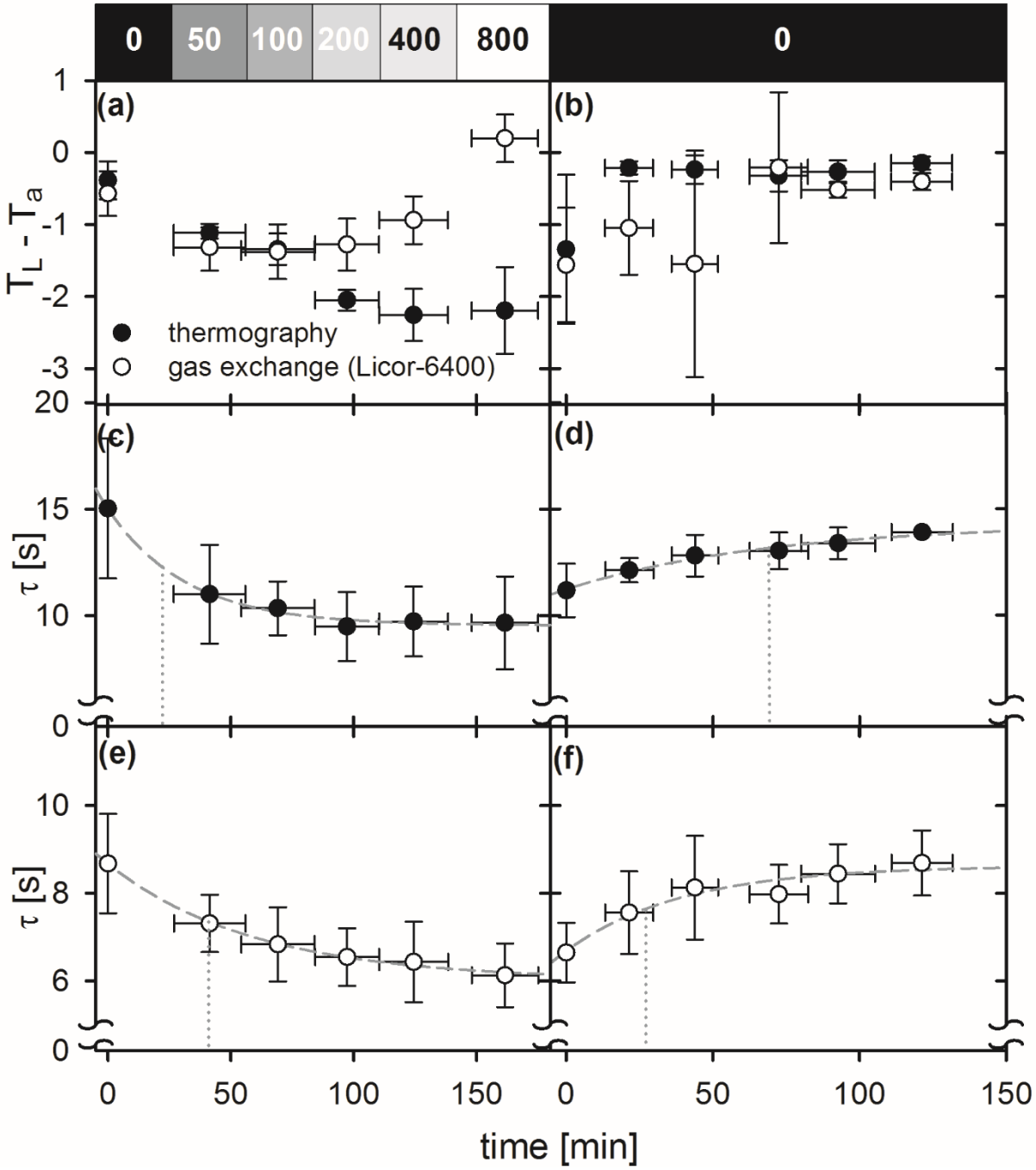

Figure 4.3.4: Comparison between active thermography and temperature measurements within a gas exchange cuvette on in spring barley (*Hordeum vulgare*) leaves. Data obtained by active thermography shown by closed circles and data obtained with the Licor-6400 gas exchange device are indicated by open circles. Measurements were performed at stepwise increases in light intensity from 0 to 800 µmol m^{-2} s^{-1}. Light intensities are given by a gray-intensity scale at the top of the graphs panels. **(a)** Measurements of the difference between leaf temperature (T_L) and ambient air temperature (T_a), T_L-T_a, in response to increasing light intensity. **(b)** T_L-T_a during re-darkening of leaves. **(c)** Time constant (τ) obtained by active thermography in response to increasing light. Exponential regression (gray dashed line): $f(x) = 9.54 + 5.49\ e^{-(x/31.74)}$, $r^2 = 0.99$ **(d)** τ obtained by active thermography in response to re-darkening. Exponential regression (gray dashed line): $f(x) = 14.30 - 3.08\ e^{-(x/69.92)}$, $r^2 = 0.97$ **(e)** τ obtained by the thermocouple of gas exchange system in response to increasing light. Exponential regression (grey dashed line): $f(x) = 6.02 + 2.65\ e^{-(x/59.27)}$, $r^2 = 0.99$ **(f)** τ obtained by gas exchange measurements in response to re-darkening. Exponential regression (gray dashed line): $f(x) = 8.63 - 1.94\ e^{-(t/27.59)}$, $r^2 = 0.90$. The solid lines indicate the time required to reach 50% of the overall decay ($t_{50\%}$) of the respective exponential function. Each point represents mean value of n=6 individual leaves. Error bars represent standard deviations of the mean.

The measured τ exponentially decreased in response to a step-wise increase in light intensity and increased to nearly initial values in the dark, for both thermographic measurements and temperature measurements in the gas exchange cuvette (Fig. 4.3.4c-f). Values obtained by active thermography were significantly higher compared to the values measured with the thermocouple integrated in the gas exchange system ($p < 0.001$). The τ dynamics obtained by active thermography were compared to τ dynamics measured within the gas exchange cuvette. For this purpose, the obtained data were exponentially fitted and the time which is required to reach 50% of the overall decay ($t_{50\%}$) was determined. For active thermography measurements under increasing light intensity, a $t_{50\%}$ of about 22 (± 3) min was observed for the τ decrease, which reveals a decrease rate twice as fast as observed with gas exchange measurements, where $t_{50\%}$ was around 41 (± 4) min (Fig. 4.3.4c and e). In contrast, the τ increase observed after exposure to darkness by active thermography was much slower ($t_{50\%}$ = 70 (±26) min) compared to the increase observed by gas exchange measurements ($t_{50\%}$ = 28 (±13) min) (Fig. 4.3.4d and f).

The heat transfer coefficient (h) was calculated for the respective heat flux densities and finally $C\ A^{-1}_{leaf}$ was calculated to quantify the impact of the respective h on τ (Fig. 4.3.5). In response to stepwise increasing light intensity h_{leaf} increased slightly from 85.0 W m^{-2} K^{-1} to 91.2 W m^{-2} K^{-1} at 800 µmol m^{-2} s^{-1}, and decreased after re-darkening towards 85.5 W m^{-2} K^{-1} (Fig. 4.3.5b). The changes in h_{leaf} were not significant ($p > 0.05$). h_H and h for long-wave radiative heat (h_{LW}) remained relatively constant around 79.1 (± 1.1) W m^{-2} K^{-1} and 5.7 W m^{-2} K^{-1}, respectively. In contrast, $h_{\lambda E}$ significantly changed ($p < 0.001$). During light exposure $h_{\lambda E}$ increased on average from 0.7 W m^{-2} K^{-1} to a maximum of 7.0 W m^{-2} K^{-1}, and decreased again in response to darkness towards a mean value of 0.2 W m^{-2} K^{-1} (Fig. 4.3.5b). The maximum contribution of $h_{\lambda E}$ was about 7.7%, which were reached at highest light intensities of 800 µmol m^{-2} s^{-1}.

According to Equation 2.2.32, $C\ A^{-1}_{leaf}$ was calculated as the product of the measured τ and the calculated h_{leaf}^{-1} (Fig. 4.3.5c). As τ changed significantly during light illumination and re-darkening ($p < 0.001$), $C\ A^{-1}_{leaf}$ also changed significantly ($p < 0.001$). In response to light illumination $C\ A^{-1}_{leaf}$ decreased from 738 (±118) J m^{-2} K^{-1} to 560 (± 80) J m^{-2} K^{-1} at 800 µmol m^{-2} s^{-1} and increased in response to exposure to darkness to a mean value of 745 (±104) J m^{-2} K^{-1}, which was slightly higher compared to the initial value, but was not significantly different ($p > 0.05$).

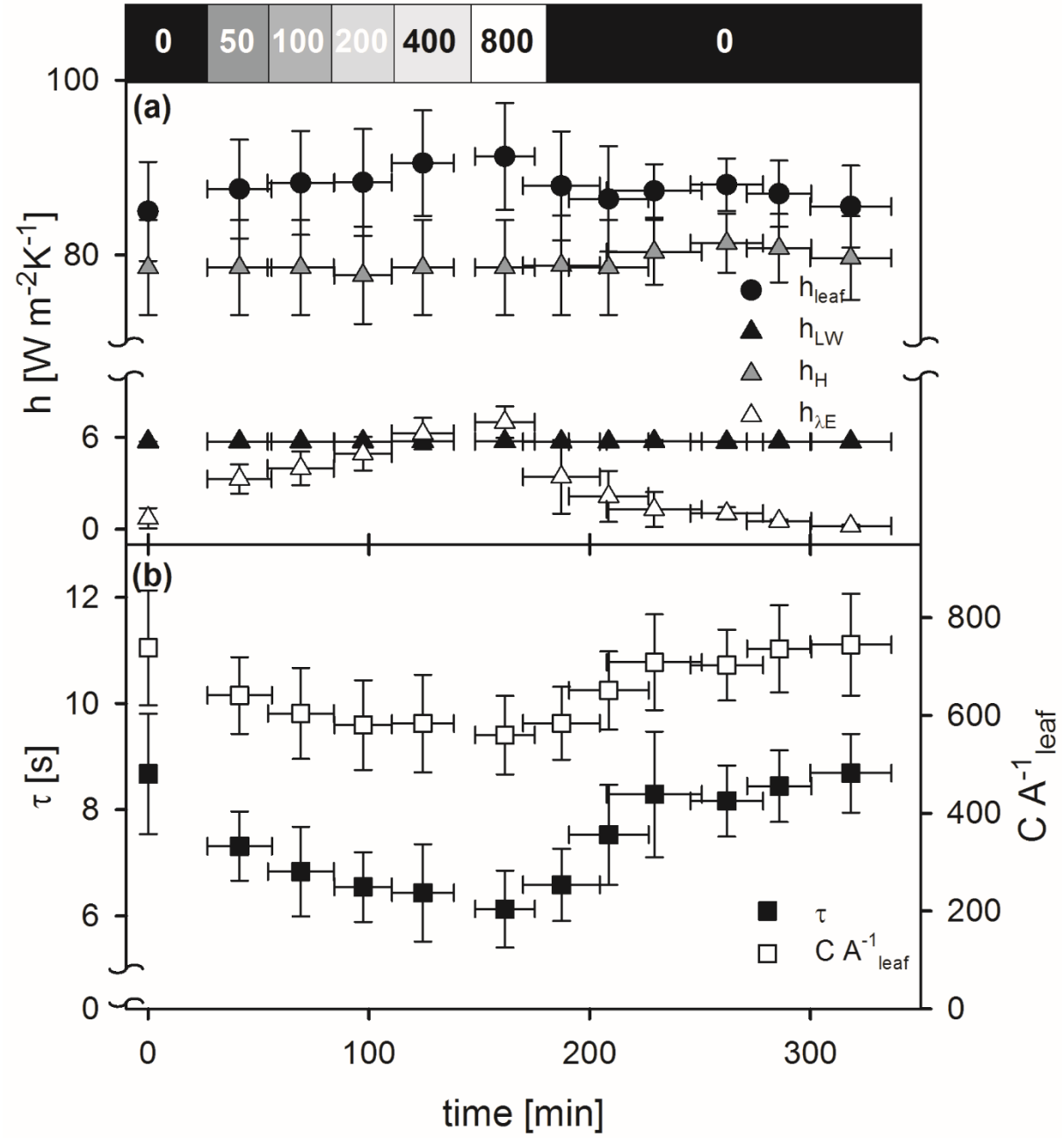

Figure 4.3.5: Light induced changes in heat dissipation parameters of spring barley (*Hordeum vulgare*) leaves in a gas exchange cuvette. Measurements were performed at stepwise increasing light intensity from 0 to 800 µmol m^{-2} s^{-1}. Light intensities are given by gray-intensity scale at the top of the graphs panels. **(a)** Dynamics in heat transfer coefficients (h). Total leaf h (h_{leaf}) shown by closed circles, h for long-wave radiation (h_{LW}) shown by closed triangles, h for convective heat (h_H) shown by grey triangles, and h for transpiration ($h_{\lambda E}$) shown by open triangles. **(b)** Time constant (τ) shown by closed squares, and specific leaf heat capacity per unit area (C A^{-1}_{leaf}), calculated with τ and h_{leaf}, given by open squares. Each measurement point represents mean value of n=6 individual leaves. Error bars represent standard deviations of the mean.

De- and rehydration processes of barley leaves were significantly correlated with transpiration rates (TR) (Fig. 4.3.6). Significant correlations between TR and τ were found ($p < 0.001$) and between TR and LWC, derived from C A^{-1}_{leaf} ($p < 0.001$). Although a general tendency of τ to decrease together with TR was found, as indicated by the correlation of the mean values, the

variation in the measurement was quite high (maximum standard deviations of about 0.73 mmol m^{-2} s^{-1} at a mean value of 1.41 mmol m^{-2} s^{-1} for TR), indicating varying responses of different leaves. However, the correlation between TR and calculated LWC illustrated that de- and rehydration of leaves respond to TR (Fig. 4.3.6b). The de- and rehydration response were divided into three phases; the initial dehydration in response to light, a transition to a steady-state phase around a light intensity of 200 µmol m^{-2} s^{-1} where values seemed to stabilize, and a rehydration phase in the dark. All phases could be interpreted by using linear regressions. These analyses indicated that the fastest rate of water loss occurred during the light period.

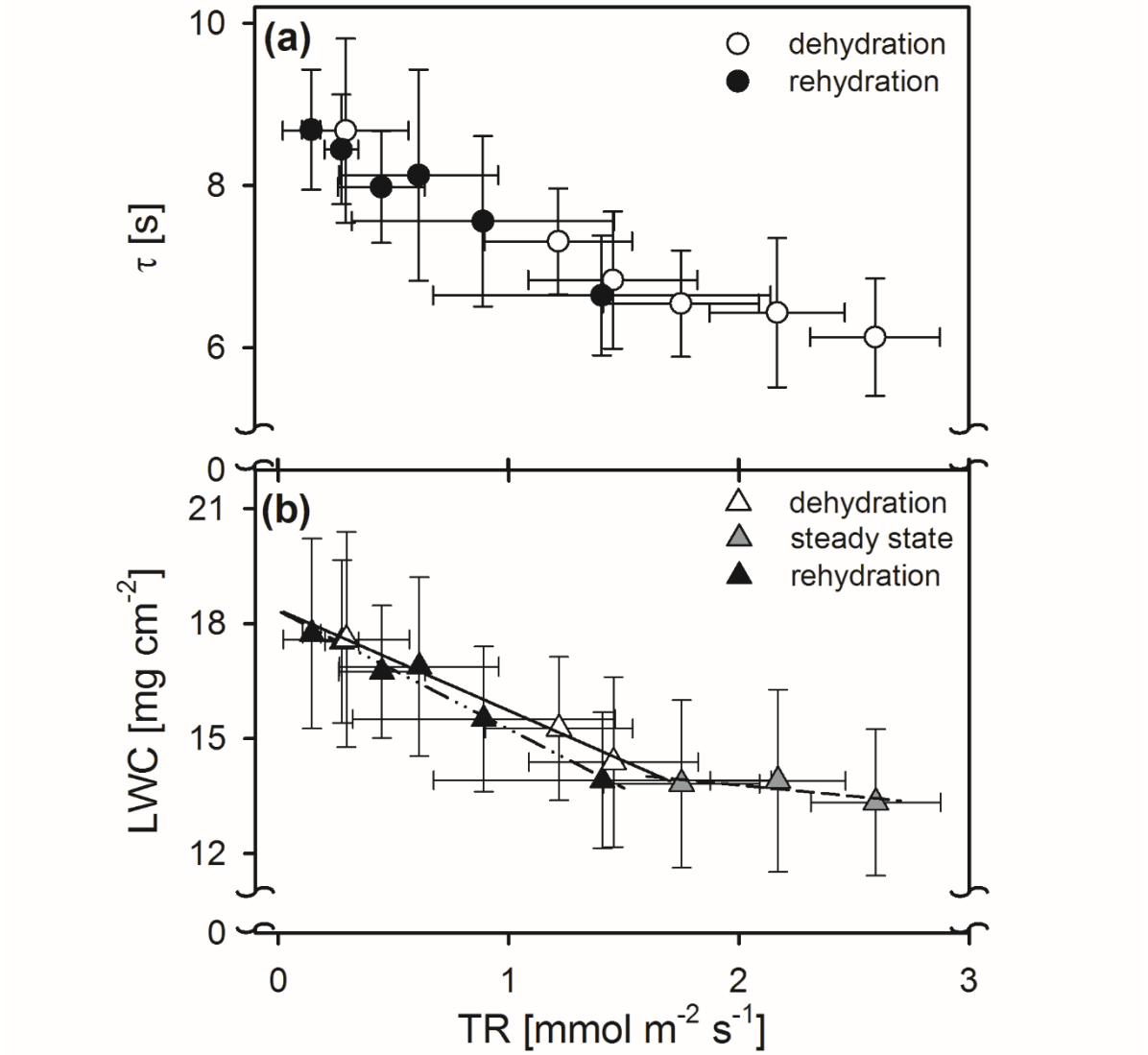

Figure 4.3.6: Leaf water loss through transpiration measured with gas exchange. **(a)** time constant (τ) in dependency of transpiration rate (TR). Dehydration phase in light indicated by open circles and rehydration in dark indicated by closed circles. **(b)** Leaf water content per unit area (LWC) in dependency of TR. Measurements are divided in three phases. Dehydration in response to illumination (open triangles) with linear regression (solid line): $y = -2.63x + 18.36$, $r^2 = 0.99$, steady state (grey triangles) with linear regression (dashed line): $y = -0.58x + 14.94$, $r^2 = 0.27$, rehydration in dark (closed triangles) with linear regression (dash-dot-dotted line): $y = -3.08x + 18.33$, $r^2 = 0.96$. Each symbol represents the mean value of n=6 individual leaves. Error bars represent standard deviations of the mean.

4.4 Discussion

In this Chapter, it was demonstrated that the active thermography approach has the potential to be used as a method to estimate LWC distribution and dynamics at the leaf scale. Irrespectively of plant species and experimental conditions, τ strongly correlates with LWC. With this approach, it was possible to spatially map τ to leaf structures, which generally have a high water content. Additionally, τ indicates dehydration and rehydration processes in response to LWC changes induced by water loss through transpiration.

According to the theory (Equation 2.2.32), τ strongly correlates with C A^{-1}_{leaf}, and thus with LWC. Additionally, the Equation 2.2.32 indicates that τ depends further on h_{leaf}. In these experiments, it was found that the relationship between τ and LWC of dark-adapted leaves changes with changing wind speeds. Increasing wind speed decreases the boundary layer thickness, which in turn increases h_{leaf}, resulting in a faster cooling and consequently lower τ (Raschke, 1960; Jones, 1992; Schuepp, 1993; Leigh *et al.*, 2012). It was observed that the slopes of the relationship between τ and LWC increases with increasing wind speed (Fig. 4.3.1), indicating that τ is more sensitive to changes in LWC in the absence of wind compared to windy conditions. However, for bean leaves, the relationship between τ and LWC was quite weak under wind-free conditions as well (Fig. 4.3.1b). Leaf area and the leaf width to leaf length ratio highly affect the leaf boundary layer and thus h_{leaf} (Dixon and Grace, 1984; Schuepp, 1993; Defraeye *et al.*, 2013). Bean leaves have a larger leaf area and also a higher leaf width to leaf length ratio compared to barley leaves, resulting in larger boundary layer thickness (Gates, 1965; Sinclair, 1970), which ultimately results in a lower h_{leaf}. Additionally, the variation in leaf area was much higher for bean leaves compared to barley leaves (standard deviation of barley leaves ± 5.49 cm², standard deviation for bean leaves ± 46 cm²), so that the measurements of bean leaves display a higher variation for boundary layers. For narrower leaves, like barley leaves, edge effects play a more important role than for wider leaves, such as bean leaves (Sinclair, 1970; Schuepp, 1993). At the leaf margins, the boundary layer is disturbed and thus heat transfer is accelerated. Because leaf edges are relatively close to each other in barley, these edge effects affect the whole leaf boundary layer structure (Gates, 1965; Sinclair, 1970; Vogel, 2009). This effect disappears as soon as leaves are exposed to wind, because wind effectively removes the boundary layer.

The relationships between τ and LWC were used to map τ and LWC spatially (Fig. 4.3.2). For both plant species, it was possible to map leaf structural properties, which are related to higher water content, such as vascular tissues (Sack and Scoffoni, 2013). Mid-veins contain more water compared to leaf lamina and thus have a higher C A^{-1}_{leaf}, resulting in higher τ-values. In

contrast to barley, which has one prominent mid-vein, visible in the images, and smaller longitudinal veins (Dannenhoffer *et al.*, 1990; Ueno *et al.*, 2006), not visible in the image, in bean leaves also minor veins could be observed by mapping τ and derived LWC (Fig. 4.3.2b). Both the first- and second- order veins narrow in diameter along their length in angiosperms (Sack and Scoffoni, 2013), which is related to an increased hydraulic capacity (McKown *et al.*, 2010). Tapering of mid-veins, and for bean also of minor veins, was illustrated by τ-gradients, which clearly decreased along the veins from leaf base to leaf tip.

In these experiments leaf dehydration in response to light was studied in detail (Fig. 4.3.3, 4.3.4 and 4.4.5). One strong advantage of combining gas exchange measurements with the active thermography, is the possibility to directly measure all parameters that are required to calculate h_{leaf} and C A^{-1}_{leaf}. Although the changes in $h_{\lambda E}$ were significant, its maximum contribution to the overall h_{leaf} was only about 7.7 %, indicating that dynamics in τ were not directly driven by dynamics in $h_{\lambda E}$, and thus in transpiration (Fig.4.3.4). Therefore, it was concluded that changes of τ in this experiment are primarily explained by changes in C A^{-1}_{leaf} and thus in LWC. However, transpiration rates had a significant effect on LWC (Fig.4.3.5) providing an indirect effect on τ. The measurements could be divided into three phases, which were characterized by their linear regressions. The slopes of the respective linear regressions provide a rate in mg $mmol^{-1}$ s^{-1}, which describes the net water loss in mg through transpiration. In the dehydration phase, under low light, a rapid decrease in LWC occurs during which the water loss through transpiration is larger than the water replacement within the leaf. In steady state phase, at increasing light, LWC still decreases slightly but seems to approach a constant value. The rehydration phase is a recovery phase in the dark, during which stomata close and water loss through transpiration is smaller than the water replacement or rehydration in the leaf, which most likely depends on the leaf hydraulic conductance. The leaf hydraulic conductance is known to increase with light in the scale of minutes to hours (Tyree *et al.*, 2005; Sack and Holbrook, 2006; Scoffoni *et al.*, 2008). It is assumed that with higher light the leaf hydraulic conductance increases and water loss through transpiration is replaced by water transport into the leaf (transitions from dehydration to steady state), which results in a lower water loss rate as indicated by the slope of the linear regression in the steady state phase. In conclusion, monitoring τ in parallel with transpiration provides information about net water loss, which also could be related to leaf hydraulic conductance.

The direct assessment of the relationship between τ and net water loss requires a stable boundary layer. In this experiment this was ensured by the gas exchange device, which provides a permanent air flow around the leaf enclosed in the gas exchange cuvette. Due to this permanent

air flow, the air from the leaf surface is removed and no boundary layer can be built up. Under these conditions, changes in τ are mainly related to changes in $C\ A^{-1}_{leaf}$ and thus LWC. Consequently, conditions where a stable and slight wind is present are preferable over non-wind conditions. However, active temperature measurements using a thermo-couple instead of a thermal camera, eliminates the advantage of the active thermography to spatially map LWC (Fig. 4.3.2). Although, it was possible to observe a decrease of τ in response to illumination with the active thermography approach, the τ decrease was much faster when compared to gas exchange measurements (Fig. 4.3.3). While the leaf enclosed in the leaf cuvette is exposed to forced convection condition, the leaf part outside the cuvette was exposed to free convection conditions. Under free convection, the boundary layer thickness is much higher compared to forced convection (Schuepp, 1993; Vogel, 2009; Defraeye *et al.*, 2013). Because h_{leaf} is much smaller at free convection compared to forced convection, h_{leaf} has a much stronger impact on τ at free convection conditions. Additionally, at free convection, the boundary layer conductance depends on buoyancy forces of air and thus on T_L-T_a (Bailey, 1993; Monteith and Unsworth, 2008), which permanently decreased during the experiment. Consequently, h_{leaf} was not stable throughout the measurements and permanently increases, resulting in a decrease of τ. In contrast, the gas exchange system provides a constant air stream around the leaf, which keeps h_{leaf} nearly constant throughout the measurements. The τ decrease observed with the active thermography approach under free convection is thus a result of both a decrease in $C\ A^{-1}_{leaf}$ and an increase in h_{leaf}. These changes finally lead to an overall faster decrease compared to the gas exchange measurements, where changes are mainly driven by $C\ A^{-1}_{leaf}$ dynamics alone.

The active thermography method can be used to estimate LWC of dark-adapted leaves directly. However, for transpiring leaves, τ seems to be affected by both hydration state and transpiration. To establish the active thermography approach as a method which can be used to evaluate plant-water relation dynamics, further understanding of how the leaf boundary layer, particularly transpiration, affects τ and how the dynamics of h_{leaf} can be considered are required.

5. Influence of leaf boundary layer and leaf heat transfer coefficients

5.1 Background and scope of the experiment

The time constant (τ) was shown to be sensitive to leaf water content per unit area (LWC), and thus to C A^{-1}_{leaf} (see Chapter 4). According to the theory (Equation 2.2.32.), τ also depends on the leaf heat transfer coefficient (h_{leaf}). It was found that τ values decrease more strongly in response to irradiance, when the leaf is exposed to free convection conditions, compared with values of leaves that are enclosed in a gas exchange cuvette and exposed to forced convection conditions. It is assumed that stomatal conductance (g_s) and thus the heat transfer coefficient for transpiration ($h_{\lambda E}$) has a stronger impact on τ in free convection compared to forced convection conditions. In contrast, the convective heat transfer coefficient (h_H) is assumed to increase with increasing wind speed, because wind accelerates heat transfer processes form leaf surfaces to the surrounding air. To test the impact of h_{leaf} on τ, the leaf boundary layer was actively manipulated with varying wind and irradiance regimes. Single leaves of spring barley (*Hordeum vulgare*) and common bean (*Phaseolus vulgaris*) were exposed to incrementally higher wind speeds and additionally measured both in dark- and light-adapted states. Spatial maps of τ revealed dynamics in LWC and h_{leaf} in response to the respective ambient conditions. Finally, the impact of h_{leaf} on τ, and to what extent the respective heat transfer coefficients affect the overall h_{leaf}, were finally tested by modeling the leaf boundary layer conductance and thus h_{leaf} with dimensionless numbers.

5.2 Material and Methods

5.2.1 Plant material

Spring barley (*Hordeum vulgare* Var. Victioriana) and common bean (*Phaseolus vulgaris* Var. Shiny) seeds were germinated as described in Chapter 4.2.
The evening before measurements, plants were shifted from the green-house to the laboratory and dark-adapted over night for at least 14 hours.

5.2.2 Measurements

For all measurements the laboratory set-up and active thermography protocol was used as described in the methodology Chapter 3.3 and 3.4, and T_a measurements and corrections were performed following the protocol in Chapter 3.1.1.
To induce changes in the boundary layer conductance, single leaves were exposed to increasing wind speeds, which was produced by a small ventilator that was integrated in the laboratory

set-up. Reference measurements for later modeling of the conductance to convective heat (g_H) were performed with dark-adapted leaves, for both barley and bean, which were exposed to wind speeds of 0.0, 0.2, 0.4, 0.6, 0.8, 1.0, 1.2, and 1.4 m s^{-1}, on a separate set of plants. For the actual experiments, dark-adapted leaves were exposed to increasing wind at speeds of 0.0, 0.4, 0.8, and 1.2 m s^{-1}. Afterwards, leaves were light-adapted to a light intensity of about 1000 µmol m^{-2} s^{-1} until T_L and g_s reached steady state values, which was usually the case after 30 to 40 minutes of exposure to light. After light adaptation, leaves were again measured at the four wind speed steps (0.0, 0.4, 0.8, and 1.2 m s^{-1}). After each induced leaf cooling kinetic, g_s was measured using the Licor-6400. Typically, within one minute g_s reached stable values, which were then recorded.

5.2.3 Model description

According to Equation 2.2.32, calculation of h_{leaf} requires the parameters τ and C A^{-1}_{leaf}. For the reference measurements with the dark-adapted leaves, C A^{-1}_{leaf} was derived from the relationships between τ and LWC obtained in Chapter 4 (Fig. 4.3.1) and multiplying LWC with the specific heat capacity of water (4200 J kg^{-1} K^{-1}). Because, the reference measurements were performed at eight wind speed steps and the relationships between τ and LWC were obtained at only three wind speed steps (Fig. 4.3.1), a wind speed dependent linear Equation to model more broadly the respective LWC of each leaf was defined.

$$LWC = f_m(u)\tau + f_y(u) \qquad \text{Equation 5.2.1}$$

where the slope m is given by the exponential function $f_m(u)$ and the y-intercept is given by the exponential function $f_y(u)$ (Fig. 5.2.1).
For barley these Equations were:

$$f_m(u) = 0.73 - 0.41\, e^{-\frac{u}{0.45}} \qquad \text{Equation 5.2.2}$$

$$f_y = 5.72 + 0.68\, e^{-\frac{u}{-0.62}} \qquad \text{Equation 5.2.3}$$

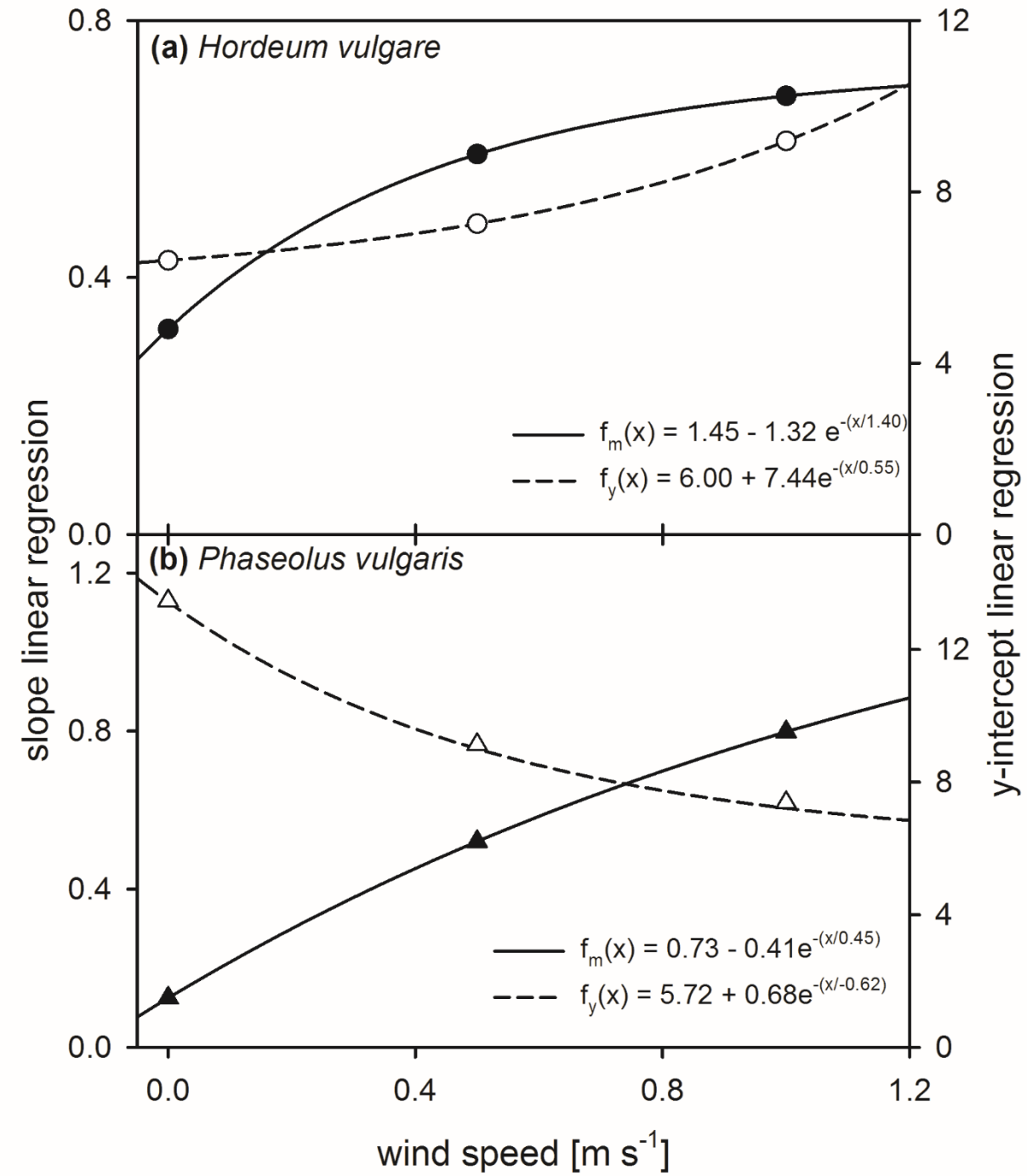

Figure 5.2.1: Linear regression model for leaf water content prediction. The slope (m) obtained by linear regression of the relationship between the time constant and leaf water content is given by closed symbols and the y-intercept of the linear regressions is given by open symbols. Change of the regression parameter in response to wind speed were fitted using exponential regressions. Equations are given in the respective panel.

And for bean these Equations were:

$$f_m(u) = 1.45 - 1.32\, e^{-\frac{u}{1.40}} \qquad \text{Equation 5.2.4}$$

$$f_y = 6.00 + 7.44\, e^{-\frac{u}{0.55}} \qquad \text{Equation 5.2.5}$$

With the modelled C A^{-1}_{leaf} and the measured τ, h_{leaf} was calculated according to Equation 2.2.29.

As g_H cannot simply be measured and is required to calculate h_H and consequently h_{leaf}, g_H was modelled using dimensionless numbers as described by the Equations 2.2.11 to 2.2.16. To calculate g_H from dimensionless numbers, the parameters a and b are required (see Equation 2.2.16), which were derived from the reference measurements.

In a first step, g_H of the dark-adapted leaves was calculated by rearranging Equation 2.2.29 and making two assumptions;

i. $h_{\lambda E}$ can be neglected for dark-adapted leaves, which is supported by measured values, i.e., g_s was very low for barley and bean leaves in the dark
ii. g_H behaves in a similar way irrespective of dark- or light-adaptation.

With these assumptions, g_H could be calculated as follows:

$$g_H = \left(\frac{\frac{C}{A_{leaf}}}{\tau} - h_{LW}\right)\left(\frac{1}{\rho_a c_p}\right) \qquad \text{Equation 5.2.6}$$

In a second step, the calculated g_H was used to calculate the respective Nusselt number (Nu). This calculated Nu was compared to theoretical Nu values, obtained by Equation 2.2.16 with the variables a and b being 1. By plotting the logarithm of the measured Nu ($\log Nu_{measured}$) against the logarithm of Equation 2.2.16 ($\log(Gr + 1.4Re^2)$), both parameters a and b were obtained (Fig. 5.2.2). The respective values for barley and bean and for free and forced convection are given in table 5.2.1.

Table 5.2.1: Parameters a and b for spring barley (*Hordeum vulgare*) and common bean (*Phaseolus vulagris*) leaves in free and forced convection.

	Hordeum vulgare		*Phaseolus vulgaris*	
	a	b	a	b
free convection	13.76	0.16	0.91	0.33
forced convection	2.41	0.25	2.58	0.25

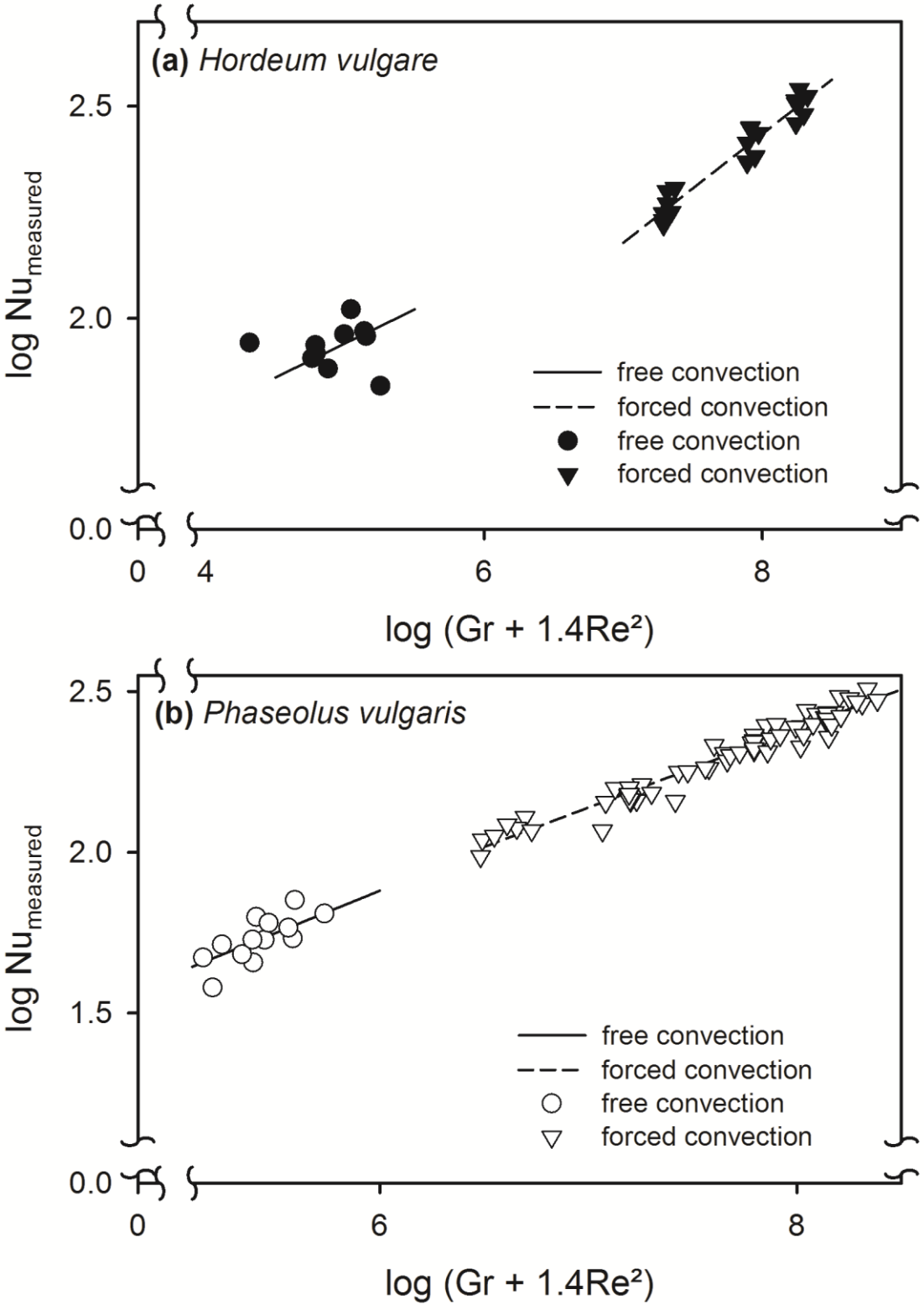

Figure 5.2.2: Derivation of the parameters a and b for the dimensionless numbers model. Logarithm of the Nusselt number (Nu) derived from measured data was plotted against the logarithm of the theoretical Nu, given by Gr + 1.4Re². **(a)** Measurements of dark-adapted spring barley leaves (*Hordeum vulgare*) at four different wind speeds (u). u steps according the legend in the panel. Two linear regressions were applied. All data indicated by solid line with y = 0.16x + 1.14, $r^2 = 0.95$, forced convection (dashed line) with y= 0.26x + 0.38, $r^2 = 0.93$. **(b)** Measurements of dark-adapted common bean leaves (*Phaseolus vulgaris*) at eight different wind speeds. u steps according to the legend in the panel. Two linear regressions were applied. For free convection (solid line): y= 0.26x + 0.30, $r^2 = 0.75$, and for forced convection (dashed line): y=0.24y + 0.43, $r^2 = 0.95$.

By substituting a and b into Equation 2.2.16, g_H could be calculated at any prevailing conditions. The modelled g_H derived from dimensionless numbers fitted well with g_H derived from actually measured data (Fig. 5.2.3.).

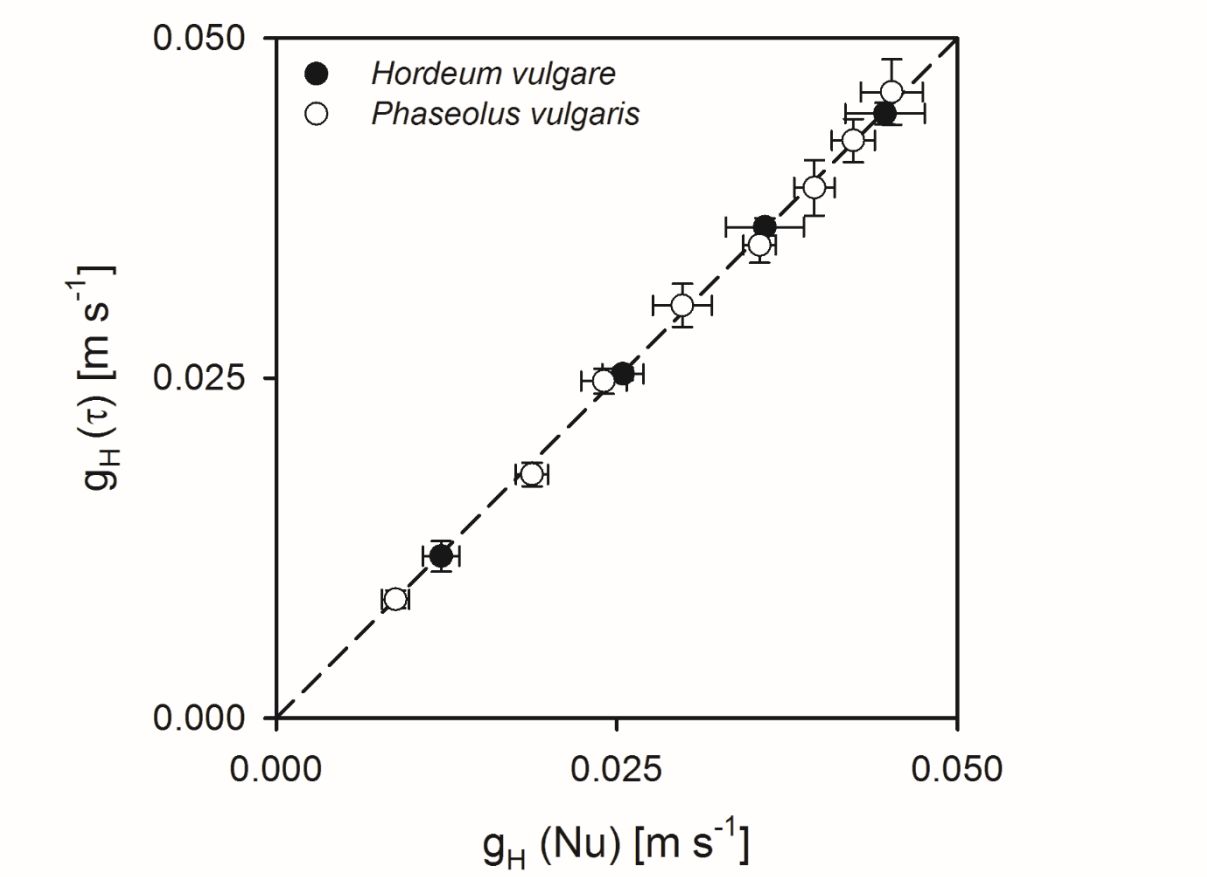

Figure 5.2.3: Comparison of conductance to convective heat (g_H) obtained by two modeling approaches. g_H was derived from time constant (τ) measurements (g_H (τ)) (see Equation 5.2.6) and compared to g_H modelled with dimensionless numbers, based on the Nusselt number (g_H (Nu)) (see Equation 2.2.16). Comparison is made for spring barley (*Hordeum vulgare*) and common bean (*Phaseolus vulgaris*).

5.2.4 Data processing and analyses

Measured cooling curves were recorded and fitted according to Equation 2.2.31 to obtain τ from the fitting, using the Origin 8.5 software (OriginLab, USA) or, for τ images the MATLAB algorithm (Chapter 3.3.2). Statistical analyses included analyses of variance (ANOVA), Pearson correlation analyses for linear relationships, and Spearman correlation analyses for non-linear relationships, which were all performed with SigmaPlot (Systat Software Inc., USA). For ANOVA, SigmaPlot automatically tests for normality of the data. In case where no normality was present, ANOVA test on the ranks were performed. In each case, the Tukey test was used for post-hoc pairwise comparison to a significance level of 5%.

5.3 Results

5.3.1 Responses of time constant to wind and light exposure

In order to quantify the effect of a changing boundary layer on τ, wind curves of dark-adapted leaves were compared with wind curves measured on light-adapted leaves (Fig. 5.3.1). For both barley and bean, significant changes of τ ($p < 0.05$) in response to increasing wind-speed were observed as well for dark- as for light-adapted leaves (Fig. 5.3.1a and b). The τ response was described by an exponential function providing a decay constant ($t_{50\%}$), which refers to the wind-speed at which τ has reached 50% of its initial value. In the dark-adapted state, obtained $t_{50\%}$-values were 0.26 m s^{-1} and 0.23 m s^{-1} for barley and bean, respectively. For light-adapted leaves, the decrease was characterized by $t_{50\%}$-values of 0.52 m s^{-1} for barley and 0.33 m s^{-1} for bean. For light-adapted leaves τ-values were significantly lower compared to dark-adapted leaves ($p < 0.05$ for barley and $p < 0.001$ for bean). Significant differences in τ between barley and bean were found at 0.0 m s^{-1} and at 0.8 m s^{-1} ($p < 0.05$). Absolute τ-values were always higher for bean leaves compared to barley leaves, particularly at 0.0 m s^{-1}, where the mean τ was more than 10 s higher for bean.

No comparable response of T_L-T_a to wind was observed (Fig. 5.3.1c and d). For barley leaves, T_L-T_a seemed to remain relatively stable throughout the measurements ($p > 0.05$), while light-adapted leaves were generally cooler compared to dark-adapted leaves. Significant differences between dark- and light-adapted leaves were only found at wind speeds of 0.0 and 0.4 m s^{-1} ($p < 0.05$). For bean leaves, exponentially decreasing T_L-T_a values were observed for dark-adapted leaves and exponentially increasing T_L-T_a values were observed for light-adapted leaves (Fig. 4.3.1d). At zero wind, light-adapted leaves were cooler compared to dark-adapted leaves. At 0.4 m s^{-1}, T_L-T_a values were similar, and for wind speeds above 0.4 m s^{-1} light-adapted leaves showed higher values compared to dark-adapted leaves. Except at 0.4 m s^{-1} the differences between dark- and light-adapted leaves were significant ($p < 0.05$).

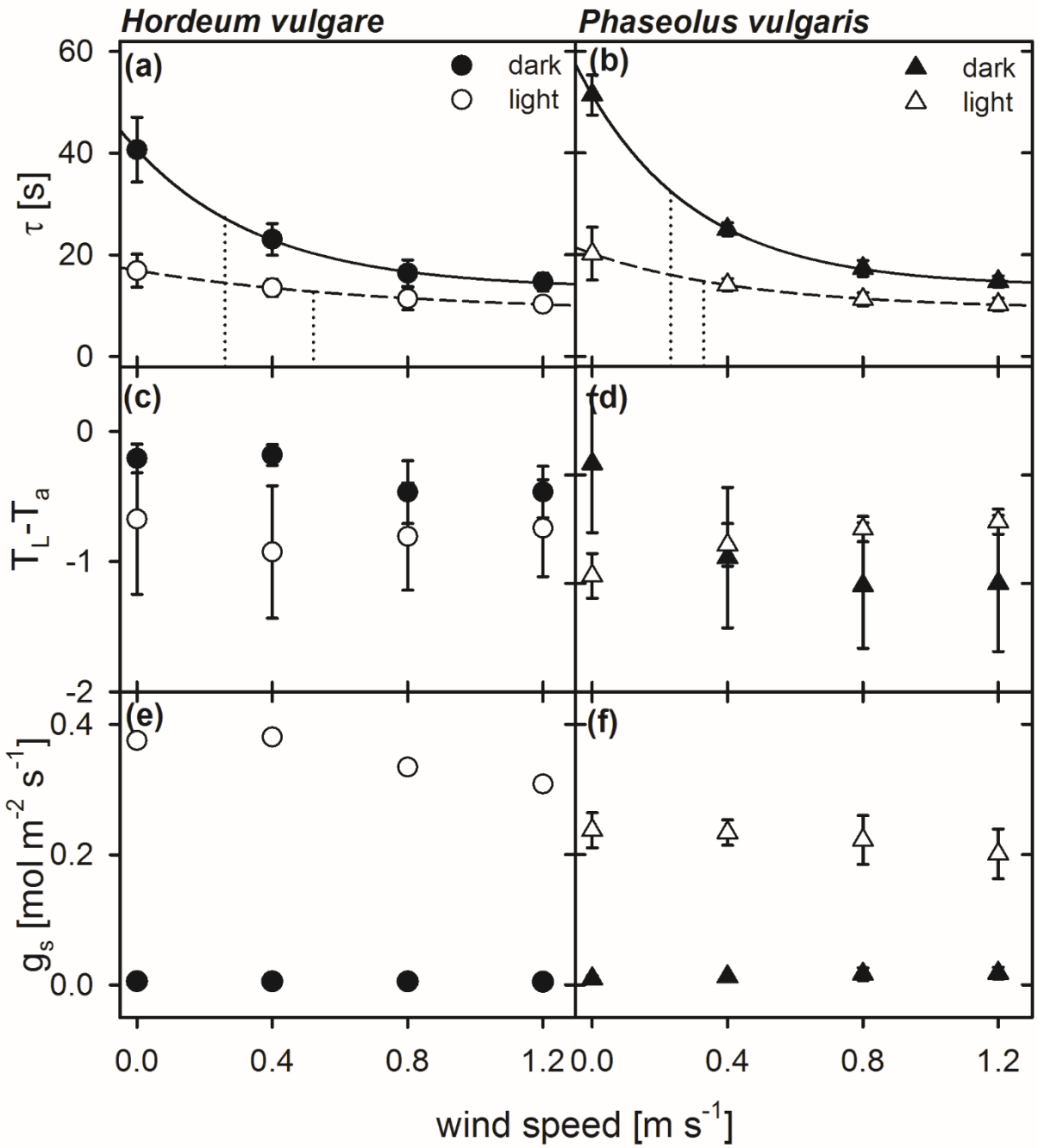

Figure 5.3.1: Wind- and light-induced changes in leaf heat transfer parameters of spring barley (*Hordeum vulgare*) and common bean (*Phaseolus vulgaris*). Measurements of dark-adapted leaves are indicated by closed symbols, and measurements of light-adapted leaves are indicated by open symbols. **(a)** and **(b)** wind- and light induced changes in time constant (τ). Dotted lines refer to the wind speed at which τ has reached 50% of the initial value ($t_{50\%}$). **(c)** and **(d)** wind- and light-induced changes in difference between leaf temperature and ambient air temperature (T_L-T_a). **(e)** and **(f)** wind- and light-induced changes in stomatal conductance (g_s). Error bars indicate standard deviation. For barley plants n = 9 individual leaves, for bean n = 10 individual leaves.

For both, barley and bean, g_s increased significantly ($p < 0.05$) in response to illumination (Fig. 5.3.1e and f). Although, g_s slightly decreased in response to wind, any significant changes were found, neither for barley nor for bean.

To evaluate changes in leaf heat transfer in response to wind and light illumination T_L-T_a was mapped spatially for representative leaves of bean and barley, respectively (Fig. 5.3.2). Generally, dark-adapted leaves had a more homogeneous distribution of T_L-T_a over the leaf surface compared to light-adapted leaves. Further, it was observed that T_L-T_a appears more homogeneous for dark-adapted leaves with increasing wind speed. In comparison to the dark-adapted leaves, light-adapted leaves showed a more heterogeneous pattern of T_L-T_a, particularly for bean leaves (Fig. 5.3.2a). For light-adapted bean leaves, areas in between major veins generally appeared cooler compared to areas with a comparably higher density of major veins. Particularly, at zero wind, leaf areas which have smaller veins, such as the leaf tip and the leaf boundaries, were cooler than the center of the leaf, where thicker veins are located. With increasing wind speed, T_L-T_a increases and areas which appeared cooler before, were warmer, particularly at the leaf tip, which was directly facing the wind source in the measurement set-up. For barley leaves, the observed patterns were not as clear as for bean leaves (Fig. 5.3.2b). While bean leaves permanently got warmer in response to increasing wind-speed, T_L-T_a of barley leaves did not show such a response and T_L-T_a were slightly fluctuating as well in the dark as upon illumination (see also Fig. 5.3.1c). Additionally, the mid-vein was only partly recognizable when leaves were light-adapted because it was warmer compared to the leaf blades (e.g. Fig. 5.3.2b at 0.0 and 0.8 m s^{-1}).

Spatial maps of τ provide information on both, water distribution in the leaves and h_{leaf}. The τ-false-color-images illustrated that with increasing wind speed and with illumination τ decreased (Fig. 5.3.3). Irrespectively of wind speed and illumination conditions, the most prominent structures, as indicated by the highest τ-values were the major veins, particularly for bean leaves (Fig. 5.3.3a). In barley leaves, only the mid-vein was visible (Fig. 5.3.3b). In dark-adapted leaves, the highest τ-values were clearly associated with thicker and more basal veins. Additionally, a gradient from high to low τ-values could be observed from the leaf base to the leaf tip and towards the leaf boundaries (see also Fig. 4.3.3 in Chapter 4). For bean leaves, it was possible to map also small minor veins, particularly when a slight wind breeze was present (e.g. Fig.5.3.3a at 0.4 m s^{-1}).

Light-adapted leaves, which generally showed lower τ-values, revealed a stronger decrease of τ in response to light in interveinal areas for bean leaves and leaf lamina for barley. Compared to the respective dark-adapted state, also the thicker major veins showed lower τ-values after illumination. Still, major and minor veins were clearly visible in bean leaves. Conspicuously, for bean leaves it was found that the highest τ-values were associated with vein-nodes, indicating an accumulation of water in these regions (e.g. Fig. 5.3.3d).

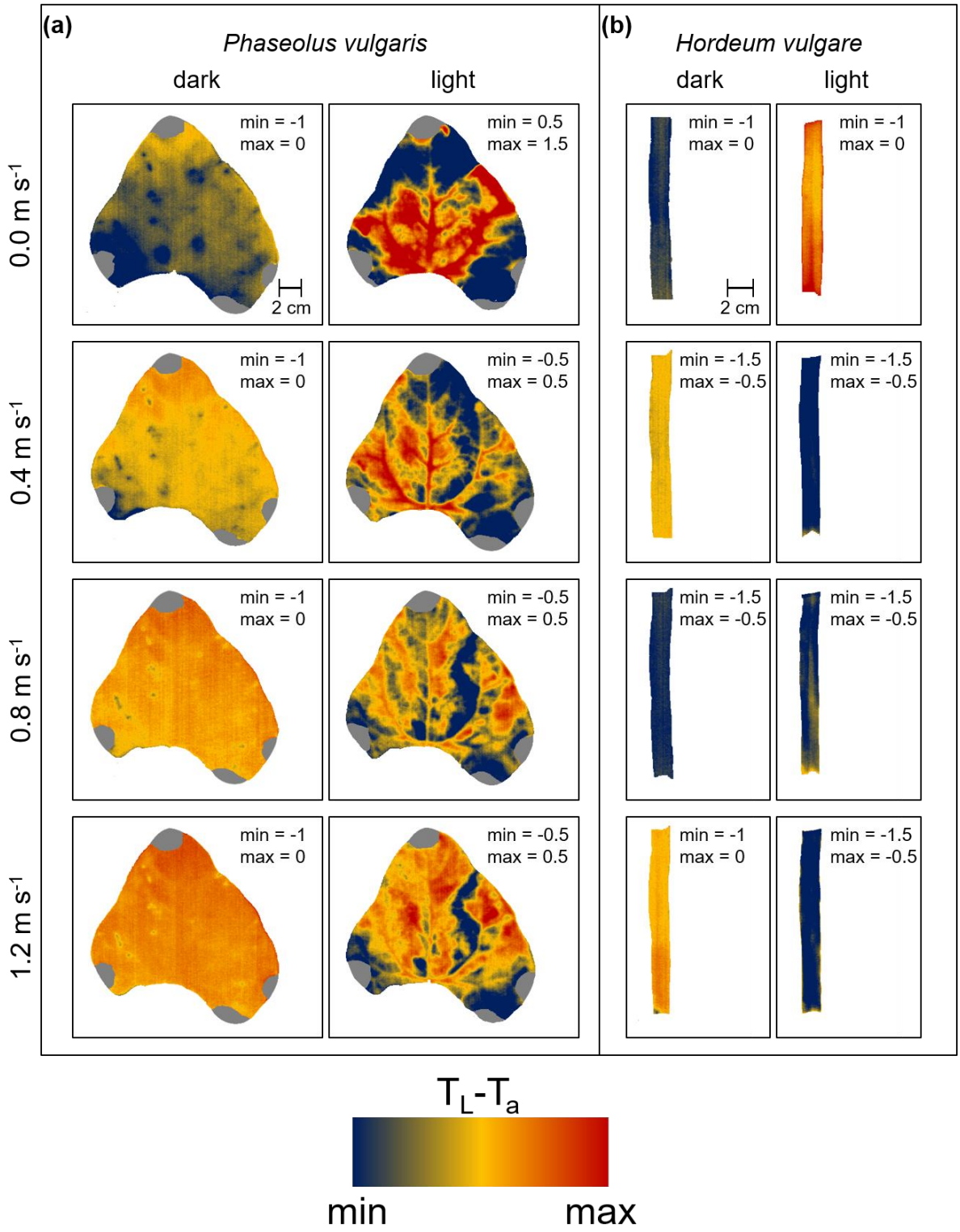

Figure 5.3.2: Spatial mapping of wind- and light-induced changes in leaf temperature to ambient air temperature difference (T_L-T_a). **(a)** representative leaf of common bean (*Phaseolus vulgaris*) and **(b)** a representative leaf of spring barley (*Hordeum vulgare*). Dark-adapted leaves are presented in the first column from the left and light-adapted leaves in second column from the left, respectively. Each line represents measurements at different wind speeds of 0.0 m s^{-1}, 0.4 m s^{-1}, 0.8 m s^{-1}, and 1.2 m s^{-1}. T_L-T_a is color-coded as indicated by the color-scale at the bottom. Minimum (min) and maximum (max) values of T_L-T_a are given in each panel.

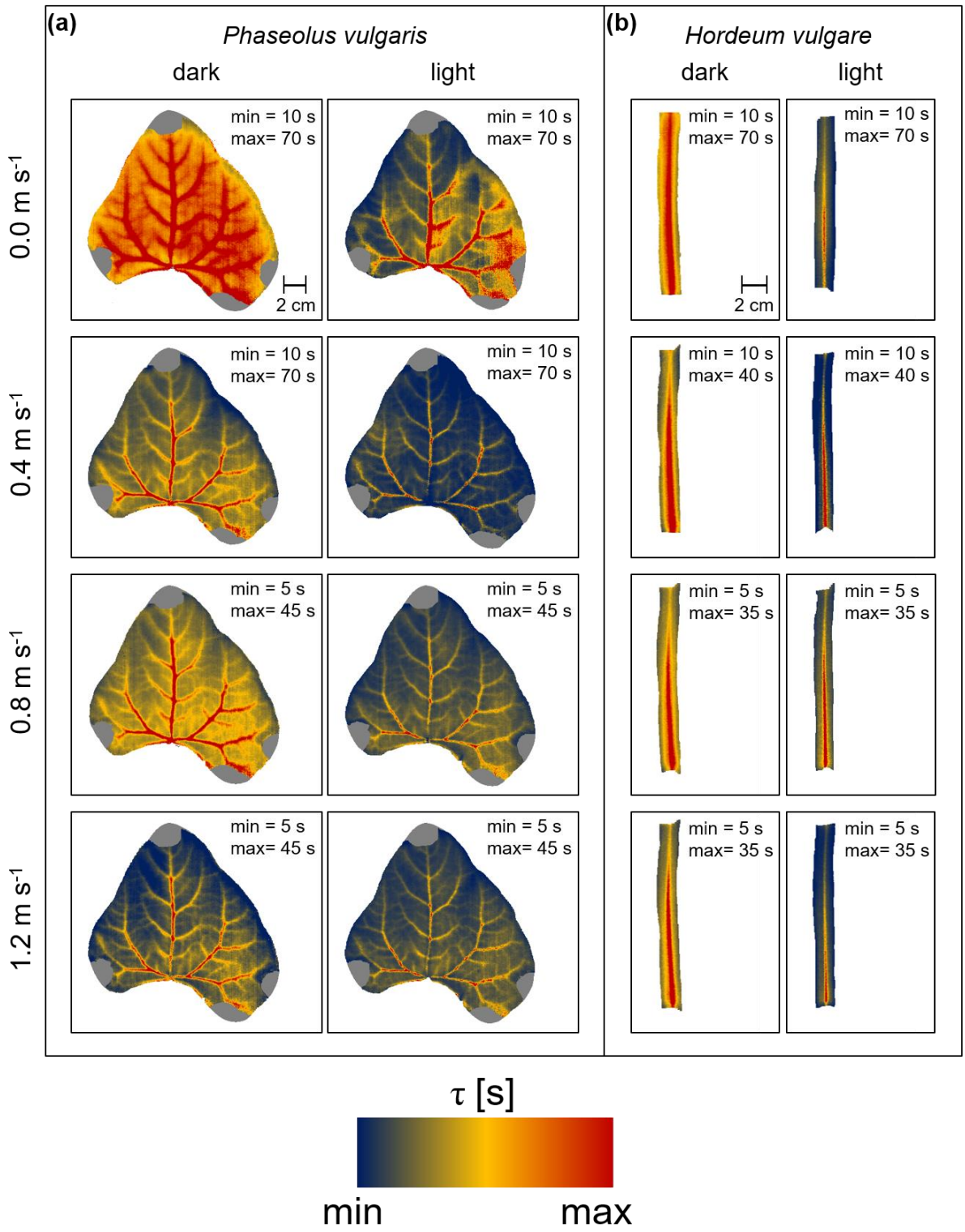

Figure 5.3.3: Spatial mapping of wind- and light-induced changes in time constant (τ). **(a)** representative leaf of common bean (*Phaseolus vulgaris*) and **(b)** a representative leaf of spring barley (*Hordeum vulgare*). Dark-adapted leaves are presented in the first column from the left and light-adapted leaves in second column from the left, respectively. Each line represents measurements at different wind speeds of 0.0 m s^{-1}, 0.4 m s^{-1}, 0.8 m s^{-1}, and 1.2 m s^{-1}. τ-values are color-coded as indicated by color-scale at the bottom. Minimum (min) and maximum (max) values of τ are given in each panel.

5.3.2. Impact of the leaf heat transfer coefficient on the time constant

For quantification of the impact of h_{leaf} on τ, $C A^{-1}_{leaf}$ was modelled using two different models. The first model was based on the linear regressions for the relationships between τ and LWC as found in earlier experiments (Fig. 5.2.1). The second model uses dimensionless numbers to calculate h_{leaf}, with which $C A^{-1}_{leaf}$ was finally calculated. Generally, both models matched well to each other (Fig. 5.3.4). For barley, a strong and highly significant linear correlation was found ($p < 0.001$, Fig. 5.3.4a). In contrast, the model using dimensionless numbers revealed some weaknesses for bean, particularly for $C A^{-1}_{leaf}$ calculations for wind-free conditions (Fig. 5.3.4b). Here the dimensionless numbers model clearly underestimated $C A^{-1}_{leaf}$ compared to the model based on the linear regressions. Because the models did not match very well for 0.0 m s^{-1}, these values were excluded for later statistical analyses. However, for the wind speeds between 0.2 and 1.2 m s^{-1} a strong and highly significant linear correlation between the two models was also found for bean ($p < 0.001$).

The leaf heat transfer coefficient calculated with modeled g_H and measured g_s correlated well with τ (Fig. 5.3.5). For both, barley and bean a highly significant correlation between h_{leaf} and τ was found ($p < 0.001$). Generally, h_{leaf} of light-adapted leaves were higher compared to h_{leaf} of dark-adapted leaves. Both curves were fitted by an exponential function, which provided high r^2 values with 0.97 and 0.89 for barley and bean, respectively. Additionally, $t_{50\%}$ values of 5.6 s for both barley and bean indicated a similar response of τ to h_{leaf}, although absolute values differed between these two species.

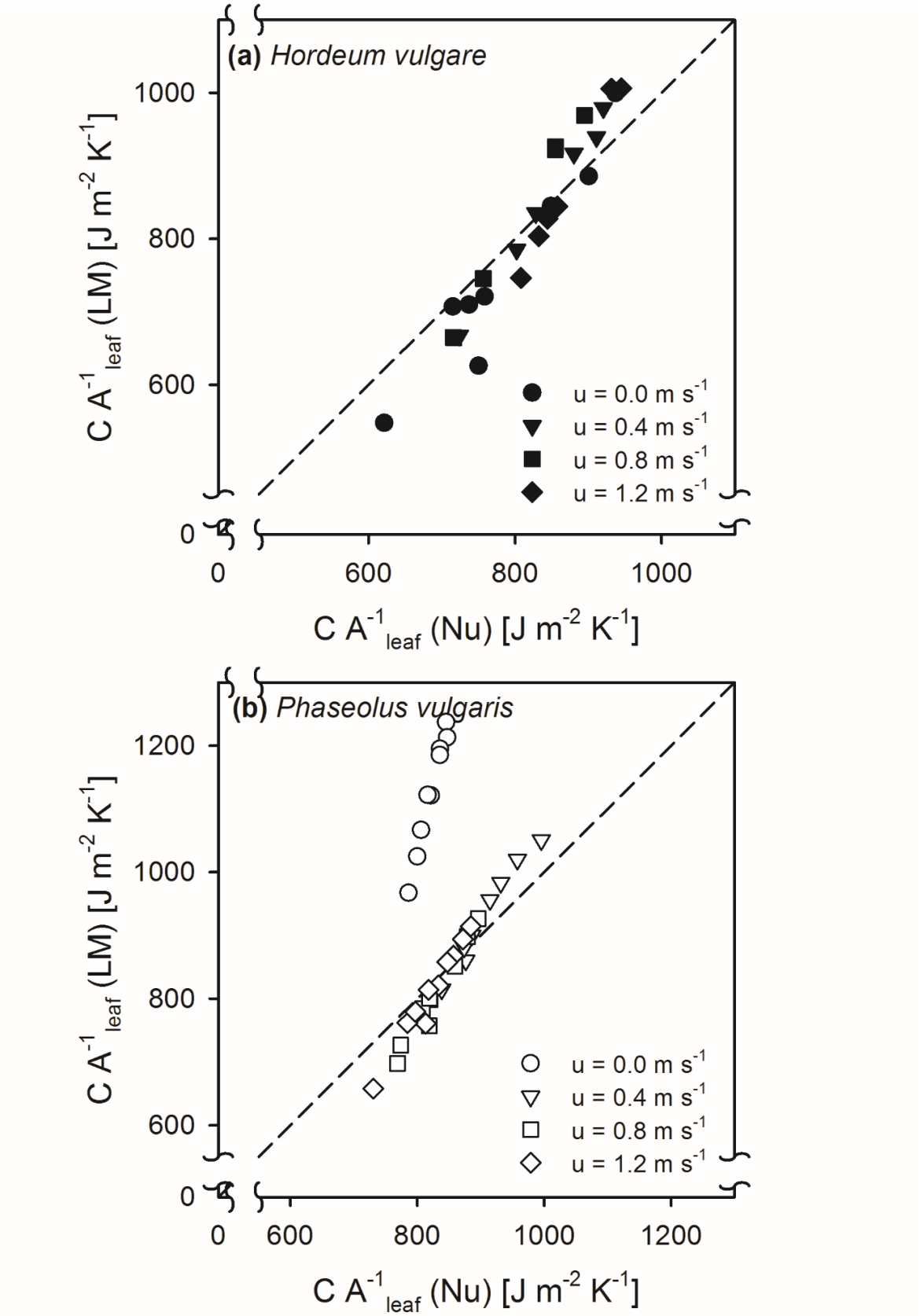

Figure 5.3.4: Comparison of two models for leaf heat capacity ($C\ A^{-1}_{leaf}$) prediction. $C\ A^{-1}_{leaf}$ derived from linear regression of the relationship between time constant and leaf water content (LM) was compared to $C\ A^{-1}_{leaf}$ derived from a dimensionless numbers model (Nu). **(a)** dark-adapted spring barley (*Hordeum vulgare*) leaves. **(b)** dark-adapted common bean (*Phaseolus vulgaris*) leaves. The modeled data are shown for measurements at four different wind speeds (u), u = 0.0 m s^{-1} shown by circles, u = 0.4 m s^{-1} shown by triangles, u = 0.8 m s^{-1} shown by squares, and u = 1.2 m s^{-1} shown by diamonds. Dashed lines represent the one-to-one line relationship.

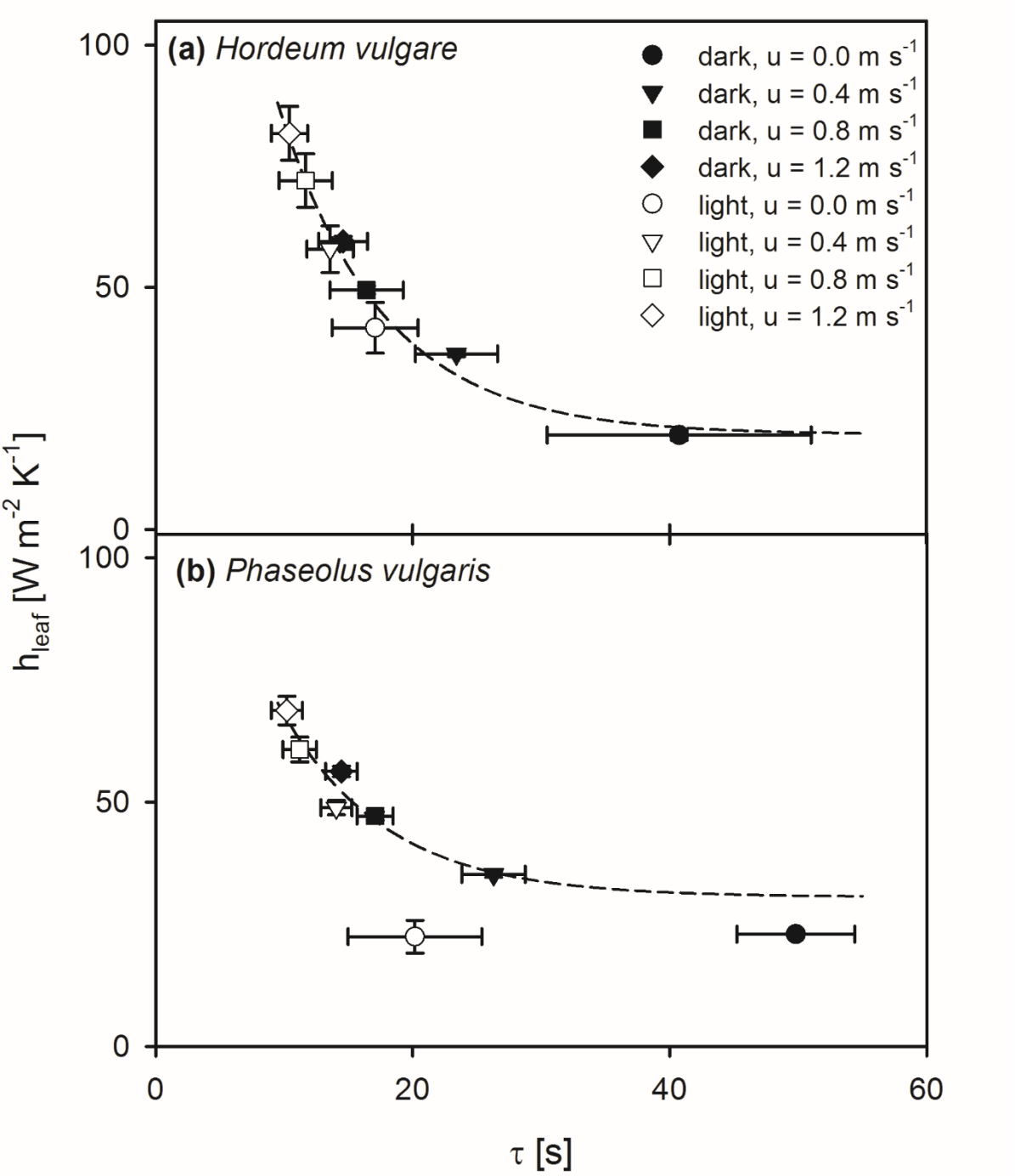

Figure 5.3.5: Correlation between modeled leaf heat transfer coefficient (h_{leaf}) and time constant (τ). Measurements were performed at four different wind speeds (u) and in dark- and light-adapted state of individual leaves. u = 0.0 m s^{-1} shown circles, u = 0.4 m s^{-1} shown by triangles, u = 0.8 m s^{-1} shown by squares, and u = 1.2 m s^{-1} shown by diamonds. Dark-adapted leaves are indicated by closed symbols and light-adapted leaves are indicated by open symbols. **(a)** Measurements of individual spring barley leaves (*Hordeum* vulgare). Exponential regression indicated by dashed line: $f(x) = 19.60 + 221.81\ e^{-012x}$, $r^2 = 0.97$. **(b)** Measurements of individual common bean leaves (*Phaseolus vulgaris*). Exponential regressions are indicated by dashed line: $f(x) = 30.56 + 128.29\ e^{-0.12x}$, $r^2 = 0.89$. Error bars represent standard deviation of single leaves. For barley n = 9, and for bean n = 10.

Finally, the impact of each heat transfer coefficient (h) on the overall h_{leaf} was evaluated. While h for long-wave radiative heat (h_{LW}) did not correlate with h_{leaf}, for both barley and bean, h_H

and $h_{\lambda E}$ showed a strong and significant correlation with h_{leaf} ($p < 0.001$). The relative contribution of each h to the overall h_{leaf} significantly changed with wind speed ($p < 0.001$) (Fig.5.3.6). While the relative contribution of h_H increased with increasing wind speed, the relative contribution of h_{LW} and $h_{\lambda E}$ decreased with increasing wind speed.

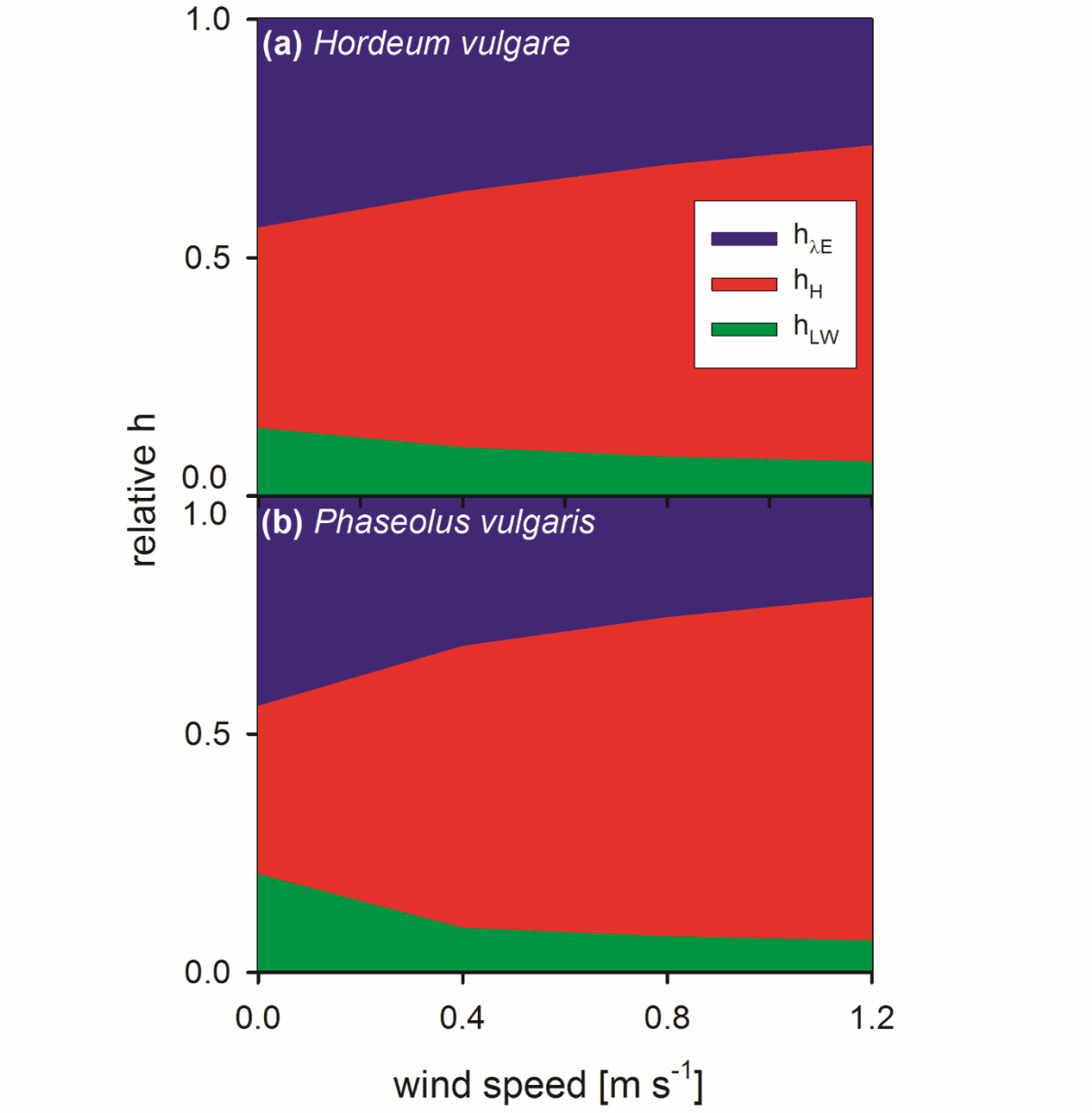

Figure 5.3.6: Relative contribution of normalized heat transfer coefficients to the total leaf heat transfer coefficient in response to wind speed. Heat transfer coefficient for evapotranspiration ($h_{\lambda E}$) in blue, heat transfer coefficient for convective heat (h_H) in red, and heat transfer coefficient for long-wave radiative heat (h_{LW}) in red. **(a)** Spring barley (*Hordeum vulagre*) and **(b)** common bean (*Phaseouls vulgaris*). Areas represent mean values of n = 9 single leaves for barley and n = 10 single leaves for bean.

At zero wind $h_{\lambda E}$ had the highest impact on h_{leaf} with about 45% of the overall h_{leaf}. At 1.2 m s^{-1} the relative contribution of $h_{\lambda E}$ remained significant, but the relative contribution to the overall h_{leaf} dropped to 26% and 21% for barley and bean, respectively.

5.4 Discussion

In this Chapter, the impact of changing h_{leaf} on τ was assessed by actively manipulating the leaf boundary layer by means of varying wind speeds and light exposure. It was possible to study quantitative relationships between components of heat exchange processes, by introducing τ in a commonly used model for estimation of leaf heat transfer using dimensionless numbers. Additionally, the spatial distributions of T_L-T_a and τ illustrated some interesting relationships between wind and light, indicating that both parameters have an impact on the leaf boundary layer.

5.4.1 Model evaluation

A good agreement between τ-based calculations and dimensionless-numbers-based calculations of g_H were found (Fig. 5.2.3). For further evaluation of the modeled data, calculated C A^{-1}_{leaf} was compared with those values, which were derived from the linear relationships found in Chapter 4 (Fig. 5.3.4). In principle, both calculations delivered comparable values. Nevertheless, some weak points occurred in the modeled data for measurements at wind-free conditions, particularly for bean, whereas the models for barley matched well. At zero wind-speed, the leaf is supposed to be exposed to free convection conditions. Because free convection highly depends on leaf area and surface 3D structure, and each leaf possesses an individual structure, a high variability in h_{leaf} is assumed under these conditions. The linear regressions of the relationship between τ and LWC therefore contained some errors. Thus, both the direct derivation of C A^{-1}_{leaf} and the calculation of C A^{-1}_{leaf} using dimensionless numbers carried errors. Both measurements and the modeling of heat transfer in non-wind conditions, where free convection is assumed, is a difficult issue and it is questionable, whether free convection on plant leaves exists at all. Particularly for light-adapted bean leaves, a highly heterogeneous T_L distribution was observed which may result in thermal instabilities of the boundary layer (Defraeye *et al.*, 2013). The heat transfer from the leaf surface is affected by a wide range of factors, such as surface roughness. For example trichomes or vascular tissue, both of which increase the leaf surface area, significantly affect leaf heat transfer by inducing small turbulent air streams (Parkhurst, 1976; Schreuder *et al.*, 2001; Defraeye *et al.*, 2013). Barley has a relatively flat surface due to its parallel vein system (Dannenhoffer *et al.*, 1990), whereas bean has a wavy surface structure with plenty of thick leaf veins that are dichotomously branched. While the air provided by the ventilator streams in parallel to the veins on the barley surface, the air stream may be disturbed on the bean surface by traversed veins, which induces small turbulences on the leaf surface. These factors, in addition to leaf area, are the reason for thermal instabilities of the boundary layer, which are most relevant at free convection conditions. Additionally, the

example of a bean leaf shows a striking area (to the right of the mid-vein), which is always cooler compared to the rest of the leaf (Fig. 5.3.2a). Probably, the leaf forms a small cavity here, where water vapor lost by transpiration accumulates. This in turn accelerates heat transfer in this area, which is indicated by lower T_L-T_a and also lower τ-values (Fig. 5.3.3a).
Finally, h_{leaf} and its components were modelled to quantify the impact of h_{leaf} on τ using dimensionless numbers (Schuepp, 1993; Monteith and Unsworth, 2008; Nobel, 2009). The modeled h_{leaf} correlated well with τ, and according to the underlying theory, an exponential relationship between these both parameters was found (Fig. 5.3.5).

5.4.2 Response of time constant to varying boundary layer conditions

The boundary layer thickness varies with low wind, and decreases in response to increasing wind, which in turn increases heat transfer (Raschke, 1960; Vogel, 2009). Thus, the observation that τ decreases in response to increasing wind speed for both barley and bean and for dark- and light-adapted leaves is in agreement with previous findings (Fig. 5.3.1). Barley leaves showed lower values, particularly at zero wind and at 0.4 m s^{-1}, which is likely due to leaf size and shape. Comparatively smaller leaves have a thinner boundary layer (Gates *et al.*, 1965; Sinclair, 1970). T_L increases with the distance from the leaf edge, which, particularly at wind-free conditions, facilitates the increase in boundary layer thickness (Vogel, 2009). T_L-T_a maps for barley seemed to be more homogeneous compared to bean leaves, as well in the dark-adapted state as in the light adapted state (Fig. 5.3.2). Roth-Nebelsick (2001) modeled T_L for leaves in response to very low wind speeds and found that T_L was far away from being uniform, indicating a complex boundary layer for larger leaves. At least for light-adapted bean leaves the experimental data correspond to this model (Fig. 5.3.2).
It was also found that τ significantly decreases in response to illumination (Fig. 5.3.1). According to the theory, it is assumed that C A^{-1}_{leaf} decreased and h_{leaf} increased. A decrease in τ of about 20 and 30 s was observed for barley and bean, respectively. Based on the linear relationships found in Chapter 4, these changes would correspond to a water loss of 20 to 30 %. This seems unlikely, because the plants were well-watered and were not exposed to any stress situation. However, both barley and bean, were transpiring at high transpiration rates (Fig. 5.3.1e and f) so that some water loss is also very likely (e.g. Scoffoni *et al.*, 2014).
It was observed that wind increased h_{leaf} and thus decreased τ. In windy conditions, forced convection becomes more relevant for the overall heat transfer (Schuepp, 1993; Vogel, 2009; Defraeye *et al.*, 2013). On the one side, the boundary layer is simply blown away, which reduces boundary layer thickness and with it boundary layer resistance. On the other side, the wind

transports the heat away from the leaf surface. The stronger the wind becomes, the smaller the boundary layer gets and the faster the heat is removed from the leaf surface, which finally results in an increased h_{leaf}. Such wind effects could be also observed by spatial T_L-T_a maps of bean leaves (Fig. 5.3.2a). The wind-leading edge (leaf tip) got warmer compared to the wind-averted leaf edge (leaf base) in response to wind, which confirms the assumption that the boundary layer is progressively eliminated following a gradient (Kitano and Eguchi, 1990). For barley leaves, this effect was not visible, which might be related to a generally more homogeneous boundary layer for small and narrow leaves (Gates *et al.*, 1965; Sinclair, 1970). Another reason may be again the smother leaf surface of barley and the parallel venation system, which offers no resistance to the air stream.

A further increase of h_{leaf} was observed in response to light illumination. Light induces stomatal opening and thus increases heat transfer by transpiration so that particularly $h_{\lambda E}$ increases (Roelfsema and Hedrich, 2005; Shimazaki *et al.*, 2007; Pieruschka *et al.*, 2010). Upon illumination, both barley and bean leaves cooled down (Fig. 5.3.1. and 5.3.2.). While light-adapted barley leaves remained cooler throughout the measurements, light-adapted bean leaves got warmer in response to illumination. However, particularly for bean leaves local T_L-T_a changes on the leaf could be observed, where leaf parts with a higher density of leaf vascular tissue, and thus a higher local LWC, as indicated by comparably higher τ-values, showed warmer patches compared to interveinal areas, where stomata density is higher. Interestingly, it was found that irrespective of wind, the leaf lamina regions which became warmer and showed a higher T_L-T_a were exactly associated to those areas where the higher local τ-values were found. For barley leaves, this effect was not directly noticeable, but for both barley and bean leaves in light- and dark-adapted state, respectively, significant and non-linear correlations between T_L-T_a and τ were found ($p < 0.05$). A further interesting observation was that the highest τ-values of light-adapted bean leaves where found at vein nodes. This may be related to a small water accumulation, which in turn is a result of changed leaf hydraulic conductance (Scoffoni *et al.*, 2008; Sack and Scoffoni, 2013).

5.4.3 Composition of the leaf heat transfer coefficient and the impact of leaf heat capacity on the boundary layer

Many of these results illustrate that barley has a higher h_{leaf} due to their smaller and narrower leaves, which was also reflected by the modeled $h_{leaf.}$ For barley, h_{leaf} was generally higher compared to that of bean leaves for dark-adapted as well as for light-adapted leaves. The relative contributions of the single components of h_{leaf}, namely h_H, $h_{\lambda E}$, and the heat transfer coefficient

for radiative heat (h_{LW}) revealed a significant influence of $h_{\lambda E}$ for light-adapted leaves (Fig. 5.3.6). However, h_H seems to have the highest contribution to the overall h_{leaf}, whereas the relative contribution of h_{LW} remained relatively low compared to the other heat transfer coefficients. The relative contribution of $h_{\lambda E}$ decreases with increasing wind. Stomatal resistance can become much larger than the convective resistance (boundary layer resistance), particularly at higher wind speeds (Cannon *et al.*, 1979; Defraeye *et al.*, 2013). Although, the experiments were performed in a low wind speed regime, this effect was already noticeable.

The results indicate the importance of h_H when modeling leaf heat transfer. Often, the main issue in plant science is to model transpiration and the convective heat is assumed to be nearly constant or at least a uniformly occurring heat flux. However, as the results strongly indicate, the convective heat is probably the most important parameter for leaf heat transfer modeling. Convective heat and transpiration are inevitably coupled because the water vapor that is released through stomata has to penetrate the boundary layer, which depends on the prevailing convective conditions. Additionally, the time scale of T_L responses depends on the thermal capacity of leaves (Vogel, 2009; Leigh *et al.*, 2012), which can be indirectly measured by τ. Correlations between local T_L-T_a and local τ were found on the leaf surface. Intuitively, the boundary layer is thicker in the center of the leaf compared to the leaf edges, and thus less or slower heat transfer occurs in these regions (Defraeye *et al.*, 2013). Additionally, vein density and thickness is higher in the leaf center (McKown *et al.*, 2010; Sack and Scoffoni, 2013), which results in higher local $C\ A^{-1}_{leaf}$, as illustrated by the τ-images. Water, the main component of $C\ A^{-1}_{leaf}$, has a very high specific heat capacity ($c_p \approx 4.2$ kJ kg^{-1} K^{-1}) and it can absorb high amounts of heat without significant temperature changes. However, water has also a low thermal conductivity ($k \approx 0.6$ W m^{-1} K^{-1}) (Jayalakshmy and Philip, 2010) so that absorbed heat is released relatively slowly. If a leaf is exposed to a high energetic environment, as it is the case upon illumination, more heat will act on the leaf surface compared to darkness and will inevitably increase T_L with time. It is concluded that the amount of water, and thus $C\ A^{-1}_{leaf}$, has a significant impact on the leaf boundary layer, because higher water content means higher heat absorption, which increases T_L due to the low thermal conductivity of water.

5.4.4 Conclusion

In this Chapter it was demonstrated that h_{leaf} and particularly the convective heat and transpiration has a strong effect on τ. However, it was possible to implement τ in a common modeling approach for heat transfer modeling. Because, τ, as the product of $C\ A^{-1}_{leaf}$ and h_{leaf}, is actually a measure of thermal inertia of the leaf, τ should be considered for leaf heat transfer modeling.

Not at least because T_L-T_a, which is also related to leaf heat transfer processes, was shown to be highly affected by thermal instabilities in the boundary layer and small turbulences on the leaf surface, which makes T_L-T_a rather unpredictable and conclusively inappropriate for modelling. Additionally, in contrast to the parameter T_L-T_a, separation between C A^{-1}_{leaf} and h_{leaf} effects is possible by the combination of τ with, for example, dimensionless numbers model. Therefore, using the active thermography provides a reliable method to study h_{leaf} and the quantitative relationships of its components, by measuring τ.

Nevertheless, the primary goal is to establish the active thermography approach as a valid method to determine leaf- or plant-water relations. It was demonstrated that under certain conditions, namely at high wind speeds (e.g. in gas exchange cuvettes), τ is dominated by LWC. However, it was also demonstrated that under certain conditions, namely at low wind speeds, τ is dominated by changes in h_{leaf}. Simply due to the measurement protocol and the requirement of leaf cooling kinetics, the application of the active thermography is more likely at wind-free or low wind conditions, particularly at plant or canopy scale. Thus, h_{leaf} has to be considered as a potential factor influencing τ, if the goal is to derive LWC from τ measurements. In any circumstances thermal measurements should be accompanied by precise wind speed measurements that address an appropriate spatial scale and granularity of observations.

6. Assessment of stress-responses of barley to a deficit irrigation in the greenhouse using the active thermography approach on canopy scale

6.1 Background and scope of the experiment

In this Chapter, the applicability of the active thermography approach in the greenhouse on canopy scale was investigated. It was tested whether it is possible to detect the stress-response of four spring barley (*Hordeum vulgare*) varieties - Apex, Barke, Heils Franken, and Victoriana to a deficit irrigation (DI). Stress reactions in response to drought or DI has been evaluated by the crop water stress index (CWSI) (Idso *et al.*, 1981; Jackson and Idso, 1981). The CWSI is assumed to be sensitive to changes in h_{leaf}, particularly to changes in transpiration. However, as the CWSI is only sensitive to transpiration and not directly sensitive to the leaf water content per unit area (LWC), the CWSI alone cannot be used to assess the overall plant-water relation dynamics in response to stress. Because LWC is a result of an equilibrium between water uptake by the roots and water loss by transpiration, its measurement is essential to fully understand the plant-water relation dynamics in response to water limitation. The time constant (τ) was shown to be sensitive to LWC dynamics (Chapter 4), but it was also sensitive to changes in h_{leaf}, particularly under non-wind conditions and in conditions of illumination, where transpiration occurs (Chapter 5). In this paragraph, it was tested for the first time, which environmental and plant physiological factors affect τ at the canopy scale. Further, τ was compared with the CWSI and both parameters were evaluated with respect to the ability to detect stress. The CWSI directly responded to stress, because it is mainly related to transpiration and thus h_{leaf}, which decreased with the increasing stress. Measurements of τ did not correlate with the stress level as the CWSI did, because τ reflects LWC and h_{leaf}. However, the combined consideration of τ and the CWSI revealed different strategies of the varieties to deal with water-limiting conditions.

6.2. Material and Methods

6.2.1 Location

The experiment was performed in a greenhouse at the Campus Klein-Altendorf, University of Bonn (50° 37’ 31.7’’ N, 6° 59’ 18.8’’ E). The climate in the greenhouse was not controlled except openable ventilation flaps on the roof.

The experiment was performed during the early summer 2015 between May 29th and July 28th. During this period the daily average maximum photosynthetic photon flux density (PPFD) was 776 (± 586) µmol m^{-2} s^{-1}, which usually occurred around midday. The absolute maximum of

1800 µmol m^{-2} s^{-1} during midday, was reached on July 6th. Mean air temperature (T_a) was 23.7 (± 3.4) °C, with an absolute maximum of 37.4 °C, which was also reached at midday on July 6th. Minimum T_a was generally reached during the night with an absolute minimum of 15.2 °C at the 22nd of June.

6.2.2 Plant material

Four spring barley varieties were used - Apex, Barke, Heils Franken, and Victoriana. These varieties differ in their diurnal plant water relation dynamics (Rischbeck *et al.*, 2014). Thirty plants were germinated in boxes of the size 37.5 cm x 26 cm x 17.5 cm, with a distance of 5 cm between each seed in each direction. The boxes were filled with about 15 liters of a peat-sand-pumice substrate (Dachstaudensubstrat SoMi 513). At the bottom of the boxes holes were drilled and the boxes were placed on water absorbing clothes in a tray to enable hydration of the substrate from below. For each variety ten plant boxes were prepared. Half of these boxes were later treated as control, the other half was treated with a DI. During the experiment some plant boxes had to be eliminated due to unusually high temperatures, which resulted in direct leaf damage for some boxes. For this reason, only two replicates per variety and per treatment were measured and two replicates per variety and per treatment were used to determine fresh weight (FW) by destructive harvest.

Plants were sown on the May 25th and germinated between May 29th and 31th. After plants had been germinated, 12 g of the long-term NPK fertilizer Plantacote 4M (Manna, Germany) was applied to each box. Harvesting was performed at two time points during the experiment on June 16th and July 8th, and were consequently about 17 and 39 days old, respectively. On July 8th first flag leaves were already present. Three plants from two boxes per variety and treatment, respectively, were harvested from the designated boxes and analyzed for FW and leaf area (LA). For LA determination all leaves were detached and scanned with the LI-3100C Area Meter (LI-COR Biosciences, USA).

6.2.3 Drought treatment

For each variety a control and a DI treatment was applied. According to the water retention curve of the used soil (Fig. 6.2.1), the soil moisture of the control treatment was kept around 55%, where the soil water retention is about -10 hPa and represents field capacity (Fig.6.2.2).

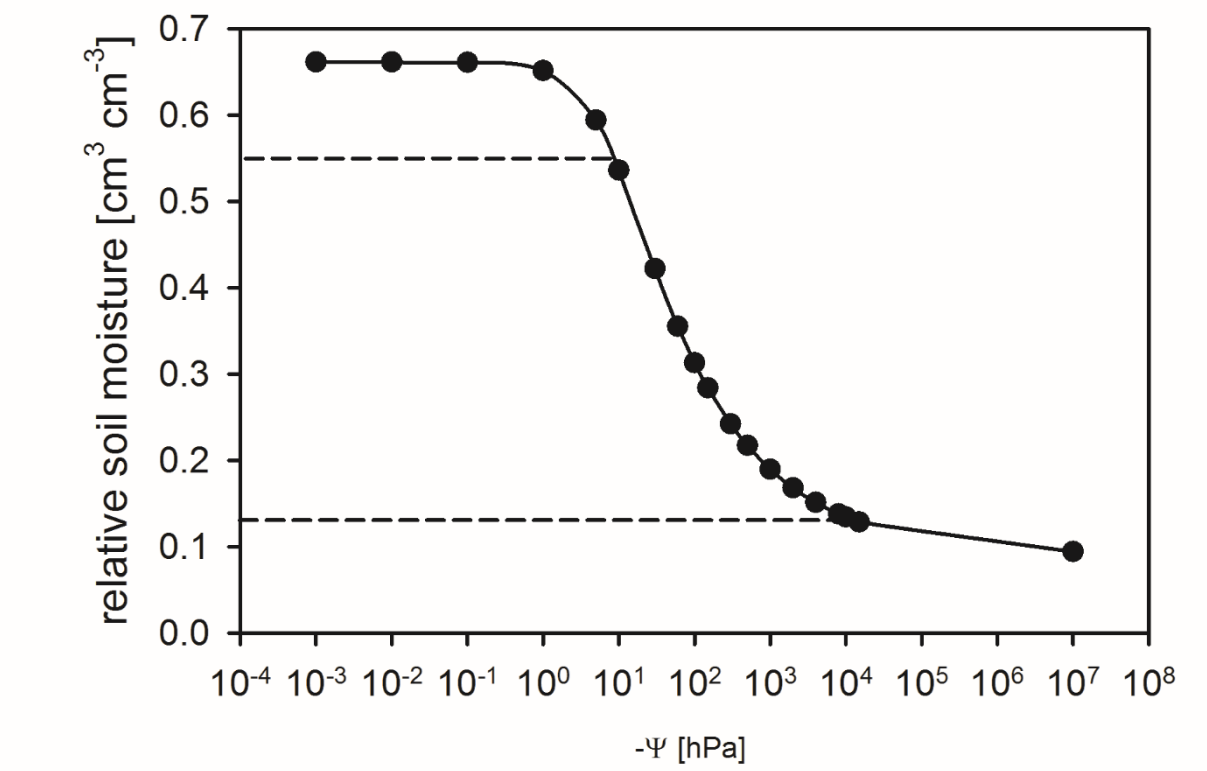

Figure 6.2.1: Soil water retention curve. Relative soil moisture in dependency on soil water retention (-ψ). Upper dashed line refers to field capacity of the soil at 55% soil moisture and lower dashed line refers to permanent wilting point at 13% soil moisture (Barboza-Barquero *et al.*, 2015).

For the DI treatment the soil moisture was kept between 20% and 30%, where soil water retention is between -100 and -500hPa. This soil moisture range already provides a water-limitation for the plants, but does not cause severe drought stress, so that the prevailing conditions refer to a mild-drought stress (Fig.A.6.1). Particularly during the weeks around June 29th and July 6th, temperatures were very high, which caused strong dehydration of the soil, so that even the soil moisture of the control treatment partly dropped below 20% (Fig.6.2.2). For this reason, between June 22nd and July 6th plants were irrigated every day.

To adjust the desired soil moisture, the boxes filled with soil were measured before seeding with a ML2x ThetaProbe (Delta-T Devices, UK) and additionally weighed. Afterwards the boxes were filled with water and one day later soil moisture and weight of the boxes were determined again. By linearly fitting these two reference points, the amount of water that has to be added could be calculated by measuring the soil moisture.

Soil moisture adjustment was performed three times a week. First, plant boxes were weighed and measured with the ThetaProbe and afterwards the calculated amount of water was added. About one hour after irrigation, the boxes were weighed and measured again to control the soil moisture adjustment. Where soil moisture did not reach the desired value, more water was added.

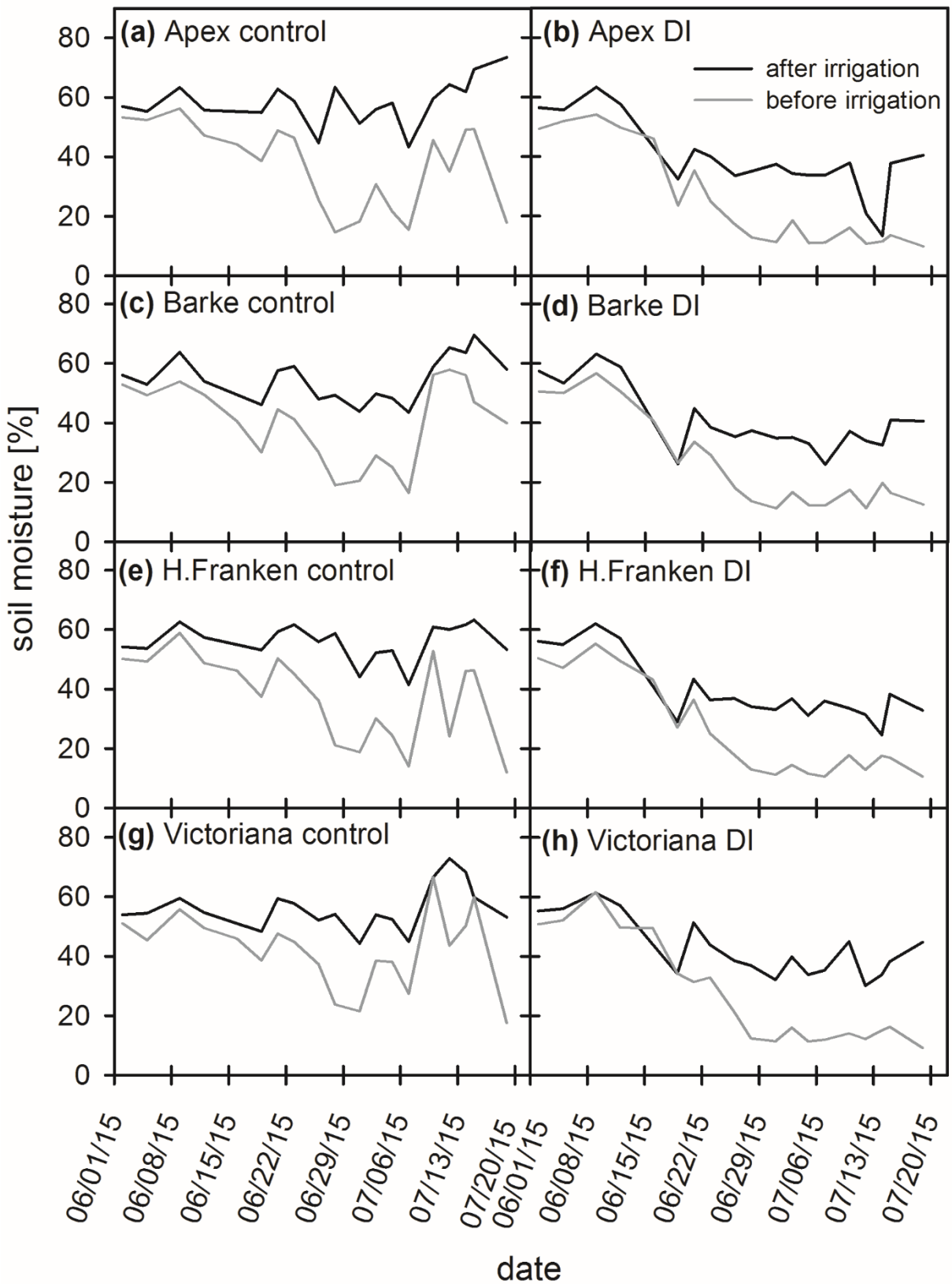

Figure 6.2.2: Soil moisture monitoring during the experiment of the spring barley canopies. Black lines are measurements after irrigation and grey lines are measurements before irrigation. Control treatment is illustrated in the left column and deficit irrigation (DI) treatment is illustrated in right column. **(a)** and **(b)** shows the variety Apex, **(c)** and **(d)** shows the variety Barke, **(e)** and **(f)** shows the variety Heils Franken (H.Franken), and **(g)** and **(h)** show the variety Victoriana. Lines represent the mean value of the two replicates.

Although plants were watered from below, water distribution within the boxes were heterogeneous. In individual cases plant canopies were over-watered resulting in a soil moisture higher than 55%. Additionally, DI treated canopies received exessive water inducing a recovery from the induced stress. This was particularly observed for the variety Victoriana around July 6th, where a stress-recovery was assumed for one DI-treated canopy and water-logging stress was assumed for one control treatment (Steffens *et al.*, 2005).
The DI treatment was induced on June 16th and soil humidity was stepwise decreased and it took about two weeks until the desired humidity between 20% and 30% was reached.

6.2.4 Measurements

The experimental set-up was used as described in Chapter 3.4.3. T_a was measured as described in Chapter 3.1.1. and PPFD was measured by a LI-190 light sensor (LI-COR Biosciences, USA). The measurements were performed according the protocols described in the Chapters 3.2 and 3.3. The active thermography approach was applied to measure τ, related to LWC and h_{leaf}, and the passive thermography was used to compute the CWSI, related to h_{leaf}.
Measurements were performed on six days during the experimental period – June 15th, June 22nd, June 29th, July 6th, July 13th, and July 20th. At each day, measurements were performed at four time points, which were around 9:00 (morning), 14:00 (midday), 18:00 (evening), and 24:00 (night), except for July 13th, where the four measurements were performed around 9:00 (morning), 12:00 (noon), 14:00 (midday), and 18:00 (evening). For each measurement two replicates of each variety and each treatment, in total 16 boxes, were used. Measurements were always performed in pairs, i.e. a control treatment was measured and the following measurement was performed with a DI treatment of the respective variety. A whole measurement set took about 90 minutes.
One hour before each measurement set, each box was weighed. Weighing was repeated directly before the measurement. With the weight-loss during the time before measurement, the mean water loss rate (WLR) of the plant box was determined as water loss in g per minute and plant box.
In parallel to the thermographic and gravimetric measurements, stomatal conductance was measured several times during the day using a Licor-6400 gas exchange device (LI-COR Biosciences, USA).

6.2.6 Data processing and analyses

Recorded image sequences were processed using the automated MatLab script (see Chapter 3.3.2) to obtain spatial maps of τ. For τ-image processing, τ-thresholds were set at 0 s and 250 s. Additionally, the r-value filter was set to 0.9487, which corresponds to a r^2-value of 0.90 for the underlying exponential function (Equation 2.2.31). Measurement artifacts in the resulting τ-maps, such as the imaging of the wet reference, were removed manually. For further analyses, the images were exported as data matrices. For further simplification and following data analyses, the data matrices were processed with an automated R-script, which eliminated missing pixel-values and stacked the pixel values column-wise.

For statistical analyses SigmaPlot (Systat Software Inc., USA) was used. For correlation analyses in SigmaPlot, the Pearson correlation analysis was performed. Analyses of Variance (ANOVA) were performed in order to evaluate genotypic and treatments effects among the measurements. For pairwise mean value comparison the Tukey test was applied, with a 5% threshold.

6.3 Results

6.3.1 Diurnal dynamics and relationship between the time constant and the crop water stress index

In general, both parameters τ and CWSI showed diurnal dynamics, which were different for different measurement days (Fig. A.6.2 and Fig. A.6.3). In order to understand which environmental and physiological factors drive dynamics in τ and CWSI, two contrasting days were analyzed in more detail. June 15th was the first measurement day and the DI treatment was not yet initiated (Fig. 6.4.1.). In contrast, on July 6th the DI treatment had been initiated since four weeks (Fig. 6.4.4.). Additionally, this day was the hottest and brightest day during the whole experiment. On both days, diurnal behavior of τ and the CWSI was observed.

6.3.1.1 Crop water stress index

On June 15th the CWSI decreased with increasing light-intensity and increasing temperatures (Fig. 6.3.1a-f). The highest light-intensity and the highest T_a were measured at midday, where the CWSI in most cases reached minimum values. The CWSI measured at midday was significantly lower compared to the other measurement time points ($p < 0.05$).

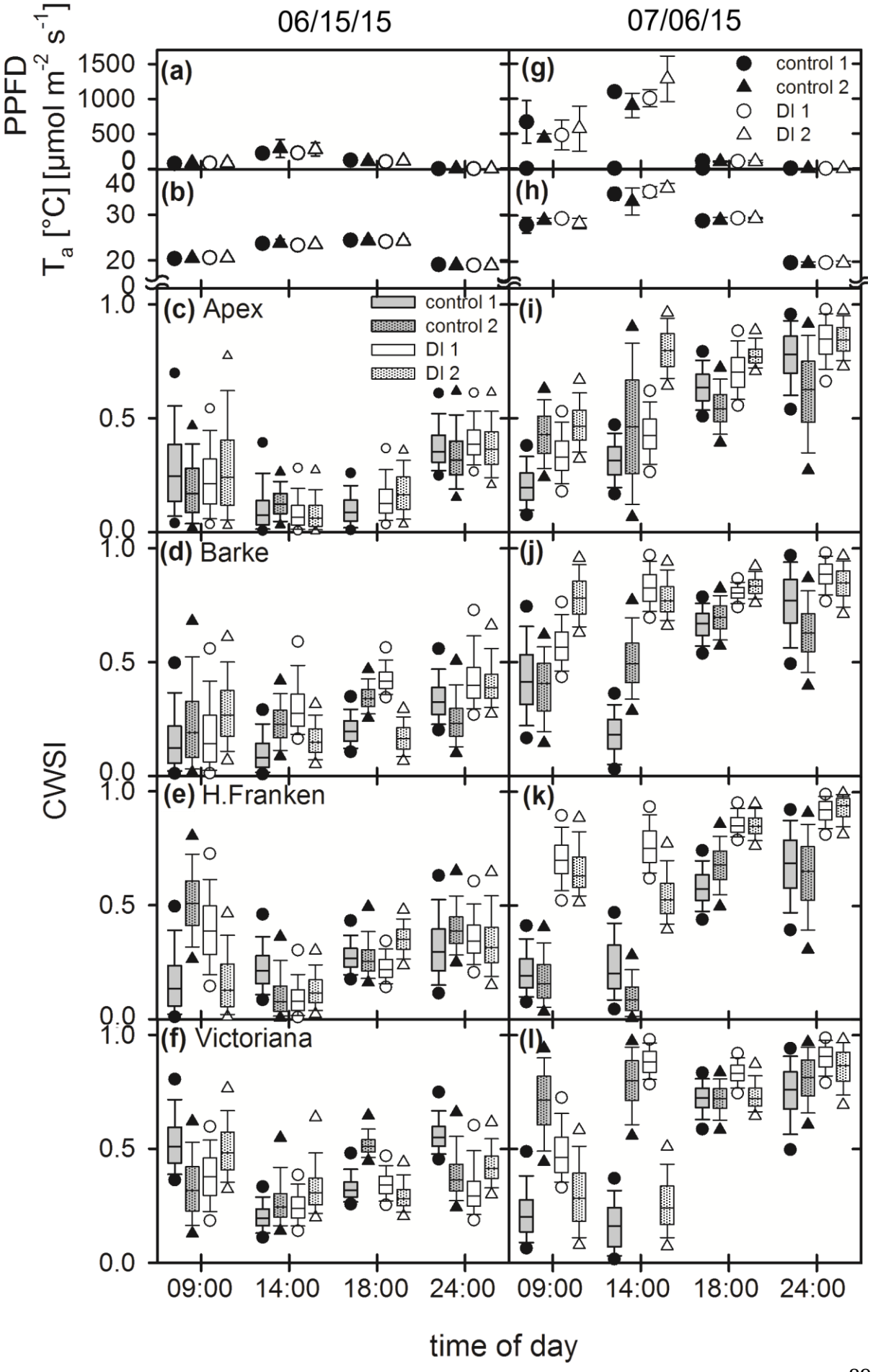
06/15/15
07/06/15
PPFD
T_a [°C] [µmol m^{-2} s^{-1}]
(a)
(b)
(g)
(h)
control 1
control 2
DI 1
DI 2
(c) Apex
(d) Barke
(e) H.Franken
(f) Victoriana
(i)
(j)
(k)
(l)
CWSI
09:00
14:00
18:00
24:00
time of day

Figure 6.3.1: Diurnal course of environmental factors and of the Crop Water Stress Index (CWSI). Measurements performed on June 15th, 2015 presented in the left column, **(a)** to **(f)**, and measurements performed on July 6th, 2015 are presented in right column, **(g)** to **(l)**. **(a)** and **(g)** Daily mean of photosynthetic photon flux density (PPFD) and **(b)** and **(h)** daily mean of ambient air temperature (T_a). Error bars are standard deviation. **(a)** and **(i)** are diurnal courses of the variety Apex, **(c)** and **(j)** are diurnal courses of the variety Barke, **(d)** and **(k)** are diurnal courses of the variety Heils Franken (H.Franken), and **(f)** and **(l)** are diurnal courses of the variety Victoriana. Control treatments are given by closed symbols, grey bars and the gray dot-patterned bars. Deficit irrigation (DI) treatments are given by open symbols, white bars and white dot-patterned bars. For each treatment two replicates are shown. There was a time difference of about one hour between the two replicates. Measurements were always performed in pairs, i.e. a control treatment was measured and the following measurements was performed with a DI treatment. One box represents one image with n pixels, where n was on average 83169 (± 33249) pixels. Boxes give the range in between the 25% and 75% quantile, the whiskers are the 5% and 95% quantiles, and symbols represent potential outliers. Lines within the boxes represent the median.

On July 6th, the mild-drought stress has been induced four weeks before. The diurnal trends of the CWSI for the different treatments showed clear differences (Fig. 6.3.1g-l). Generally, the DI treatments had a significantly higher CWSI throughout the day compared to the control treatments ($p < 0.001$). The lowest CWSI for the control treatment was generally observed for the measurements in the morning and during midday, where light-intensities and T_a were highest. Additionally, the strongest differences in the CWSI were observed between the control and the DI treatments in the morning and at midday. Both, morning and midday measurements differed significantly from measurements in the evening and during night ($p < 0.001$). In the evening and during the night CWSI did not show as large differences between the treatments as during the day, but the DI treatments still showed slightly higher CWSI values compared to the control treatments.

6.3.1.2 Time constant

As observed for the CWSI, τ reached minimum values around midday, where the highest light-intensity and T_a was measured (Fig. 6.3.2). Measurements during the night resulted in significantly higher τ values compared to the other time points ($p < 0.05$). The strongest differences were found between night and midday measurements of τ ($p < 0.001$). Generally, the diurnal trends of τ seemed to be similar for the different varieties and no significant differences were found. The diurnal tendencies were observed on both days June 15th (Fig. 6.3.2a-f) and July 6th (Fig. 6.3.2g-l). However, on July 6th τ values were generally lower compared to June 15th. Additionally, τ was rather low in the morning, as already high light-intensities and high T_a were measured in the morning. It was also observed on both days that τ measurements around midday showed fluctuations, so that partly τ-values were obtained which were comparably high as the night measurements (e.g. Fig. 6.3.2c, f, and k).

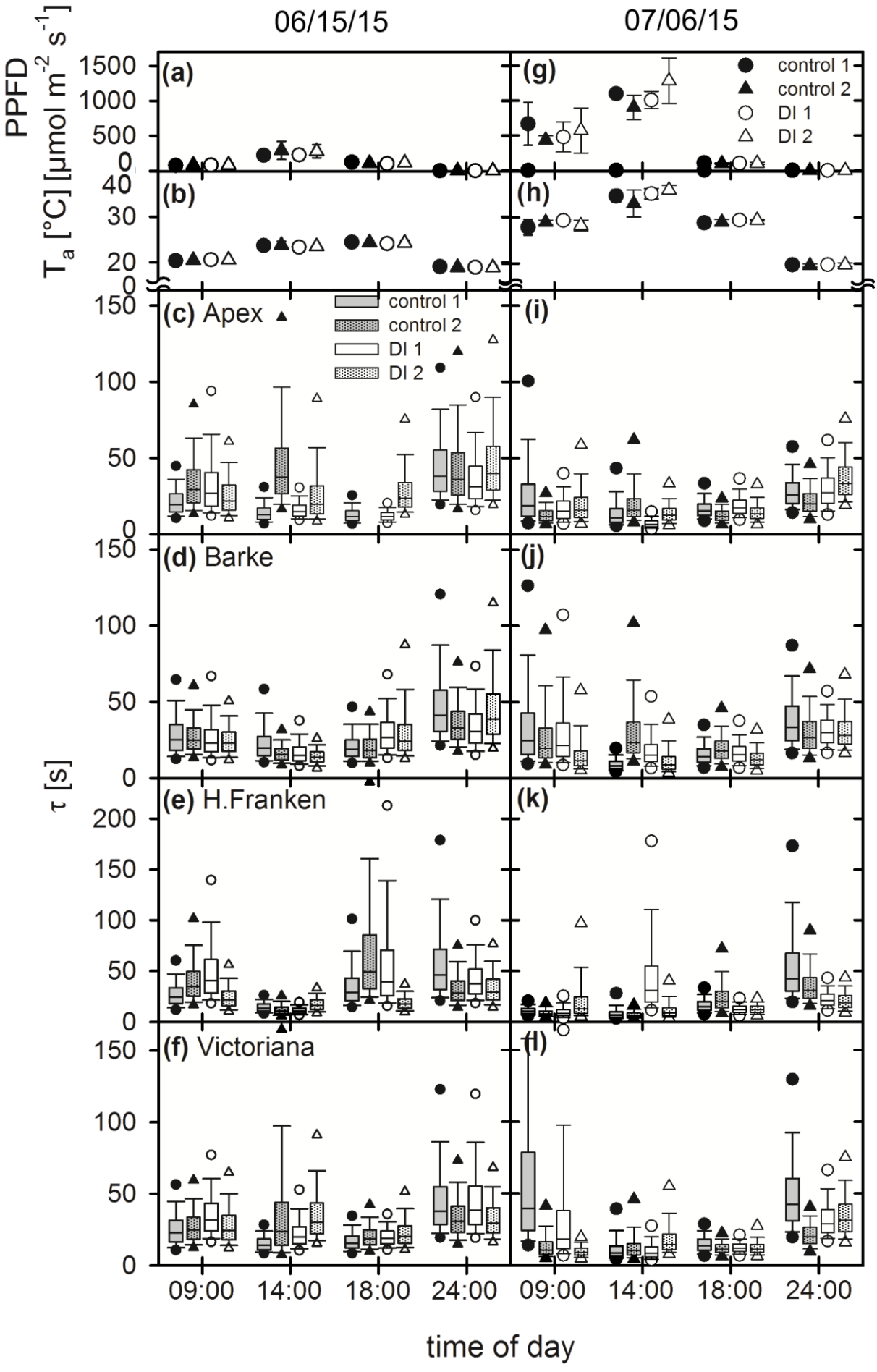
06/15/15
07/06/15
PPFD
T_a [°C] [µmol m^{-2} s^{-1}]
(a)
(b)
(c) Apex
(d) Barke
(e) H.Franken
(f) Victoriana
(g)
(h)
(i)
(j)
(k)
(l)
control 1
control 2
DI 1
DI 2
τ [s]
09:00
14:00
18:00
24:00
time of day

Figure **6.3.2:** Diurnal course of environmental factors and of time constant (τ). Measurements performed on June 15th, 2015 presented in the left column, **(a)** to **(f)**, and measurements performed on July 6th, 2015 are presented in right column, **(g)** to **(l)**. **(a)** and **(g)** Daily mean of photosynthetic photon flux density (PPFD) and **(b)** and **(h)** daily mean of ambient air temperature (T_a). Error bars are standard deviation. **(a)** and **(i)** are diurnal courses of the variety Apex, **(c)** and **(j)** are diurnal courses of the variety Barke, **(d)** and **(k)** are diurnal courses of the variety Heils Franken (H.Franken), and **(f)** and **(l)** are diurnal courses of the variety Victoriana. Control treatments are given by closed symbols, grey bars and the gray dot-patterned bars. Deficit irrigation (DI) treatments are given by open symbols, white bars and white dot-patterned bars. For each treatment two replicates are shown. There was a time difference of about one hour between the two replicates. Measurements were always performed in pairs, i.e. a control treatment was measured and the following measurements was performed with a DI treatment. One box represents one image with n pixels, where n was on average 83169 (± 33249) pixels. Boxes give the range in between the 25% and 75% quantile, the whiskers are the 5% and 95% quantiles, and symbols represent potential outliers. Lines within the boxes represent the median.

6.3.1.3 Spatial distribution of time constant and the crop water stress index within the canopy

Spatial maps of τ and CWSI revealed spatial distribution of these parameters within the canopies (Fig. 6.3.3) In general, τ-images appear more heterogeneous compared to the CWSI images (Fig. A.6.4a and b). On both days, images taken at midday revealed the highest variation in τ and showed thus the highest heterogeneity. Images taken on July 6th showed a higher heterogeneity compared to images taken on June 15th (Fig. A.6.4a and b). Heterogeneity resulted from different τ-distribution within the canopies. Leaf structures, such as the mid-veins were visible and associated with higher τ values compared to the leaf lamina. Additionally, lower layers in the canopy and tissue portions which are deeper within the canopy revealed higher τ-values compared to leaves that protrude of the canopy. Upper canopy portions were more associated with lower τ-values, whereas the lower canopy layers were associated with higher τ-values. On July 6th, upper portions of the canopies were associated with lower τ-values compared to the June 15th and lower parts in the canopy showed comparably high values on both days.

Compared to τ, the CWSI was more homogeneously distributed in the canopy (Fig. 6.3.3 and Fig. A.6.4c and d). Additionally, the CWSI distribution in the canopy showed a more homogeneous distribution on July 6th compared to June 15th.

Images revealed some interesting pattern of τ and the CWSI. For example, the variety Apex showed a high τ on June 15th, whereas the CWSI was very low (Fig. 6.4.3a). A contrary pattern could be observed for example for the variety Victoriana on July 6th (Fig. 6.4.3d).

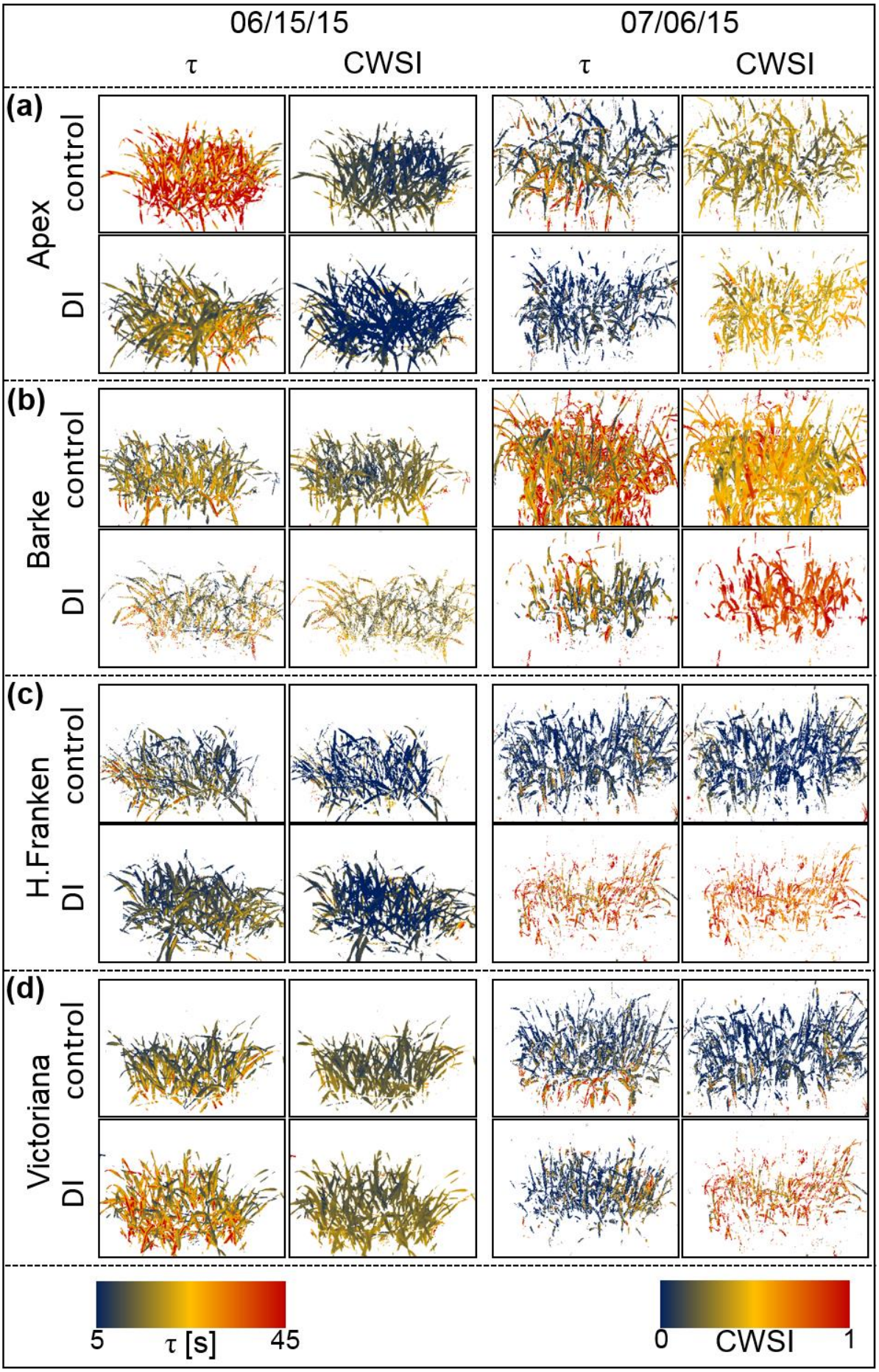
06/15/15
07/06/15
τ
CWSI
τ
CWSI
(a)
Apex
control
DI
(b)
Barke
control
DI
(c)
H.Franken
control
DI
(d)
Victoriana
control
DI
5
τ [s]
45
0
CWSI
1

Figure 6.3.3: Spatial distribution of time constant (τ) and Crop Water Stress Index (CWSI) of midday measurements. Measurements performed on June 15th, 2015 are presented in the two on the left-hand side and measurements performed on July 6th, 2015 are presented in the two columns on the right-hand side. Images of τ are presented in the left column of the respective day and the CWSI is presented in the right column of the respective day. For each variety two rows of images are shown. In the first row an example for a control treatment is given and in the second row an example for the deficit irrigation (DI) treatment is given. **(a)** shows the variety Apex, **(b)** shows the variety Barke, **(c)** shows the variety Heils Franken (H.Franken), and **(d)** shows the variety Victoriana. Both parameter τ and CWSI are represented by color-code as indicated by the color-bars at the bottom. Blue color refers to low values and red color refers to high values.

6.3.1.4 Relationship between the time constant and the crop water stress index

Using the Pearson correlation analysis, the relationship between τ and the CWSI was tested, as well as the relationship of both parameters to T_L-T_a, which is an approximation of heat flux densities and h_{leaf}, (Fig. 6.3.4). On June 15th a weak positive correlation between τ and the CWSI was found ($p > 0.05$), but this correlation could not be observed on July 6th (Fig. 6.3.4a and b). However, if one examines the treatment groups separately, for both groups significant relationships between τ and CWSI could be found (Tab. A.6.1). The relationships seemed to be stronger on June 15th compared to that found for July 6th. While on June 15th both parameters clearly tended to increase together, on July 6th low τ-values were distributed over the whole CWSI range (Fig. 6.3.4b). Low CWSI values were mainly associated with low τ-values, in contrast, low τ-values were not necessarily related to low CWSI values. Particularly for the DI treatments, low τ-values were frequently associated with high CWSI values.

According to the theory τ is related to LWC and h_{leaf}, and the CWSI is related to h_{leaf}. As the measurements were performed at conditions close to free convection, h_{leaf} should be strongly related to T_L-T_a (see Chapter 5). Generally, both parameter τ and CWSI correlated well and positively with T_L-T_a, while the CWSI showed a much stronger relationship to T_L-T_a on both days (Fig. 6.3.4c-f and Tab. A.6.1). On June 15th for both parameters, the relationship to T_L-T_a was less strong compared to July 6th. Particularly for the CWSI, the relationship to T_L-T_a on the 15th of June revealed a clustering, which was related to the time of day, where T_L-T_a reached lower values at midday and in the evening compared to measurements in the morning and at night (Fig. 6.3.4.e). But considering the treatment groups, control and DI treatment, separately, the correlations became stronger on June 15th. The relationship between the CWSI and T_L-T_a was highly significant ($p < 0.001$) for both days and both treatments and on July 6th the relationship revealed a nearly linear relationship ($r > 0.9$) (Fig. 6.3.4f). In contrast, τ showed weaker relationships to T_L-T_a, although these relationships were also significant (Tab. A.6.1).

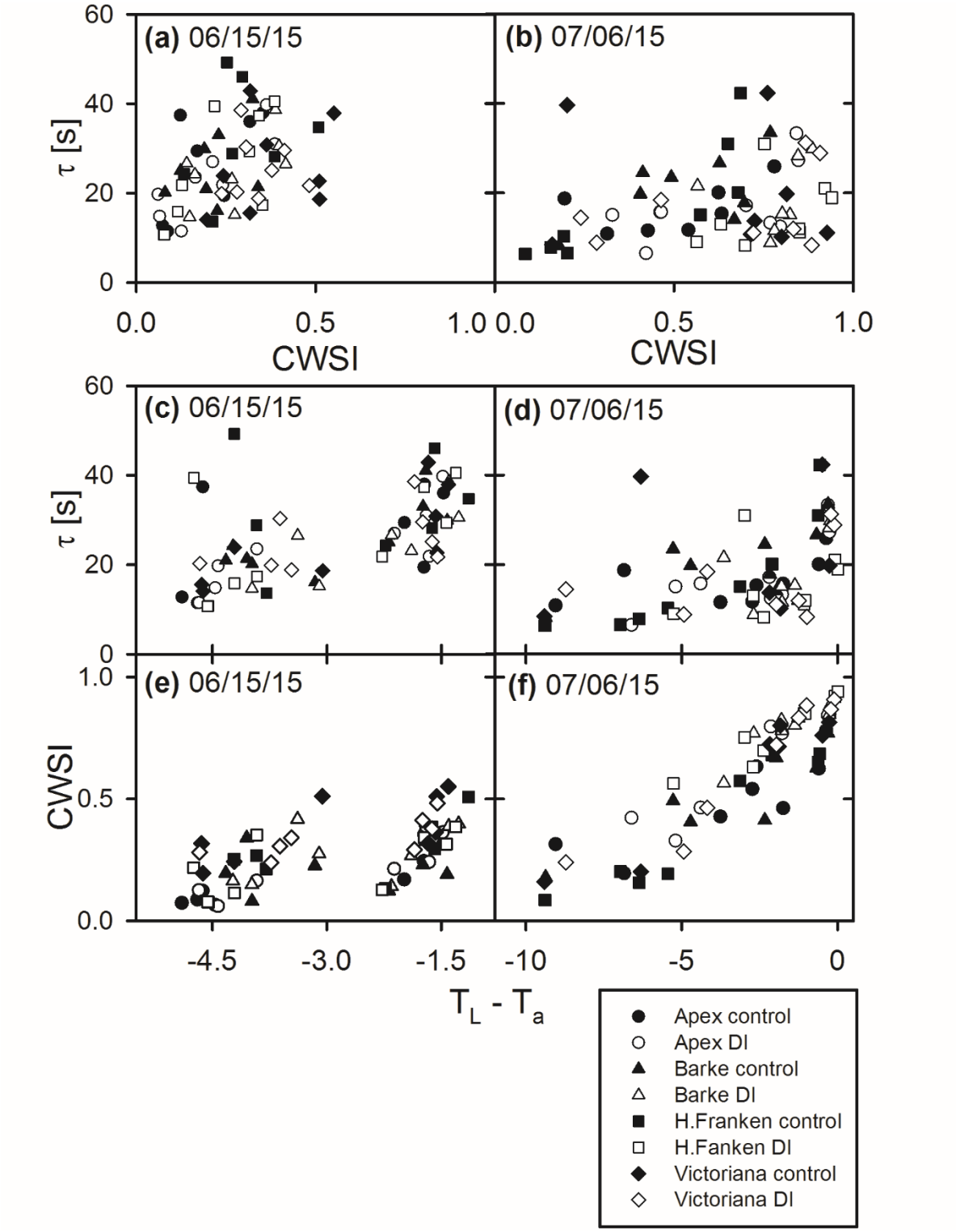

Figure 6.3.4: Relationship between the time constant (τ) and the crop water stress index (CWSI), and the relationship to the difference between leaf temperature to ambient air temperature (T_L-T_a) of the respective parameter. **(a)** Relationship between the diurnally measured τ and CWSI on June 15th, 2015. **(b)** Relationship between the diurnally measured τ and CWSI on July 6th, 2015. **(c)** Relationship between diurnally measured τ and T_L-T_a on June 15th, 2015. **(d)** Relationship between diurnally measured τ and T_L-T_a on July 6th, 2015. **(e)** Relationship between diurnally measured CWSI and T_L-T_a on June 15th, 2015. Cluster on the left-hand side is related to midday and evening measurements, and the cluster on the right-hand side is related to measurements in the morning and at night. **(f)** Relationship between diurnally measured CWSI and T_L-T_a on July 6th, 2015. The variety Apex is indicated by circles, the variety Barke by triangles, the variety Heils Franken (H.Franken) by squares, and the variety Victoriana by diamonds. The respective control treatments are shown by closed symbols and the respective deficit irrigation (DI) treatment is indicated by open symbols.

As observed before, τ measurements at midday and at night showed the strongest differences in the diurnal courses. Additionally, the strongest differences in the CWSI were usually found around midday. Therefore, τ and CWSI were tested for their relationship during the experiment and to WLR by using the Pearson correlation analyses (Fig. 6.3.5). In contrast to the diurnal courses where a positive correlation was found between τ and CWSI, for the data of the whole experimental period significant negative relationships between τ and CWSI were found (Fig. 6.3.5a and b, Tab. A.6.2). Interestingly, the correlation between τ measured at night and the midday CWSI was stronger compared to the correlation between τ measured at midday and the CWSI. However, for the control treatments, no correlation between the midday τ and the CWSI was found, but between the night τ and the CWSI. In contrast, for the DI treatments both midday τ and night τ correlated with the CWSI, where the night τ showed a stronger relationship to the CWSI.

6.3.2 Variety differences

6.3.2.1 Biomass

Plants were harvested and analyzed for biomass parameter, such as FW and LA at two time points, in the early stage of the experiment on July 18th and in the middle of the experiment on July 8th (Fig. 6.3.6).

FW per plant increased during the experiment for both control and DI treatment, except for the DI treatment of the variety Heils Franken, where the biomass was similar at both stages (Fig. 6.3.6a). After the first harvest, all varieties had similar FW except the variety Victoriana, which had a slightly lower FW. However, differences among the varieties were not significant. After the second harvest, the control treatments of each variety had experienced a stronger increase in FW compared to the DI treatments. Among the control treatment, the variety Barke reached the highest FW, whereas Victoriana had the lowest, and Apex and Heils Franken were in between with similar biomass. Among the DI treatment, Apex reached the highest FW, while the other three varieties had a similar FW. Relatively to the control FW, the variety Victoriana had the lowest reduction of FW in response to DI treatment. The strongest reduction of FW was observed for the variety Barke.

Leaf area per plant showed a similar pattern compared to FW per plant (Fig. 6.3.6b). The variety Barke reached the highest LA, but had also the strongest reduction of LA, when comparing the DI treatment to the control treatment. Again, the variety Victoriana had the relative lowest reduction of LA, but had also the lowest LA among all varieties.

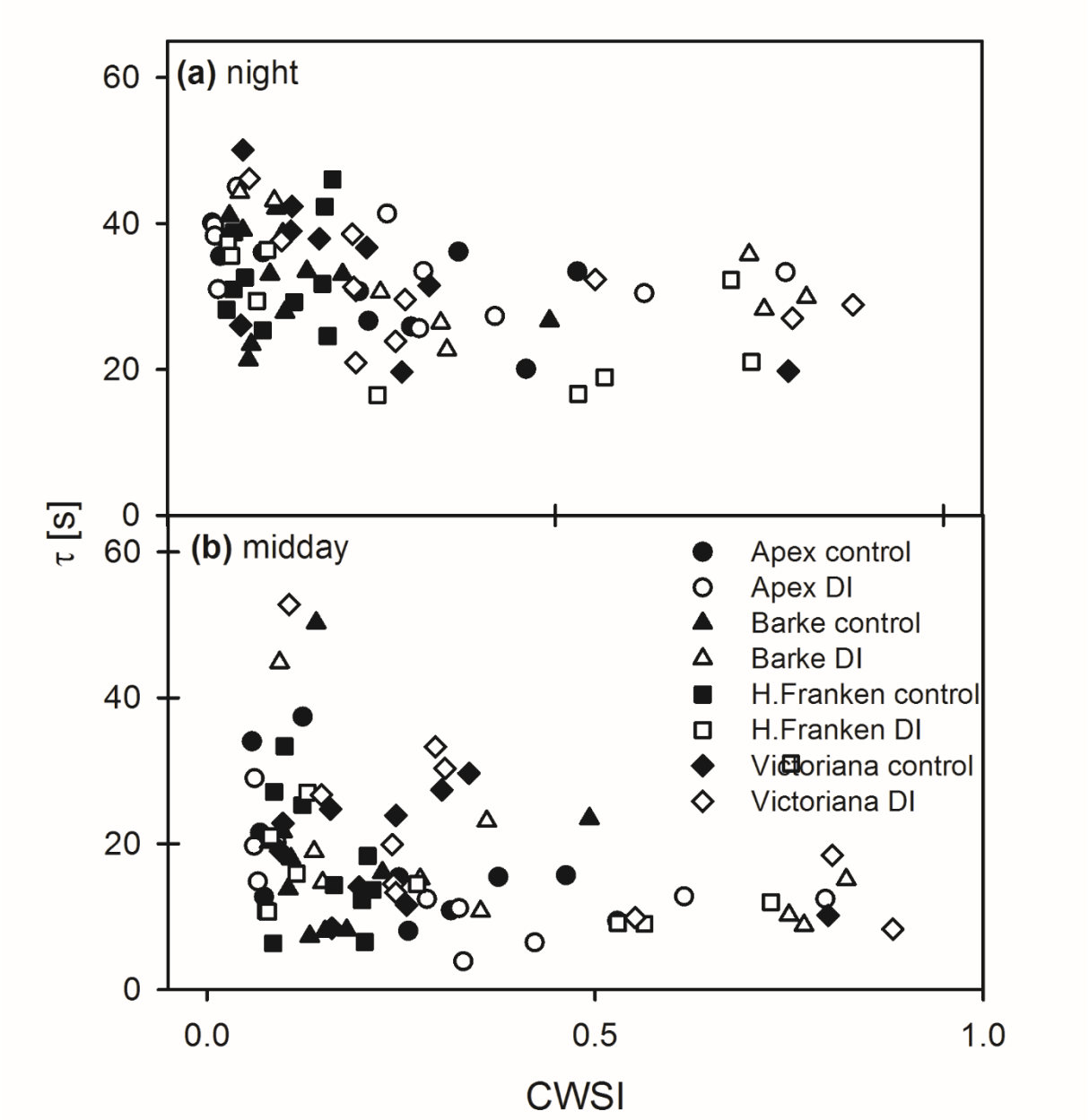

Figure 6.3.5: Temporal relationship between time constant (τ) and the Crop Water Stress Index (CWSI). **(a)** Relationship between τ and CWSI both measured at midday. **(b)** Relationship between τ measured during night and CWSI measured at midday. The control treatments are given by closed symbols and the deficit irrigation (DI) treatments are given by open symbols. The variety Apex is shown by circles, the variety Barke by triangles, the variety Heils Franken (H.Franken) by squares, and the variety Victoriana by diamonds. Each point represents one measurement. Measurements performed on 15th June, 22nd June, 29th June, 6th July, and 20th July are presented. Data obtained on 13th July are excluded, because no measurements were performed at night.

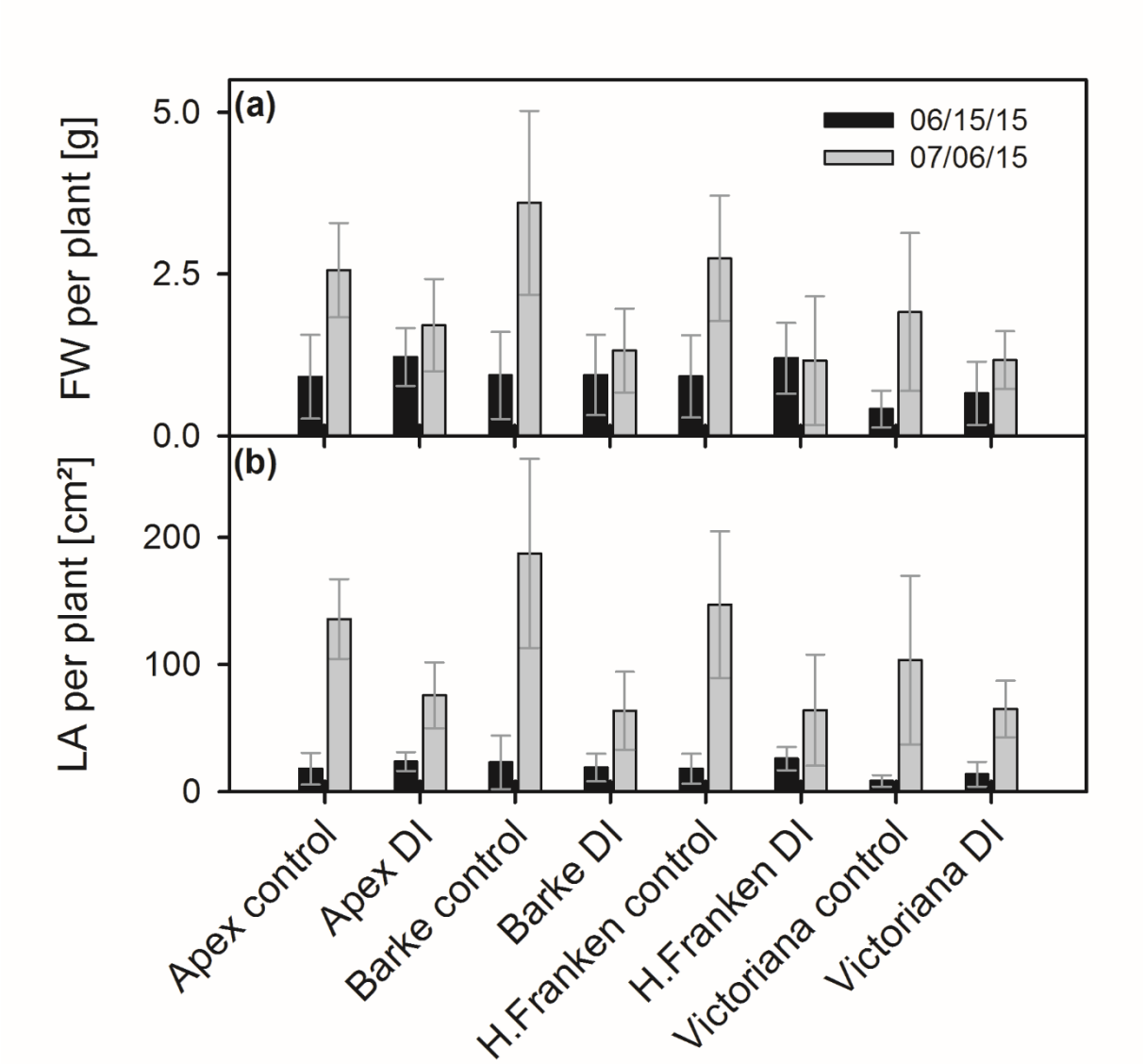

Figure 6.3.6: Biomass parameters of each variety. Biomass parameter of the varieties Apex, Barke, Heils Franken (H.Franken), and Victoriana were determined at two time points, on June 15th, 2015, related to non-stress conditions and July 6th, 2015, related to stress conditions. Biomass parameter were separately determined for the control treatment and the deficit irrigation (DI) treatment. **(a)** Fresh weight (FW) per plant, and **(b)** leaf area (LA) per plant. For each variety and each treatment, three plants from two different boxes were analyzed, respectively.

6.3.2.2 Water loss rates and stomatal conductance

To evaluate the transpiration behavior throughout the experiment, WLR and g_s was measured (Fig. 6.3.7). Particularly WLR showed a temporal behavior with changing maxima (Fig. 6.3.7c), whereas maximum values of g_s remained relatively constant during the whole experiment (Fig. 6.3.7d). WLR was clearly affected by light-intensity (Fig. 6.3.7a) and T_a (Fig. 6.3.7b). On the first two measurement days where light-intensity and T_a was relatively low, WLR values were also comparatively low (Fig. 6.3.7c). On June 29th and July 6th, which were the brightest and hottest days, WLR increased substantially and reached values which were threefold higher compared to the first two measurement days. On the last two measurement days, PPFD and T_a decreased again and with it WLR. The measurements of g_s did not reveal a comparable course during the experiment (Fig. 6.3.7d). The measured maximum values of g_s remained nearly constant during the experiment.

However, differences between the control and the DI treatment could be found for both, WLR and g_s. On the first two days, WLR and g_s remained in the same range for the control and the DI treatment, respectively (Fig. 6.3.7c and d). But on June 29th and July 6th clear differences between the two treatments could be found. In comparison to the control treatment, the DI treatment showed suppressed WLR and g_s, resulting in a clustering of the DI treatments at lower WLR and g_s values, respectively. Moderate differences between the two treatments were also found at the last two measurement days, particularly for the WLR measurements. While WLR for the DI treatment was still suppressed on both days July 13th and July 20th, the difference in g_s was only visible on July 13th.

By observing the WLR, differences between the varieties were visible as trend, but hardly any differences between the varieties could be found by observing g_s. Particularly on the both hot and bright days (June 29th and July 6th), the variety Apex reached higher WLR compared to the other varieties for both, control and DI treatment (Fig. 6.3.7c). The differences between the other varieties was not that clear, but by tendency the varieties Barke and Victoriana reached lower WLR values compared to the varieties Apex and Heils Franken.

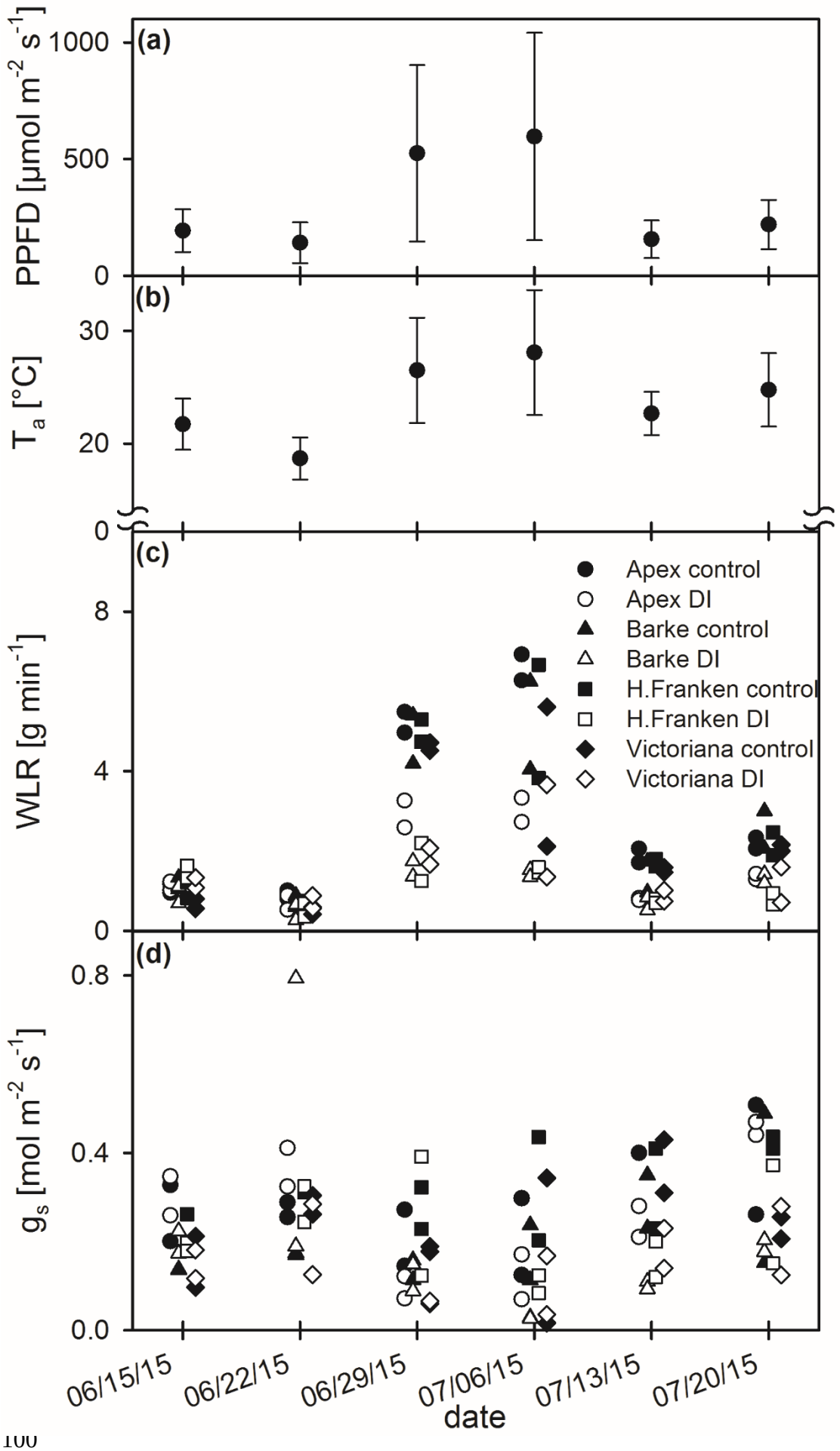
(a)
PPFD [µmol m-2 s-1]
1000
500
0
(b)
Ta [°C]
30
20
0
(c)
WLR [g min-1]
8
4
0
Apex control
Apex DI
Barke control
Barke DI
H.Franken control
H.Franken DI
Victoriana control
Victoriana DI
(d)
gs [mol m-2 s-1]
0.8
0.4
0.0
06/15/15
06/22/15
06/29/15
07/06/15
07/13/15
07/20/15
date

100

Figure 6.3.7: Seasonal measurements of environmental conditions, water loss rate per plant box and stomatal conductance (g_s). **(a)** Mean photosynthetic photon flux density (PPFD). **(b)** Mean air temperature (T_a). Error bars are the standard deviation of the complete day. **(c)** Daily maximum water loss rate per plant box (WLR). Closed symbols refer to control treatment and open symbols refer to deficit irrigation (DI) treatment. The variety Apex, a water-spending variety, is indicated by circles. Barke, a variety that switches between a water-spending and a water-saving strategy, is indicated by triangles. Heils Franken (H.Franken), also a variety that switches between a water-spending and a water-saving strategy, is indicated by squares. Victoriana, awater-saving variety, is indicated by diamonds. **(d)** Daily maximum of g_s. Meaning of symbols as in (c). Each symbol represents a single plant box.

6.3.2.3 Variety differences in the time constant and the crop water stress index

As described in section 6.4.1. τ and the CWSI showed diurnal dynamics, which were different between June 15th and July 6th, particularly for the CWSI (Fig. 6.3.8).

On June 15th the variety Apex had τ values which were among the lowest in the morning and in the evening (Fig. 6.3.8a). At midday τ was in the midrange and partly reached the diurnal maximum. For the variety Barke the measured τ values were always in the midrange and nothing conspicuous was observed. The variety Heils Franken showed τ values in the morning and in the evening which were among the highest. However, at midday Heils Franken showed the lowest τ values compared to the other varieties. For the variety Victoriana, as well high as low τ values were observed in the morning and at midday. In the evening τ was comparatively low. On July 6th (Fig. 6.4.8b), τ was generally lower compared to June 15th. Throughout the day, the variety Apex showed relatively stable τ values, which were in the midrange of the measurements. The variety Barke showed a similar behavior compared to the variety Apex, but also showed τ values which were among the highest in the morning and at midday. The measurements of the variety Heils Franken revealed the lowest τ values in the morning and at midday, but in the evening τ was found in the midrange. The variety Victoriana again showed both high as well low values, particularly in the morning and at midday. In the evening the values were comparable to the other varieties.

On June 15th, the CWSI did not exceed 0.5 (Fig. 6.3.8c). At all daytimes, the CWSI measured for the variety Apex tended to comparatively low values. Except in the morning, the CWSI obtained for the variety Barke tended to be among the highest values. The variety Heils Franken showed as well high as low CWSI values throughout the day. At all measurement time points, the CWSI of the variety Victoriana reached the highest values compared to the other varieties. On July 6th, the DI treatments showed clearly higher CWSI values compared to the control treatments (Fig. 6.3.8d). The CWSI obtained for the variety Apex seemed to be in the midrange for both control and DI treatments and remained below 0.5 in the morning and at midday, except for one DI treated canopy. In contrast, the variety Barke showed CWSI values which were spread over the whole range of the measured CWSI values. Probably the strongest difference

between the control and the DI treatments were found for the variety Heils Franken. While the control treatments showed the lowest CWSI values, the DI treatments were among the highest. However, the highest CWSI values were reached by the variety Victoriana. Comparable to the variety Heils Franken, the variety Victoriana showed very high but also very low CWSI values, particularly at midday.

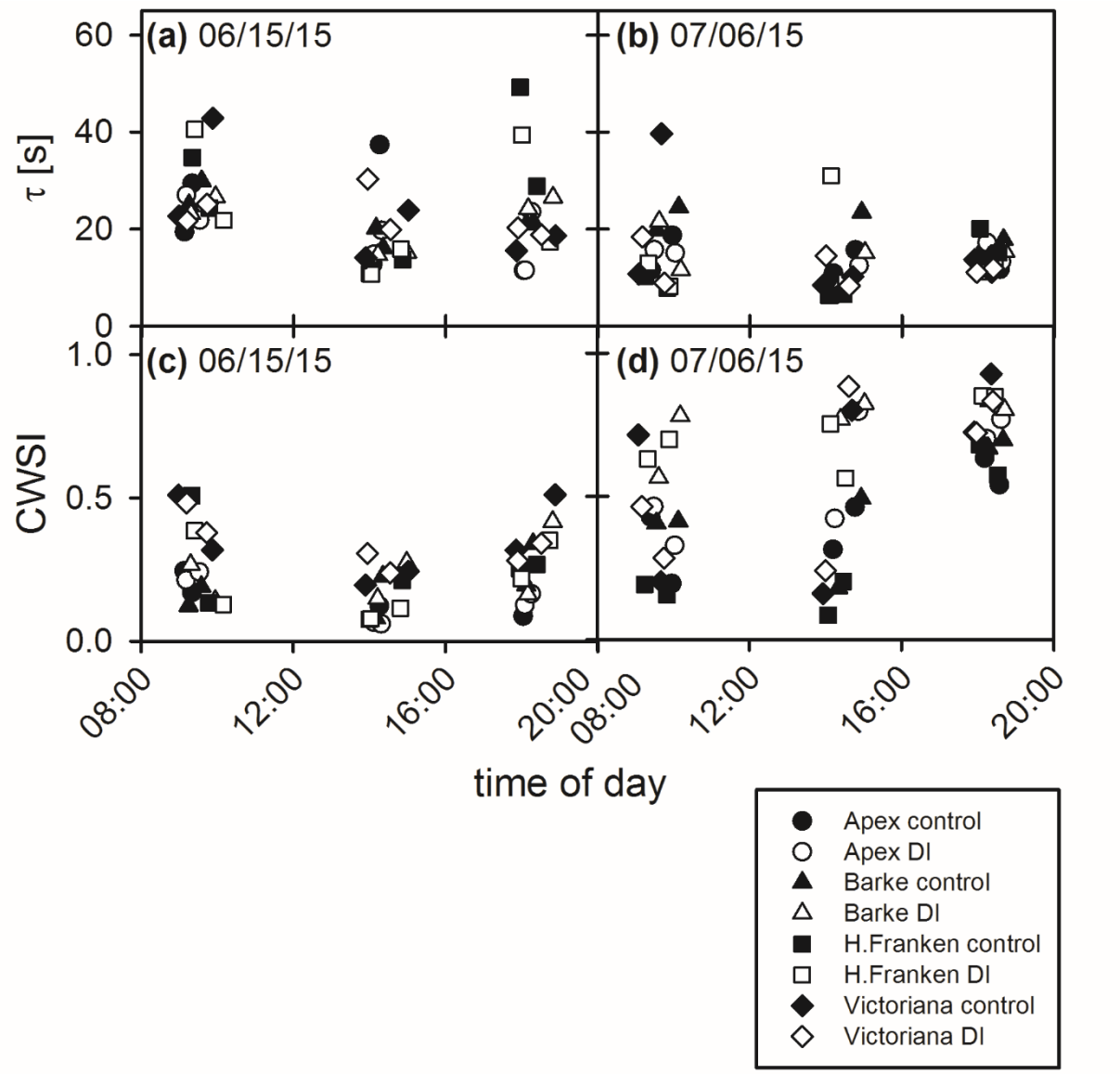

Figure 6.3.8: Median values of the diurnal trends of the time constant (τ), and the crop water stress index (CWSI). **(a)** and **(c)** are measurements of the respective parameter on the 15th of June. **(b)** and **(d)** are measurements of the respective parameter on the 6th of July. Control treatments are represented by closed symbols, deficit irrigation (DI) treatments are represented by open symbols. The variety Apex is indicated by circles, the variety Barke by triangles, the variety Heils Franken (H.Franken) by squares, and the variety Victoriana by diamonds.

6.4 Discussion

The active thermography approach was successfully transferred from single leaf measurements in the laboratory to canopy measurements in the greenhouse. It was extensively tested, whether the measurement of τ can be used to detect stress responses to a deficit irrigation. Additionally, diurnal dynamics of τ were compared with the diurnal dynamics of the CWSI, which is a commonly used parameter to detect drought stress. While the CWSI allowed a direct stress detection, τ seemed to be unaffected. However, considering both parameters in parallel allowed the derivation of different stress-avoidance strategies for a mild drought- stress.

6.4.1 Diurnal dynamics

6.4.1.1 Diurnal dynamics of the crop water stress index

As observed during this experiment, the relationship between T_L-T_a and leaf heat fluxes are affected by several environmental, physical, and physiological factors and therefore can differ between different time points during the day (Fig. 6.3.4.e). To overcome this effect, the CWSI was developed, which is a normalization of the leaf heat fluxes (Jackson and Idso, 1981). The CWSI was shown to be strongly related to changes in transpiration and h_{leaf} (Jones, 1999*b*), which was also confirmed by the strong relationship between the CWSI and T_L-T_a (Fig. 6.3.4). In this experiment it was demonstrated that the CWSI shows a diurnal behavior with lowest values around midday, particularly for the control treatments (Fig. 6.3.1). Usually, PPFD and T_a reached a maximum around midday which affects stomatal opening and closure and thus transpiration (Hall and Kaufmann, 1975; Mott *et al.*, 1997; Roelfsema and Hedrich, 2005; Pieruschka *et al.*, 2010). Consequently, the PPFD and T_a driven transpiration results in a low CWSI.

On July 6th plants had been exposed to water-limiting conditions for already four weeks. Additionally, the hot and sunny conditions during this day intensified the drought stress effect. It was observed that the CWSI was clearly increased for the DI treatments compared to the control treatments. On both days, fluctuations around midday were found, where relatively high CWSI values were also measured for the control treatments. On the one side, transpiration is suppressed by drought (Medrano *et al.*, 2002; Flexas *et al.*, 2006; Chaves *et al.*, 2009) and on the other side, g_s measurements revealed a midday-depression (Fig. A.6.5), which occurs in response to hot and dry conditions in order to reduce water loss (Olioso *et al.*, 1996). In both cases, measurements result in an increased CWSI indicating that the CWSI is not necessarily related to stress alone, but is affected by diurnal dynamics in the transpiration behavior of

plants. Therefore, a single measurement of the CWSI may lead to a misinterpretation regarding the stress situation of plants.

6.4.1.2 Diurnal dynamics of the time constant

As demonstrated in the Chapters 4 and 5, τ responses to both LWC and h_{leaf}. Therefore, a low τ can be result of dehydration, or increased h_{leaf}, or a combination of both. It was observed that τ, comparable to the CWSI, showed the lowest values at midday and the highest values at night (Fig. 6.3.2). During midday, PPFD and T_a reached maximum values, which increases transpiration. Increased transpiration results in an increased h_{leaf}. Additionally, barley is an anisohydric plant species that allows relatively strong tissue dehydration in order to keep transpiration and photosynthesis high (Tardieu and Simonneau, 1998; Sade *et al.*, 2009, 2012). Thus, low τ values at midday are a result of increased h_{leaf} and plant tissue dehydration. In contrast, high τ values at night refer to a tissue rehydration and a low h_{leaf} because no transpiration occurs. Also on the 6th of July τ showed a comparable diurnal pattern and no clear differences were found between the control and the DI treatments. Plants which are exposed to water-limiting conditions transpire less (Medrano *et al.*, 2002; Flexas *et al.*, 2006; Chaves *et al.*, 2009) so that h_{leaf} for these plants have to be relatively low in comparison to plants which are not stressed due to water-limitation. However, the DI treatments showed comparably low τ-values compared with the control treatments, indicating that τ alone cannot be used to differentiate between control and DI treatments. As transpiration and tissue dehydration is strongly coupled, control plants show a low τ, which is in this case a mixture of increased h_{leaf} and decreased LWC. The plants in the DI treatments will also keep transpiration as high as possible to drive photosynthesis and, therefore, will dehydrate stronger compared to the control treatments as the mobilization of water from the soil is increasingly reduced and the internal water storage decreases (Levitt, 1972). Consequently, both treatments show low τ values, but the relative contribution of h_{leaf} and LWC to τ, respectively, is different.

6.4.1.3 Midday fluctuations and the relationship between the time constant and the crop water stress index

In anisohydric plants, such as barley, transpiration is inevitably coupled with plant dehydration (Tardieu and Simonneau, 1998; Sade *et al.*, 2009, 2012). Thus, the findings that the diurnally measured τ and CWSI showed a negative relationship could be expected (Fig. 6.3.4a and b). Additionally, it was partly observed that canopies showed fluctuations of τ and the CWSI around midday (Fig. 6.3.3). Particularly, after the mild drought stress induction the relationship

between τ and the CWSI became weaker, because low CWSI were related to low τ values, but low τ values were not necessarily related to low CWSI values. High CWSI around midday indicates a midday-depression, where transpiration is suppressed (Fig. A.6.5) in order to reduce water loss, which is necessary to prevent too strong dehydration (Martin and Ruiz-Torres, 1992; Tardieu and Simonneau, 1998; Flexas *et al.*, 2006; Chaves *et al.*, 2009). If LWC would decrease below a certain threshold the risk of xylem embolism increases. Stomata have to close in order to save water and to enable rehydration of the leaves, which avoids xylem embolism and preserves the water potential gradient that is required to transport water through the plants (Cowan, 1972; Scoffoni *et al.*, 2008). The dehydration results in a low τ and thus a combination of low τ and high CWSI occurs, which indicates that the plants are not transpiring at the moment but must have transpired before, because the plant is dehydrated. In the opposite case, plants can rehydrate during the midday-depression, because the water loss is reduced (Olioso *et al.*, 1996), which then results in a high τ. After rehydration, plants can transpire again resulting in a low CWSI. Studies have demonstrated that g_s and LWC show diurnal oscillation, where g_s and LWC show time-shifted amplitudes (Cowan, 1972; Hennessey and Field, 1991). These fluctuations in LWC and transpiration were tracked by the diurnal dynamics of τ and the CWSI.

On the temporal scale, the relationship between τ and the CWSI switches to a positive correlation, which is particularly due to the DI treatments and the midday fluctuations (Fig. 6.3.5), where a low τ reflects dehydration and a high CWSI reflects suppressed transpiration. Similar observations were done by Cohen *et al.* (2005), who found a positive correlation between the seasonal CWSI and the leaf water potential, both measured at midday. In the present work, it was found that τ measured at night showed a stronger correlation with the midday CWSI than τ measured at midday. Particularly plants of the DI treatments dehydrated stronger compared to the control plants, so that the plants were not fully rehydrated at night, which then results in a lower τ compared to the control plants that were presumably fully rehydrated. However, it should be argued that this seasonal relationship between τ and the CWSI is only valid under certain conditions, namely if severe dehydration induces stomatal closure (Cowan, 1972; Syvertsen, 1982; Martin and Ruiz-Torres, 1992; Tardieu and Simonneau, 1998), so that a low τ is accompanied by a high CWSI.

The relationships between τ and the CWSI found in this work indicate that single measurements of τ as well as of the CWSI for the assessment of plant-water relations require careful interpretation. On the one hand, τ does not allow a clear differentiation between control and DI treatments. On the other hand, the CWSI represents only a snapshot related to dynamics of transpiration, which is not necessarily related to stress, but may reflect a midday-depression where

stomata transiently close in order to allow the plants to rehydrate. Therefore, the interpretation of the CWSI can highly benefit from the measurement of τ, which allows an estimation of the hydration status.

6.4.2 Spatial distribution of the time constant and the crop water stress index in the canopy

On the single leaf scale, spatial maps of τ illustrated regions of thermal inertia, which are closely linked to leaf structures containing a relatively high amount of water, such as veins (Chapter 4 and 5). Also spatial maps of canopy-τ allow the localization of high water content leaf structures and regions, where a comparatively higher biomass is accumulated (Fig. 6.3.3). For example, leaf veins are visible and appear as regions with a higher τ compared to leaf lamina. In the previous Chapters it was shown that this is due to a higher amount of water, which is accumulated in the veins (Sack and Scoffoni, 2013). Additionally, lower layers in the canopies are generally associated with higher τ-values than the upper layers of the canopy. In the lowest layers, probably the most biomass is accumulated, which is due to thick and high water containing stems. Additionally, stems have negligible transpiration, so that the heat transfer is rather low, which further results in high τ values. High water content and low heat transfer indicates a canopy region with a high thermal inertia and thus with a poor heat dissipation (e.g. Finnigan (2000)). Interestingly, the CWSI does not show such strong differences within the canopy (Fig. 6.3.3 and Fig. A.6.4), indicating also relatively low temperatures in the lower canopy region. This is most likely related to accumulation of water vapor originating from leaf transpiration but also from soil evaporation. In contrast to the lowest layers of the canopy, τ values in the upper canopy region were comparatively low, particularly for leaves protruding out of the canopy. Leaves have a relatively low water content compared to stems, and have usually substantial transpiration decreasing h_{leaf} and potentially LWC. Both of which are factors that results in a decrease of τ. Additionally, leaves protruding out of the canopy are surrounded by the ambient air, which increases the heat exchange with the environment, because the boundary layer is much thinner compared to leaves that are deeper in the canopy, where, for example water vapor concentration is much higher, which increases the boundary layer.

6.4.3 Variety differences

The comparison between τ, the CWSI, WLR and biomass production revealed different drought-stress avoidance strategies of the four barley varieties. According to Levitt (1972), different strategies for drought stress resistance are conceivable. Plants with a water-spending

strategy use as much water as possible as long as it is available, which results in a high biomass production. Also under water-limiting conditions the water uptake rate from the soil is kept high to further produce biomass. For short-term and mild drought this is a preferable strategy, but as soon as the stress is severe, this strategy results in a drastic reduction of the productivity, because the soil water was reduced before (Bodner *et al.*, 2015). In contrast, plants with a water-saving strategy do not use as much water as available. Usage of internally stored water is preferred over the uptake of water from the soil, which results in a stronger dehydration of the plants (Tardieu and Simonneau, 1998; Sade *et al.*, 2012) and finally saves soil water. This strategy is preferable for severe drought stress, because the soil water extraction is modulated and thus used more efficiently (Blum, 2009).

The variety Apex produced a high amount of biomass under non-stress conditions, where sufficient water was available (Fig. 6.3.6). However, also under water-limiting conditions this variety still showed a relatively high biomass production in comparison to the other varieties. Additionally, the variety Apex reached the highest WLR in comparison to the other varieties as well under non-stressed as under stressed conditions (Fig. 6.3.7). The CWSI was comparably low, whereas τ-values ranged in the middle of all varieties (Fig. 6.3.8). These results indicate that the variety Apex is a water-spending variety, which maintains a high transpiration rate in order to run photosynthesis and does not allow a strong dehydration. As the DI treatments in this experiment was kept at a soil moisture range between 20% and 30%, plants were never exposed to a severe drought for a longer period, so that always little amounts of water were accessible for the plants.

The variety Victoriana showed a comparatively low biomass production under control conditions, but also had a comparable high biomass under stress conditions when compared to the other varieties (Fig. 6.3.6). Among all varieties, Victoriana had the lowest biomass reduction due to the mild drought stress. The WLR values for the control treatment were comparatively low, but for the DI treatments the WLR was comparatively high compared to the varieties Barke and Heils Franken, but still low in comparison to the variety Apex (Fig. 6.3.7). As well for τ as for the CWSI, Victoriana showed a high fluctuation with as well high as low values, where the low CWSI values still were comparably high compared to the other varieties (Fig. 6.3.8). Fluctuating τ values indicate a permanent de- and rehydration of the plants, which frequently induces stomatal closure. These results indicate that the variety Victoriana is a water-saving variety. Although sufficient water was available, low transpiration rates were maintained and the water was primarily used from internal storages, inducing a strong dehydration and subsequently stomatal closure accompanied by rehydration.

The variety Barke seemed to show a mixture of both strategies. Under non-stressed conditions, Barke had the highest amount of biomass, but also showed the strongest biomass reduction in response to water-limitation (Fig. 6.3.6). However, biomass for the DI treatments was comparable to the biomass of the other varieties. Additionally, a similar behavior was found in the WLR (Fig. 6.3.7). Under non-stress conditions, WLR was comparatively high but was strongly suppressed by water-limitation. Additionally, the variety Barke showed the strongest reduction in the WLR and biomass production compared to the other varieties. Also the CWSI showed a large difference between the control and the DI treatments indicating that this variety switches between a water-spending strategy under non-stress conditions and a water-wasting strategy under water-limiting conditions (Fig. 6.3.8). In contrast, for τ nothing obvious could be observed and values ranged in the middle of the measured τ-range for all varieties. With respect to the dynamics of the CWSI, and thus h_{leaf}, the τ measurements revealed that the hydration state is kept rather high under non-stress conditions whereas under water-limiting conditions the plants dehydrate much stronger compared to the control treatments. In biomass production Barke was the most efficient variety under non-stress conditions. Although the biomass was strongly reduced in response to water-limitation, the produced biomass under water-limiting conditions was comparable to the other varieties.

The variety Heils Franken showed a similar behavior as the variety Barke and seemed also to switch between the water-spending and water-saving strategy, because the CWSI showed similar dynamics (Fig. 6.3.8). However, the variety Heils Franken reached the lowest τ values among all varieties, indicating that this variety does not only transpire at high rates, as indicated by the CWSI, but also allows a strong dehydration. In comparison to the variety Barke, Heils Franken produced less biomass and was thus less effective. Additionally, the produced biomass under water-limiting conditions seemed to be the lowest among all varieties. These results indicate that the variety Heils Franken is a rather inefficient variety and requires high amounts of water to produce an appropriate biomass.

6.4.4 Conclusion

In this Chapter, it was demonstrated that the active thermography approach is applicable to greenhouse conditions and on the canopy level. Although, τ was found to be highly sensitive to environmental parameter affecting the heat transfer, such as wind (Chapter 5), the usage of the method is possible and gives consistent results, when the environmental parameters are controlled properly. In this experiment, an experimental set-up was chosen, which excludes the impact of wind on the canopy. Wind would induce canopy movements and finally would make

the measurements technically impossible. Under these experimental conditions, free convection is most likely because no wind occurs, which induces forced convection. As demonstrated in Chapter 5, under free convection τ is more sensitive to transpiration than under forced convection. Therefore, τ has to be considered to be a measurement of both, LWC and h_{leaf}. It was demonstrated that τ and the CWSI show a diurnal behavior which is driven by transpiration and accompanied dehydration. But the CWSI or τ alone do not reflect the overall plant performance and single measurements cannot provide appropriate information about the overall plant-water-relations. The parallel consideration of the CWSI and τ revealed different mild drought-stress stress avoidance strategies of the plants. Conclusively, the interpretation of the CWSI highly benefits from the inclusion of τ, whereas the CWSI is indispensable for the interpretation of τ. As demonstrated in this experiment and in previous studies, LWC and transpiration are fluctuating throughout the day (Cowan, 1972; Hennessey and Field, 1991) and, therefore, diurnal assessment of both parameters τ and CWSI is necessary for the full comprehension of the plant-water relations.

7. The dehydration index

The crop water stress index (CWSI) is mainly affected by transpiration and thus, under certain circumstances, by the leaf heat transfer coefficient (h_{leaf}). The time constant (τ), however, is affected by the leaf water content (LWC) and h_{leaf} (Chapter 4 and 5). The assessment of the overall plant-water relation measuring only one of these parameters at a single time point is questionable, because both parameters underlie physiological and physical dynamics and furthermore are coupled to each other. In Chapter 6, it was demonstrated that the CWSI is not necessarily related to stress but may also reflect common physiological responses, such as the midday depression, which occur under bright and hot conditions. By contrast, τ provides useful information on LWC but is also affected by h_{leaf} and thus needs the CWSI for an adequate interpretation. Therefore, the single measurement may lead to misinterpretation of the respective plant-water status, which can be mitigated by considering both parameters in parallel. Conclusively, combining both parameters in one index seem convenient. In the following, a first attempt of such an index is introduced. The dehydration index (DHI), an empirically derived index, combines the CWSI with relative diurnal changes of τ.

7.1. Calculation of the dehydration index

The DHI is based on Equation 2.2.32 (Chapter 2.2.8), where the product of τ and h_{leaf} provides the leaf heat capacity per unit area ($C\ A^{-1}_{leaf}$) that is proportional to LWC. Because modeling of h_{leaf} requires some calibration measurements (Chapter 5), the CWSI was used as an approximation for h_{leaf}. Following assumptions were made:

i. The CWSI reflects changes in leaf heat fluxes and thus has to be proportional to h_{leaf}
ii. If CWSI equals 0, h_{leaf} is at its maximum, and if CWSI equals 1, h_{leaf} is at its minimum
iii. τ measured at night (τ_{night}) refers to fully hydrated plants and to minimum h_{leaf}
iv. a decrease in τ measured at any time during the day (τ_t) refer to either decreased LWC, increased h_{leaf} or both

The DHI was finally calculated as follows:

$$\frac{dehydrated}{hydrated} \sim DHI = 1 - \left(\frac{\tau_{night} - \tau_t}{\tau_{night}}\right) \times CWSI \qquad \text{Equation 7.1.1}$$

The τ-ratio describes the relative deviation of τ during the day from the fully hydrated τ (τ_{night}). Here, 1 refers to 100% hydration and any value below 1 refers to a deviation expressed as a percent with respect to the fully hydrated state. The higher the CWSI the more the changes of

τ are driven by dehydration and in opposite direction, the lower the CWSI the more are τ-changes driven by h_{leaf}. Thus, the multiplication of the τ-ratio with the CWSI provides the relative amount of dehydration driven changes. By subtracting this term from 1, the DHI describes the deviation from a fully hydrated state.

7.2. Diurnal and temporal trends of the dehydration index

The use of the DHI illustrates differences between the both treatments, which were a control and a deficit irrigation (DI) treatment, and between the four barley varieties (Fig. 7.1.1 and Fig. 7.1.2), which were difficult to observe by considering τ or the CWSI alone.

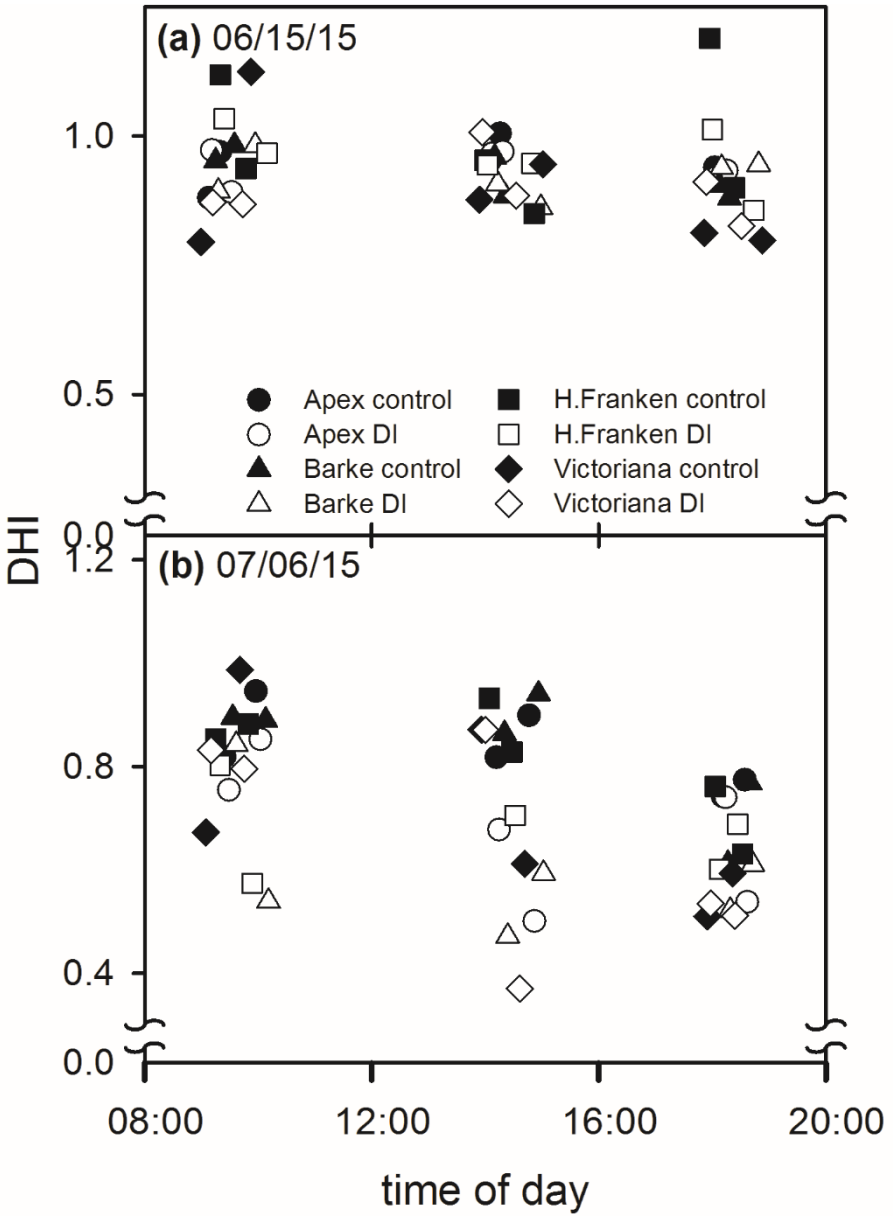

Figure 7.1.1: Diurnal trends of dehydration index (DHI). **(a)** DHI calculated for June 15th, 2015. **(b)** DHI calculated for July 6th, 2015. Control treatments are indicated by closed symbols and deficit irrigation (DI) treatment is indicated by open symbols. The variety Apex is shown by circles, the variety Barke by triangles, the variety Heils Franken (H.Franken) by squares, and the variety Victoriana by diamonds.

The diurnal changes tracked by the DHI seem likely, because barley is an anisohydric plant species, which loses water throughout the day in order to keep transpiration rates high to maintain photosynthesis (Alvarez *et al.*, 2007; Sade *et al.*, 2012). Under non-stress conditions, as it was the case on the 15th of June, suffcient water was available and the lost water was replaced relatively quickly, which implies only a moderate dehydration of the plants. As soon as stress occurs, as it was the case on July 6th, water was limited and not easily accessible for the plants (Tardieu and Davies, 1993). Under these conditions, anisohydric plants strongly dehydrate in order to keep transpiration and accompanied photosynthesis running. Particularly the DI treatments were already slightly dehydrated in the morning, because unusually high air temperatures (T_a) and photosynthetic photon flux density (PPFD) were already reached in the morning, so that photosynthesis and transpiration were induced early on this day (Fig. A.6.5). This resulted in an early dehydration of the DI treated canopies, so that they were forced to close stomata during the day in order to reduce water loss by transpiration. Due to the water-limitation, DI treated canopies were not able to rehydrate during the day resulting in a similarly low DHI in the evening compared to the midday. The control canopies also reached the highest g_s in the morning (Fig. A.6.5), but dehydrated less compared to DI plants, because sufficient water was available. First in the evening, a clear dehydration was observed. Soil moisture measurements on the next day revealed that soil moisture has partly dropped below 20% within one day (Fig. 6.2.2). Although the plants were appropriately watered before the measurements, the unusual hot and bright conditions induced high evapotranspiration rates (Bunce, 2000). It is likely, that also the control plants were transiently exposed to water-limiting conditions, which finally resulted in a stronger dehydration compared to cooler days. These effects were also observed in the trend of the daily minimum of the DHI during the whole experiment (Fig. 7.1.2). On days which were comparatively cooler and darker, plants did not dehydrate as strongly as compared to the hot and bright days.

Additionally, the variety differences which were discussed in Chapter 6.4.3 were also feasible in the DHI. The variety Apex showed relatively high and stable DHI values compared to the other varieties indicating a water-spending strategy, in which the plant tissue hydration state is kept high. However, the variety Victoriana was assumed to be highly risk-taking and soil-water saving, by first using internally stored water resources. Also the DHI of Victoriana revealed the lowest values which, is in accordance with the raised hypothesis.

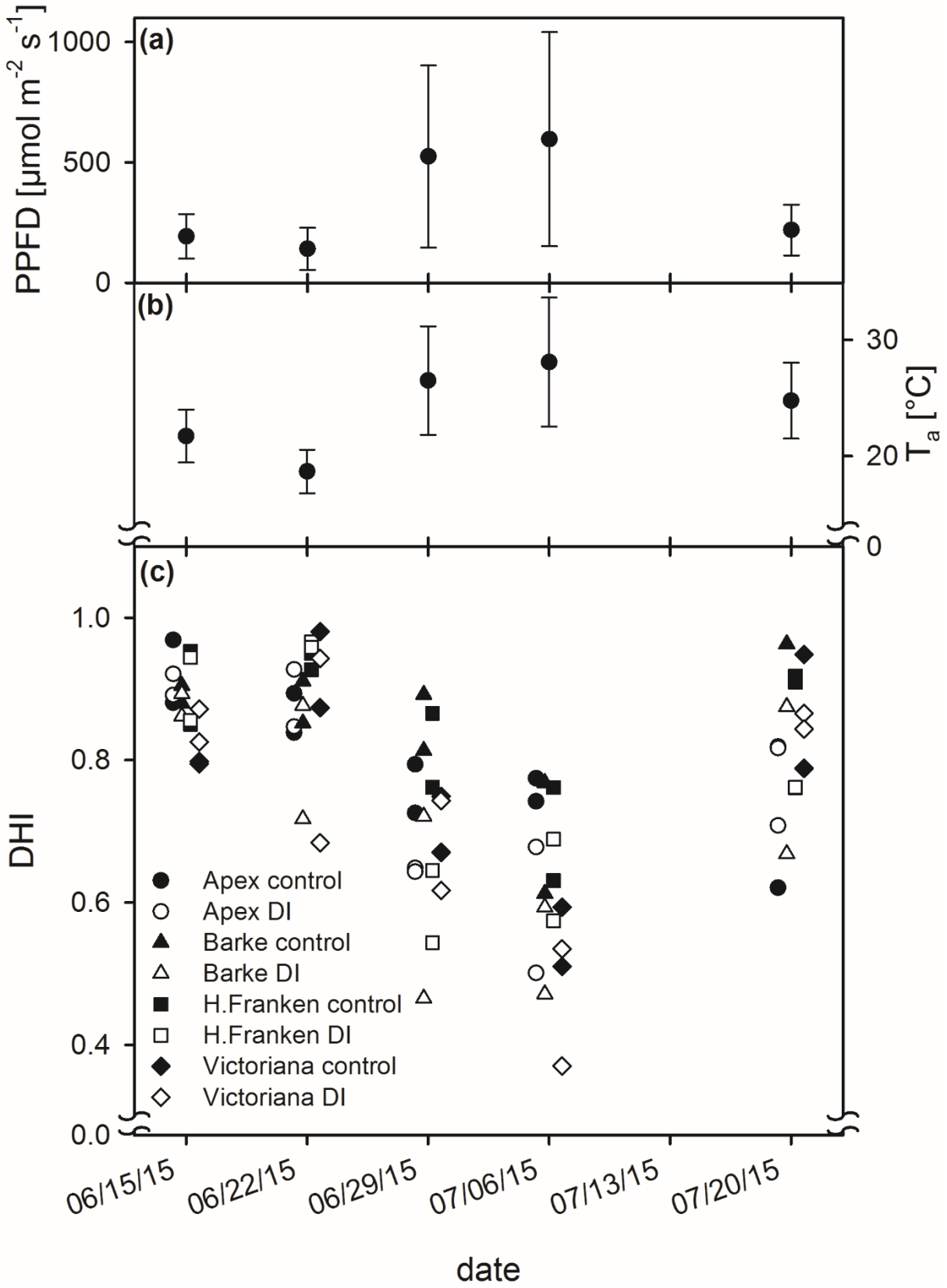

Figure 7.1.2: Seasonal trend of environmental factors and the dehydration index (DHI). **(a)** Mean photosynthetic photon flux density (PPFD). **(b)** Mean air temperature (T_a). **(c)** Daily minimum of DHI. Closed symbols represent control treatment and open symbols represent deficit irrigation (DI) treatment. The variety Apex is indicated by circles, the variety Barke by triangles, the variety Heils Franken (H.Franken) by squares, and the variety Victoriana by diamonds.

The varieties Barke and Heils Franken were assumed to switch between the water-spending and the water-saving strategy. As the DHI of these varieties show large differences between the control and the DI treatments, the DHI also supports this hypothesis.

7.3. Limits of the dehydration index and conclusion

An index which combines τ measurements with the CWSI would be highly attracting, since the CWSI is already a commonly used parameter in plant science but does not directly reflect the hydration state of plants. However, the dehydration behavior of plants is an important parameter to understand drought-stress avoidance strategies, particularly for breeding studies aiming for drought-stress tolerant plants.

The DHI is an empirically derived index, which is based on several assumptions. Therefore, it carries some uncertainties which need consideration and improvement in future works. For example, night-τ is assumed to provide a τ of fully hydrated plants. This may be true for non-stressed plants, but for stressed plants this is unlikely, because plants may not have rehydrated fully during night (see 6.4.1.3). Certainly, this is a measurement problem which could be overcome by simply measuring predawn-τ that is more likely to represent a fully hydrated plant. Additionally, the experiment was not designed to develop an index, such as the DHI, so that the DHI could not be confirmed with real measured LWC data. A further problem of the DHI is the weighting of the CWSI in this index. From Equation 7.1.1 it is clear that a CWSI near zero, which refers to a fully transpiring plant, would indicate that τ is only driven by transpiration and nearly no dehydration has occurred. But it is very unlikely that anisohydric plants, such as barley, do not dehydrate when transpiring at full potential (Alvarez *et al.*, 2007; Sade *et al.*, 2012).

Although the DHI reflects reliable dehydration behavior and was in accordance with the raised hypotheses regarding the stress-avoidance strategies of the different varieties, this index needs further quantitative and qualitative validations and improvements. Additionally, the impact of transpiration and dehydration on τ needs to be considered, for example by weighting factors for the CWSI, as this will be different for different varieties and different plant species. The DHI is a first attempt to develop an index to measure plant dehydration from passive and active thermography. Despite the fact that this particular index needs further improvements, the benefit of such an index is beyond all questions, as the greenhouse experiment (Chapter 6) has demonstrated the difficulties to assess the overall plant-water relation by using a single index or parameter.

8. Conclusions

Leaf water content (LWC) is a result of an equilibrium between water uptake and water loss (Berger *et al.*, 2010) and thus LWC is an integrator of drought stress (Jones, 2007). Monitoring of LWC is an important parameter, which is relevant for a wide range of research questions in basic plant science as well as in applied research towards breeding for drought tolerance (Berger *et al.*, 2010; Maes and Steppe, 2012; Costa *et al.*, 2013), or modeling of hydrological cycles in ecosystems (Foley *et al.*, 2010).

In this work, the active thermography method was introduced and extensively tested on different plant species and under varying environmental conditions. Stemming from the pioneering works of Kümmerlen *et al.* (1999) and Garbe *et al.* (2002), the active thermography approach was further developed as a non-invasive method and its potential for characterizing plant water status was thoroughly tested at different scales, from the single leaf scale in the laboratory to the canopy scale in the greenhouse. The measured time constant (τ) was shown to be an adequate parameter to assess plant-water relations. The applicability and the limits of the active thermography were examined in this work.

8.1 How is the measured time constant related to the leaf water content?

In the laboratory on the leaf level, τ was shown to be linearly related to LWC for different plant species and under different experimental conditions (Chapter 4). When the environmental conditions were kept constant, a direct derivation of LWC form the linear relationship between τ and LWC was possible. Additionally, the combination of active temperature measurements with the Licor-6400 gas exchange system provided a straightforward and robust experimental approach to observe LWC dynamics in parallel with transpiration rates. Dehydration responses among different plants species cannot be assumed to be invariant, as these depend on an isohydric or anisohydric behavior (Levitt, 1972; Tardieu and Simonneau, 1998; Alvarez *et al.*, 2007; Sade *et al.*, 2012). Therefore, non-invasive measurement of LWC dynamics is of interest to assess plant behavior, particularly in response to water-limiting conditions, such as drought. Additionally, LWC dynamics can provide information about the leaf hydraulic conductance, which is usually measured destructively (Scoffoni *et al.*, 2008). The Licor gas exchange system is also applicable to field studies, which enables active temperature measurements in the field without regarding the environmental conditions, because the leaf is enclosed in a gas exchange cuvette and thus exposed to a well-defined boundary layer condition.

However, the combination of active temperature measurements with a gas-exchange device has the big disadvantage that no spatial information can be obtained. It was demonstrated in this

work that the relationship between τ and LWC is valid under varying environmental conditions and it is possible to derive LWC, if the ambient conditions are regarded properly. With the active thermography LWC can be mapped spatially, providing local differences in LWC, which is a result of different leaf structures, such as vascular tissues that are known to have a relatively higher water content (Sack and Scoffoni, 2013). The non-invasive spatial mapping of LWC is a clear advantage over destructive measurements, like the pressure bomb technique (Scholander *et al.*, 1965; Tyree and Hammel, 1972), because leaves are not destroyed and provide local LWC information. Other non-invasive methods to measure LWC were recently developed, for example the terahertz time-domain spectroscopy (Castro-Camus *et al.*, 2013) and microwave cavity resonance (Menzel *et al.*, 2009). These techniques can have a high accuracy but do not provide spatial information on the water distribution within the leaf, as it can be obtained with the active thermography. Besides local differences in LWC, temporally resolved measurements may also reveal water fluxes within the leaf and thus provide leaf hydraulic conductance.

8.2 How is the measured time constant affected by a varying boundary layer conductance?

Results in this work show that τ is highly affected by a variable boundary layer conductance. But it was also demonstrated that τ can be used to properly model the leaf heat transfer coefficient (h_{leaf}) (Chapter 5). Therefore, the derivation of LWC is still possible under variable environmental conditions, as long as the relevant parameters, such as wind-speed, illumination, and air temperature (T_a) are either controlled or tightly monitored. Results also show that the convective heat transfer and transpiration cannot be separated and the modeling of convection, therefore, is an important issue in studies of the plant-water relations. The active thermography has the potential to be implemented in leaf heat transfer studies. By definition, τ is related to LWC and h_{leaf}, which together describe the thermal inertia of a leaf. It was demonstrated that this thermal inertia causes “hot spots” on the leaf, e.g. at thicker veins locations, that very likely affect boundary layer and thus the overall leaf heat transfer. Particularly under free convection conditions, modeling or measurements of h_{leaf} is a difficult issue, because leaf geometry and the varying difference between leaf temperature (T_L) and T_a (T_L-T_a) highly affect h_{leaf} (Saldin and Barthakur, 1971; Schuepp, 1993). Spatial maps of τ, and thus of the thermal inertia, may help to model free convection behavior on leaves more precisely, which could significantly improve our knowledge of leaf heat transfer processes. In previous studies, τ was already considered as a parameter to measure h_{leaf} (Kumar and Barthakur, 1971; Parlange and Waggoner, 1971; Saldin and Barthakur, 1971; Pearman *et al.*, 1972). The background principle is the same as the one underlying the active thermography method. Single leaves or canopies are warmed up and the

following leaf cooling kinetic is recorded and quantified with τ. However, in previous studies usually thermocouples were used, providing a single point measurement of T_L without the possibility to obtain spatial information. In other studies, h_{leaf} was derived from artificial leaves that were made of copper (Pearman *et al.*, 1972). However, copper cannot reflect real leaf heat transfer properties, because it has a much higher thermal conductivity ($k \approx 400$ W m^{-1} K^{-1}) than for example pure water ($k \approx 0.6$ W m^{-1} K^{-1}), which is even higher compared to real leaves (in maximum $k \approx 0.5$ W m^{-1} K^{-1}) (Jayalakshmy and Philip, 2010). Therefore, in copper "leaves" lateral heat conduction will occur, which is very unlikely in real leaves. Additionally, leaf structures, such as veins, introduced local variabilities in thermal conductivity, resulting in "hot spots" that can be detected with the active thermography. Besides unrealistic comparisons, in these studies h_{leaf} was derived from a mean value of τ, which may not reflect the reality. Thus, the spatial resolution of τ is essential to monitor local differences in h_{leaf} and to model h_{leaf} adequately. Finally, modeling of the heat transfer between plants and the environment is crucial for predicting plant-water relations and plant productivity (Shibuya *et al.*, 2006; Schymanski and Or, 2015).

8.3 How is the measured time constant at canopy scale related to water-limiting conditions?

In the present work, it was found that τ showed a diurnal behavior where the lowest τ-values were usually reached around midday and the highest during the night (Chapter 6). This behavior was expected as LWC varies diurnally due to water loss through transpiration (Cowan, 1972; Hennessey and Field, 1991; Schmidhalter *et al.*, 1998; Tardieu and Simonneau, 1998). Additionally, barley is an anisohydric plant species which is known as a risk-taking, meaning that these species allow partial dehydration in order to keep photosynthesis high (Alvarez *et al.*, 2007; Sade *et al.*, 2012). Plants were exposed to a deficit irrigation (DI), where the soil moisture was kept below 30% and thus provides a mild drought stress, because low amounts of water are still available but the availability was already limited. Although plants under DI reached in total lower τ-values compared to the control treatment, these observations were not consistent and not significant throughout the experiment. Thus, τ alone did not reveal stress responses or differences between the screened barley varieties. In Chapter 5 it was shown that transpiration and convection can have a strong impact on τ, particularly under conditions where the plants are exposed to free convection. Because wind induces movements of the plants in a canopy, measurements are technically challenging in windy conditions at the canopy scale, because the leaf movements induced by wind would affect T_L cooling kinetics. Therefore, the exclusion of wind was required, which in turn produced free convection conditions and therefore made τ more

sensitive to transpiration. Thus, under these experimental conditions τ reflects both LWC and h_{leaf}, and thus h_{leaf} needs to be considered to adequately derive LWC dynamics from τ measurements.

8.4 How is the time constant related to the crop water stress index and can both parameters reveal overall insights in the plant water relations?

Because stomata tend to close in response to decreasing LWC (Cowan, 1972; Syvertsen, 1982; Martin and Ruiz-Torres, 1992; Tardieu and Simonneau, 1998) it is unlikely that τ measured in the DI treatment was driven by transpiration and thus by a high h_{leaf}. The underlying theory of the CWSI shows that the CWSI reveals information about the heat transfer of plants, particularly about transpiration (Idso *et al.*, 1981; Jackson *et al.*, 1981). The CWSI also showed a diurnal pattern, which was in accordance with the measured canopy water loss rates (WLR) and stomatal conductance (g_s). However, Cohen *et al.* (2005) also found that the CWSI correlates with leaf water potential during seasonal development of water deficit, where high CWSI values were associated with low leaf water potential values indicating a concurrently low LWC. In this work, seasonal observations of the τ-development also showed a negative relationship to the CWSI, where midday-τ and night-τ decreased with increasing CWSI, indicating that a high CWSI is related to a low LWC. However, in the experiments presented in this thesis during the diurnal cycles this relationship is reverted, so that high CWSI values are associated with high τ-values and vice versa. This observation in turn indicates a relationship between both parameters that is based on changes in h_{leaf}. Transpiration and LWC show diurnal oscillations with time-shifted amplitudes. It was concluded, that the positive relationship between LWC and the CWSI was only valid under certain conditions, namely if the leaf was dehydrated and transpiration was suppressed. Therefore, high CWSI values, indicating low h_{leaf}, can be correlated with low τ and low leaf water potential, indicating low LWC. While τ and leaf water potential are affected by long-term water loss through transpiration, the CWSI reflects only the state of the system at the measured time point.

By considering both parameters in parallel, hypotheses regarding the stress avoidance strategies of the four barley varieties could be raised, which were in accordance with the measured WLR and the biomass production (Levitt, 1972). These results strongly indicate that the interpretation of the CWSI highly benefits from the inclusion of τ. In contrast, to understand the dynamics of τ the assessment of the CWSI is inevitable. However, both parameters together reveal valuable information about the plant water status, which cannot be obtained by measuring τ or the CWSI

alone. Therefore, the combination of τ and the CWSI in one index would be advantageous for studies aiming at the drought stress avoidance strategies of plants.
A first idea of such an index was suggested with the dehydration index (DHI). Although this index seemed to track reliable diurnal plant dehydration behavior and the raised hypotheses regarding the stress avoidance strategies could be also observed with the DHI, this index needs further validation and improvements. Nevertheless, as τ and the CWSI provide valuable information on the plant water status, the benefit of combining both parameters is beyond all questions.

8.5 Overall conclusion

This works demonstrates that the assessment of a single component of the plant-water relations, such as g_s, is not sufficient to make assumptions about the overall plant-water relations. Because all parameters are interlinked and vary during the day, an overall monitoring and long-term monitoring is unavoidable for an adequate assessment of the plant-water relations. Characterization of soil properties and soil moisture measurements are required to obtain information about the potential water availability. Monitoring of heat transfer processes, such as transpiration, which for instance can be assessed with the CWSI, are required to estimate the plant water loss and provide information of the actual state of the overall system. And last but not least, the monitoring of LWC dynamics are of high importance, because the LWC is the link between water availability (soil moisture) and the water loss (transpiration), and thus refers to the net water loss (Berger *et al.*, 2010). Without LWC monitoring, conclusions about the plant strategies to cope with water-limitation appears hardly possible. Cohen *et al.* (2005) have already claimed that an optimal determination of the plant water status from thermal images should always be based on an overall view of the physical status of the plants and the original results presented in this thesis strongly support that view.

References

Alchanatis V, Cohen Y, Cohen S, Moller M, Sprinstin M, Meron M, Tsipris J, Saranga Y, and Sela E. 2009. Evaluation of different approaches for estimating and mapping crop water status in cotton with thermal imaging. Precision Agriculture **11**, 27–41.

Allan AC, Fricker MD, Ward JL, Beale MH, and Trewavas AJ. 1994. Two transduction pathways mediate rapid effects of abscisic acid in Commelina guard cells. The Plant Cell **6**, 1319–1328.

Alvarez E, Scheiber SM, Beeson RC, and Sandrock DR. 2007. Drought tolerance responses of purple lovegrass and 'Adagio' maiden grass. HortScience **42**, 1695–1699.

Araus JL, Bort J, Steduto P, Villegas D, and Royo C. 2003. Breeding cereals for mediterranean conditions: Ecophysiological clues for biotechnology application. Annals of Applied Biology **142**, 129–141.

Asner G. 1998. Biophysical and biochemical sources of variability in canopy reflectance. Remote Sensing of Environment **253**, 234–253.

Aston AR and van Baverl CHM. 1971. Soil surface water depletion and leaf temperature. Agronomy Journal **64**, 368–373.

Bailey BJ. 1993. Modelling leaf convective heat transfer. Acta Holticulturae **399**.

Baker JT, Gitz DC, Pyton P, Wanjura DF, and Upchurch DR. 2007. Using leaf gas exchange to quantify drought in cotton irrigated based on canopy temperature measurements. Agronomy Journal **99**, 637–644.

Barboza-Barquero L, Nagel KA, Jansen M, Klasen JR, Kastenholz B, Braun S, Bleise B, Brehm T, Koornneef M, and Fiorani F. 2015. Phenotype of Arabidopsis thaliana semi-dwarfs with deep roots and high growth rates under water-limiting conditions is independent of the GA5 loss-of-function alleles. Annals of Botany **116**, 321–331.

Berger B, Parent B, and Tester M. 2010. High-throughput shoot imaging to study drought responses. Journal of experimental botany **61**, 3519–28.

Bird R, Stewart W, and Lightfoot E. 2002. *Transport phenomena*. New York: Wiley.

Blum A. 2009. Effective use of water (EUW) and not water-use efficiency (WUE) is the target of crop yield improvement under drought stress. Field Crops Research **112**, 119–123.

Bodner G, Loiskandl W, and Kaul HP. 2007. Cover crop evapotranspiration under semi-arid conditions using FAO dual crop coefficient method with water stress compensation. Agricultural Water Management **93**, 85–98.

Bodner G, Nakhforoosh A, and Kaul HP. 2015. Management of crop water under drought: a review. Agronomy for Sustainable Development **35**, 401–442.

Bunce JA. 1985. Effect of boundary-layer conductance on the response of stomata to humidity. Plant Cell and Environment **8**, 55–57.

Bunce JA. 2000. Responses of stomatal conductance to light, humidity and temperature in winter wheat and barley grown at three concentrations of carbon dioxide in the field. Global Change Biology **6**, 371–382.

von Caemmerer S and Farquhar GD. 1981. Some relationships between the biochemistry of photosynthesis and the gas exchange of leaves. Planta **153**, 376–387.

Cannon JN, Krantz WB, and Kreith F. 1979. A study of transpiration from porous flat plates simulating plant leaves. International Journal of Heat and Mass Transfer **22**, 469–483.

Castro-Camus E, Palomar M, and Covarrubias AA. 2013. Leaf water dynamics of Arabidopsis thaliana monitored in-vivo using terahertz time-domain spectroscopy. Scientific reports **3**, 2910.

Chaves MM, Flexas J, and Pinheiro C. 2009. Photosynthesis under drought and salt stress: Regulation mechanisms from whole plant to cell. Annals of Botany **103**, 551–560.

Cohen Y, Alchanatis V, Meron M, Saranga Y, and Tsipris J. 2005. Estimation of leaf water potential by thermal imagery and spatial analysis. Journal of experimental botany **56**, 1843–52.

Costa JM, Grant OM, and Chaves MM. 2013. Thermography to explore plant-environment interactions. Journal of experimental botany **64**, 3937–49.

Cowan IR. 1972. Oscillations in stomatal conductance and plant functioning associated with stomatal conductance: Observations and a model. Planta **106**, 185–219.

Dannenhoffer JM, Ebert W, and Evert RF. 1990. Leaf vasculature in barley, Hordeum vulgare (Poaceae). American Journal of Botany **77**, 636–652.

Defraeye T, Verboven P, Ho QT, and Nicolai B. 2013. Convective heat and mass exchange predictions at leaf surfaces: Applications, methods and perspectives. Computers and Electronics in Agriculture **96**, 180–201.

Dixon M and Grace J. 1983. Natural convection from leaves at realistic Grashof numbers. Plant, Cell and Environment **6**, 665–670.

Dixon M and Grace J. 1984. Effect of Wind on the Transpiration of Young Trees. Annals of Botany **53**, 811– 819.

Ehrler W. 1972. Cotton leaf temperatures as related to soil water depletion and meteorological factors. Agronomy Journal **65**, 404–409.

Finnigan J. 2000. Turbulence in plant canopies. Annual Review of Fluid Mechanics **32**, 519–571.

Flexas J, Bota J, Galmés J, Medrano H, and Ribas-Carbó M. 2006. Keeping a positive carbon balance under adverse conditions: Responses of photoysnthesis and respiration to water stress. Physiologia Plantarum **127**, 343–352.

Foley JA, Costa MH, Delire C, Ramankutty N, Costaz MH, and Snyder P. 2010. Green surprise? How terrestrial ecosystems could affect earth's climate. Frontiers in Ecology and the Environment **1**, 38–44.

Fuchs M. 1990. Infrared measurement of canopy temperature and detection of plant water stress. Theoretical and Applied Climatology **261**, 253–261.

Garbe C, Schurr U, and Jaehne B. 2002. Thermographic measurements on plant leaves. AeroSense 2002.

García-Tejero IF, Durán-Zuazo VH, Muriel-Fernández JL, and Jiménez-Bocanegra JA. 2011. Linking canopy temperature and trunk diameter fluctuations with other physiological water status tools for water stress management in citrus orchards. Functional Plant Biology **38**, 106–117.

Gates D. 1965. Energy, plants, and ecology. Ecology **46**, 1–13.

Gates DM, Tibbals EC, and Kreith F. 1965. Radiation and convection for Ponderosa pine. American Journal of Botany **52**, 66–71.

Gausman HW and Allen WA. 1973. Optical parameters of leaves of 30 plant species. Plant physiology **52**, 57–62.

Gaussorgues G. 1994. *Infrared Thermography*. London: Chapman & Hall.

Glückert U. 1992. *Erfassung und Messung von Wärmestrahlung: Eine praktische Einführung in die Pyrometrie und Thermografie*. München: Franzis-Verlag GmbH & Co KG.

Gollan T, Schurr U, and Schulze E-D. 1992. Stomatal response to drying soil in relation to changes in the xylem sap composition of Helianthus annuus. I. The concentration of cations, anions, amino acids in, and pH of, the xylem sap. Plant, Cell & Environment **15**, 551–559.

González-Dugo MP, Moran MS, Mateos L, and Bryant R. 2006. Canopy temperature variability as an indicator of crop water stress severity. Irrigation Science **24**, 233–240.

Grace J. 1974. The effect of wind on grasses 1. Cuticular and stomatal transpiration. Journal of Experimental Botany **25**, 542–551.

Grant OM, Tronina L, Jones HG, and Chaves MM. 2007. Exploring thermal imaging variables for the detection of stress responses in grapevine under different irrigation regimes. Journal of experimental botany **58**, 815–25.

Hall AE and Kaufmann MR. 1975. Stomatal Response to Environment with Sesamum indicum. L. Plant physiology **55**, 455–9.

Hennessey TL and Field CB. 1991. Circadian Rhythms in Photosynthesis. Plant physiology **96**, 831–836.

Hillel D. 1980. *Applications of soil physics*. Academic Press.

Idso SB, Jackson RD, Pinter PJ, Reginato RJ, and Hatfield JL. 1981. Normalizing the stress-degree-day parameter for environmental variability. Agricultural Meteorology **24**, 45–55.

Jackson RD, Idso SB, Reginato RJ, and Pinter PJ. 1981. Canopy temperature as a crop water stress indicator. Water Resources Research **17**, 1133.

Jackson RD, Reginato RJ, and Idso SB. 1977. Wheat canopy temperature: a practical tool for revaluating water requirements. Water Resources Research **13**, 651–656.

Jayalakshmy MS and Philip J. 2010. Thermophysical Properties of Plant Leaves and Their Influence on the Environment Temperature. International Journal of Thermophysics **31**, 2295–2304.

Jones HG. 1992. *Plants and microclimate*. Cambridge: Cambridge University Press.

Jones HG. 1999*a*. Use of infrared thermometry for estimation of stomatal conductance as a possible aid to irrigation scheduling. Agricultural and Forest Meteorology **95**, 139–149.

Jones HG. 1999*b*. Use of thermography for quantitative studies of spatial and temporal variation of stomatal conductance over leaf surfaces. Plant, Cell and Environment **22**, 1043–1055.

Jones HG. 2007. Monitoring plant and soil water status: Established and novel methods revisited and their relevance to studies of drought tolerance. Journal of Experimental Botany **58**, 119–130.

Khan HUR, Link W, Hocking TJ, and Stoddard FL. 2007. Evaluation of physiological traits for improving drought tolerance in faba bean (Vicia faba L.). Plant and Soil **292**, 205–217.

Kitano M and Eguchi H. 1990. Buoyancy effect on forced convection in the leaf boundary layer. Plant, Cell and Environment **13**, 965–970.

Kumar A and Barthakur N. 1971. Convective heat transfer measurements. Boundary-Layer Meteorology **2**, 218–227.

Kümmerlen B, Dauwe S, Schmundt D, and Schurr U. 1999. Thermography to Measure Water Relations of Plant Leaves. Handbook of Computer Vision and Applications, Volume 3: Systems and Applications.763–7881.

Langer K, Levchenko V, and Fromm J. 2004. The poplar K+ channel KPT1 is associated with K+ uptake during stomatal opening and bud development. The Plant Journal **37**, 828–838.

Leigh A, Sevanto S, Ball MC, Close JD, Ellsworth DS, Knight CA, Nicotra AB, and Vogel S. 2012. Do thick leaves avoid thermal damage in critically low wind speeds? The New Phytologist **194**, 477–487.

Levchenko V, Konrad KR, Dietrich P, Roelfsema MRG, and Hedrich R. 2005. Cytosolic abscisic acid activates guard cell anion channels without preceding Ca2+ signals. Proceedings of the National Academy of Sciences of the United States of America **102**, 4203–8.

Levitt J. 1972. *Responses of plants to environmental stresses*. Academic Press.

Linacre E. 1972. Leaf temperatures, diffusion resistances, and transpiration. Agricultural Meteorology **10**, 365-382.

Lockhart JA. 1967. Physical nature of irreversible deformation of plant cells. Plant Physiology **42**, 1545–1552.

Maes WH, Achten WMJ, Reubens B, and Muys B. 2011. Monitoring stomatal conductance of Jatropha curcas seedlings under different levels of water shortage with infrared thermography. Agricultural and Forest Meteorology **151**, 554–564.

Maes WH and Steppe K. 2012. Estimating evapotranspiration and drought stress with ground-based thermal remote sensing in agriculture: a review. Journal of experimental botany **63**, 4671–4712.

Martin B and Ruiz-Torres NA. 1992. Effects of water-deficit stress on photoysnthesis, its components and component limitations, and on water use efficiency in wheat (Triticum aestivum L.). Plant Physiology **100**, 733–739.

McKown AD, Cochard H, and Sack L. 2010. Decoding Leaf Hydraulics with a Spatially Explicit Model: Principles of Venation Architecture and Implications for Its Evolution. The American Naturalist **175**, 447–460.

Medrano H, Escalona JM, Bota J, Gulías J, and Flexas J. 2002. Regulation of photosynthesis of C3 plants in response to progressive drought: Stomatal conductance as a reference parameter. Annals of Botany **89**, 895–905.

Menzel MI, Tittmann S, Bühler J, Preis S, Wolters N, Jahnke S, Walter A, Chlubek A, Leon A, Hermes N, Offenhäuser A, Gilmer F, Blümler P, Schurr U, and Krause HJ. 2009. Non-invasive determination of plant biomass with microwave resonators. Plant, Cell & Environment **32**, 368–79.

Möller M, Alchanatis V, Cohen Y, Meron M, Tsipris J, Naor A, Ostrovsky V, Sprintsin M, and Cohen S. 2007. Use of thermal and visible imagery for estimating crop water status of irrigated grapevine. Journal of experimental botany **58**, 827–38.

Monteith JL. 1981. Evaporation and surface temperature. Quarterly Journal of the Royal Meteorological Society **107**, 1–27.

Monteith JL and Unsworth MH. 2008. *Principles of environmental physics*. Burlington: Elsevier Academic Press.

Mott KA., Denne F, and Powell J. 1997. Interactions among stomata in response to perturbations in humidity. Plant, Cell and Environment **20**, 1098–1107.

Nautiyal PC, Rajgopal K, Zala P V., Pujari DS, Basu M, Dhadhal BA, and Nandre BM. 2008. Evaluation of wild Arachis species for abiotic stress tolerance: I. Thermal stress and leaf water relations. Euphytica **159**, 43–57.

Nelder J and Mead R. 1965. A simplex method for function minimization. Computer journal **7**, 308–313.

Nguyen HT, Babu R, Chandra R, and Blum A. 1997. Breeding for drought resistance in rice: Physiology and molecular genetics considerations. American Journal of Agronomy **37**, 1426–1434.

Nobel PS. 2009. *Physicochemical and environmental plant physiology*. Oxford, UK: Elsevier Academic Press.

Olioso A, Carlson TN, and Brisson N. 1996. Simulation of diurnal transpiration and photosynthesis of a water stressed soybean crop. Agricultural and Forest Meteorology **81**, 41–59.

Parkhurst DF. 1976. Effects of Verbascum Thapsus leaf hairs on heat and mass transfer: A reassessment. New Phytologist **76**, 453–457.

Parlange JY, and Waggoner PE. 1971. Boundary layer resistance and temperature distribution on still and flapping leaves: I. Theory and laboratory experiments. Plant Physiology **48**, 437–442.

Pearman GI, Weaver HL, and Tanner CB. 1972. Boundary layer heat transfer coefficients under field conditions. Agricultural Meteorology **10**, 83–92.

Penman HL. 1948. Natural evaporation from open water, bare soil and grass. Proceedings of the Royal Society A: Mathematical, Physical and Engineering Sciences **193**, 120–145.

Pieruschka R, Huber G, and Berry JA. 2010. Control of transpiration by radiation. Proceedings of the National Academy of Sciences of the United States of America **107**, 13372–13377.

Raschke K. 1960. Heat transfer between the plant and the environment. Annual Review of Plant Physiology, 111–126.

Reynolds M, Manes Y, Izanloo A, and Langridge P. 2009. Phenotyping approaches for physiological breeding and gene discovery in wheat. Annals of Applied Biology **155**, 309–320.

Riederer M and Schreiber L. 2001. Protecting against water loss: analysis of the barrier properties of plant cuticles. Journal of Experimental Botany **52**, 2023–2032.

Rischbeck P, Baresel P, Elsayed S, Mistele B, and Schmidhalter U. 2014. Development of a diurnal dehydration index for spring barley phenotyping. Functional Plant Biology **41**, 1249–1260.

Rodriguez-Iturbe I, D'Odorico P, Porporato A, and Ridolfi L. 1999. On the spatial and temporal links between vegetation, climate, and soil mositure. Water Resources Research **35**, 3709–3722.

Roelfsema MRG and Hedrich R. 2005. In the light of stomatal opening: new insights into 'the Watergate'. The New phytologist **167**, 665–91.

Roth-Nebelsick A. 2001. Computer-based analysis of steady-state and transient heat transfer of small-sized leaves by free and mixed convection. Plant, Cell and Environment **24**, 631–640.

Sack L, Holbrook NM. 2006. Leaf hydraulics. Annual Review of Plant Biology **57**, 361–81.

Sack L, Scoffoni C. 2013. Leaf venation: Structure, function, development, evolution, ecology and applications in the past, present and future. New Phytologist **198**, 983–1000.

Sade N, Gebremedhin A, Moshelion M. 2012. Risk-taking plants: Anisohydric behavior as a stress-resistance trait. Plant Signaling & Behavior **7**, 767–770.

Sade N, Vinocur BJ, Diber A, Shatil A, Ronen G, Nissan H, Wallach R, Karchi H, and Moshelion M. 2009. Improving plant stress tolerance and yield production: Is the tonoplast aquaporin SlTIP2;2 a key to isohydric to anisohydric conversion? New Phytologist **181**, 651–661.

Saldin TF and Barthakur N. 1971. Heat transfer between Phaseolus vulagris and the environment. Canadian Journal of Botany **49**, 833–838.

Sánchez FJ, Manzanares M, De Andrés EF, Tenorio JL and Ayerbe L. 2001. Residual transpiration rate, epicuticular wax load and leaf colour of pea plants in drought conditions. Influence on harvest index and canopy temperature. European Journal of Agronomy **15**, 57–70.

Schmidhalter U, Burucs Z and Camp KH. 1998. Sensitivity of root and leaf water status in maize (Zea mays) subjected to mild soil dryness. Australian Journal of Plant Physiology **25**, 307–316.

Scholander PF, Hammel HT, Bradstreet ED and Hemmingsen EA. 1965. Sap Pressure in Vascular Plants. Science **148**, 339–346.

Schopfer P. 2006. Biomechanics of plant grwoth. American Journal of Botany **93**, 1415–1425.

Schreuder MD, Brewer CA, Heine C. 2001. Modelled influences of non-exchanging trichomes on leaf boundary layers and gas exchange. Journal of Theoretical Biology **210**, 23–32.

Schuepp PH. 1993. Leaf boundary layers. New Phytologist **125**, 477–507.

Schulze E-D and Caldwell MM. 1995. *Ecophysiology of Photosynthesis*. Berlin Heidelberg: Springer Berlin Heidelberg.

Schurr U, Gollan T, and Schulze E-D. 1992. Stomatal response to drying soil in relation to changes in the xylem sap composition of Helianthus annuus. II. Stomatal sensitivity to abscisic acid imported from the xylem sap. Plant, Cell & Environment **15**, 561–567.

Schwartz A, Wu WH, Tucker EB, and Assmann SM. 1994. Inhibition of inward K+ channels and stomatal response by abscisic acid: an intracellular locus of phytohormone action. Proceedings of the National Academy of Sciences of the United States of America **91**, 4019–23.

Schymanski SJ and Or D. 2015. Wind increases leaf water use efficiency. Plant, Cell & Environment, Open access article.

Scoffoni C, Pou A, Aasamaa K, and Sack L. 2008. The rapid light response of leaf hydraulic conductance: new evidence from two experimental methods. Plant, Cell & Environment **31**, 1803–12.

Scoffoni C, Vuong C, Diep S, Cochard H, and Sack L. 2014. Leaf shrinkage with dehydration: coordination with hydraulic vulnerability and drought tolerance. Plant Physiology **164**, 1772–88.

Seelig HD, Hoehn A, Stodieck LS, Klaus DM, Adams III WW, and Emery WJ. 2008. The assessment of leaf water content using leaf reflectance ratios in the visible, near-, and short-wave-infrared. International Journal of Remote Sensing **29**, 3701–3713.

Seelig HD, Hoehn A, Stodieck LS, Klaus DM, Adams III WW, and Emery WJ. 2009. Plant water parameters and the remote sensing R 1300/R 1450 leaf water index : controlled condition dynamics during the development of water deficit stress. Irrigation Science **27**, 357–365.

Shibuya T, Tsuruyama J, Kitaya Y, and Kiyota M. 2006. Enhancement of photosynthesis and growth of tomato seedlings by forced ventilation within the canopy. Scientia Horticulturae **109**, 218–222.

Shimazaki K, Doi M, Assmann SM, and Kinoshita T. 2007. Light regulation of stomatal movement. Annual review of plant biology **58**, 219–47.

Sinclair R. 1970. Convective heat transfer from narrow leaves. Australian Journal of Biological Sciences **23**, 309–322.

Steffens D, Hütsch BW, Eschholz T, Losak T, and Schubert S. 2005. Water logging may inhibit plant growth primarily by nutrient deficiency rather than nutrient toxicity. Plant, Soil and Environment **51**, 545–552.

Stocker O. 1956. Die Abhängigkeit der Transpiration von den Umweltfaktoren. Water Relations of Plants.436–488.

Subbarao G V, Johansen C, Slinkard AE, Nageswara RC, Saxena NP, and Chauhan YS. 1995. Strategies For Improving Drought Resistance In Grain Legumes. Critical Reviews in plant Sciences **14**, 469–523.

Syvertsen J. 1982. Minimum leaf water potential and stomatal closure in citrus leaves of different ages. Annals of botany, 827–834.

Taiz L and Zeiger E. 2006. *Plant Physiology*. Sunderland: Sinauer Associates, Inc.

Tardieu F and Davies WJ. 1993. Integration of hydraulic and chemical signalling in the control of stomatal conductance and water status of droughted plants. Plant, Cell & Environment **16**, 341–349.

Tardieu F and Simonneau T. 1998. Variability among species of stomatal control under fluctuating soil water status and evaporative demand: modelling isohydric and anisohydric behaviours. Journal of Experimental Botany **49**, 419–432.

Tyree MT and Hammel HT. 1972. The Measurement of the Turgor Pressure and the Water Relations of Plants by the Pressure-bomb Technique. Journal of Experimental Botany **23**, 267–282.

Tyree MT, Nardini A, Salleo S, Sack L, and El Omari B. 2005. The dependence of leaf hydraulic conductance on irradiance during HPFM measurements: Any role for stomatal response? Journal of Experimental Botany **56**, 737–44.

Tyree MT, Service UF, Forestry A, Box PO, and Burlington S. 1997. The Cohesion – Tension theory of sap ascent : current controversies. Journal of Experimental Botany **48**, 1753–1765.

Tyree MT and Sperry JS. 1989. Vulnerability of xylem to cavitation and embolism. Annual Review of Plant Physiology and Plant Molecular Biology **40**, 19–38.

Ueno O, Kawano Y, Wakayama M, and Takeda T. 2006. Leaf Vascular Systems in C3 and C4 Grasses: A Two-dimensional Analysis. Annals of Botany **97**, 611–621.

Vogel S. 2009. Leaves in the lowest and highest winds: temperature, force and shape. The New phytologist **183**, 13–26.

Wallace J. 2000. Increasing agricultural water use efficiency to meet future food production. Agriculture, Ecosystems & Environment **82**, 105–119.

Watt M, Silk WK, and Passioura JB. 2006. Rates of root and organism growth, soil conditions, and temporal and spatial development of the rhizosphere. Annals of Botany **97**, 839–855.

Wilkinson S and Davies WJ. 2002. ABA-based chemical signalling: the co-ordination of responses to stress in plants. Plant, Cell and Environment **25**, 195–210.

Appendix

Appendix – Chapter 2

Table A.2.1 Abbreviation list

symbol	description	unit
A	area	m^2 or cm^2 or mm^2
a	numerical constant describing the geometry of a leaf	
b	numerical constant describing the geometry of a leaf	
bl	boundary layer	
b_W	Wien's displacement constant	m K
C	heat capacity	$J\ K^{-1}$
$C\ A^{-1}_{leaf}$	leaf heat capacity per unit area	$J\ K^{-1}\ m^{-2}$
C_{leaf}	leaf heat capacity	$J\ K^{-1}$
c_p	specific heat capacity of air	$J\ kg^{-1}\ K^{-1}$
d	characteristic dimension of a leaf	cm
d_s	stomatal distribution on the leaf surfaces	
E	transpiration rate	$W\ m^{-2}$ or $mol\ m^{-2}\ s^{-1}$
e	partial water vapor pressure	Pa
e_s	saturation vapor pressure	Pa
FIR	far-infrared radiation (15 to 100 µm)	nm or µm
FPA	focal plane array	
g	gravitational acceleration	$m\ s^{-2}$
g_H	conductance to convective heat	$m\ s^{-1}$
g_{LW}	conductance to long-wave radiative heat	$m\ s^{-1}$
Gr	Grashof number	
g_W	leaf conductance to water vapor	$m\ s^{-1}$ or $mol\ m^{-2}\ s^{-1}$
H	convection	$W\ m^{-2}$
h	heat transfer coefficient	$W\ m^{-2}\ K^{-1}$
h_H	heat transfer coefficient for convective heat	$W\ m^{-2}\ K^{-1}$
h_{leaf}	total leaf heat transfer coefficient	$W\ m^{-2}\ K^{-1}$
h_{LW}	heat transfer coefficient for long-wave radiative heat	$W\ m^{-2}\ K^{-1}$
$h_{\lambda E}$	heat transfer coefficient for transpiration	$W\ m^{-2}\ K^{-1}$
I_{LW}	longwave irradiance	$W\ m^{-2}$
IR	infrared radiation (0.7 to 100 µm)	nm or µm
I_s	solar irradiance	$W\ m^{-2}$
j	energy flux	$J\ s^{-1}$
k	thermal conductivity of air	$W\ m^{-1}K^{-1}$
LW	heat loss by long-wave infrared radiation	$W\ m^{-2}$
LWC	leaf water content per unit area	$mg\ cm^{-2}$
LWIR	Long-wave infrared radiation (8 to 15 µm)	nm or µm
M	heat used for metabolic processes	$W\ m^{-2}$

MWIR	middle-wave infrared radiation (3 to 8 µm)	nm or µm
NIR	near-infrared radiation (0.75 to 1.4 µm)	nm or µm
Nu	Nusselt number	
PPFD	photosynthetic photon flux density (0.4 to 0.7 µm)	µmol m^{-2} s^{-1}
Q	energy	J
r_{aW}	boundary layer resistance to water vapor	s m^{-1} or s^1 m^2 mol^{-1}
Re	Reynold's number	
r_S	stomatal resistance	s m^{-1} or s^1 m^2 mol^{-1}
r_W	leaf resistance to water vapor	s m^{-1} or s^1 m^2 mol^{-1}
s	slope relating saturation vapor pressure to temperature	
S	physically stored heat by leaves	W m^{-2}
SWIR	short-wave infrared (1.4 to 3 µm)	
T	Temperature	K or °C
T_a	air temperature	K or °C
TIR	thermal infrared radiation	nm or µm
T_L	leaf temperature	K or °C
T_L'	new steady state leaf temperature	K or °C
u	wind speed	m s^{-1}
UV	ultra-violet radiation (0.3 to 0.4 µm)	nm or µm
VIS	visible electromagnetic radiation (0.38 to 0.78 µm)	nm or µm
α_Φ	absorptance of radiation	
β	thermal expansion coefficient of air	K^{-1}
γ	psychrometric constant	kPa $°C^{-1}$
Δe	water vapor pressure deficit (also referred to as VPD)	Pa or kPa
δe	water vapor pressure deficit of ambient air	Pa or kPa
ε	emissivity	
λ	latent heat of vaporization	J g^{-1} or J mol^{-1}
λE	leaf (evapo-)transpiration	W m^{-2} or mol m^{-2} s^{-1}
λ_{max}	peak wavelength at which maximum emission occurs	nm or µm
ν	kinematic viscosity of air	m^2 s^{-1}
ρ_a	density of air	kg m^{-3}
ρ_Φ	reflectance of radiation	
σ	Stefan Boltzmann constant	W m^{-2} K^{-4}
τ	time constant	s
τ_Φ	transmittance of radiation	
Φ	electromagnetic radiation	W m^{-2}
Φ_{bg}	background radiation	W m^{-2}
Φ_{in}	incoming heat	W m^{-2}
Φ_M	measured electromagnetic radiation	W m^{-2}

Φ_{net}	net energy flux density	W m^{-2}
Φ_{ni}	net isothermal radiation	W m^{-2}
Φ_{ρ}	reflected radiation	W m^{-2}

Appendix – Chapter 6

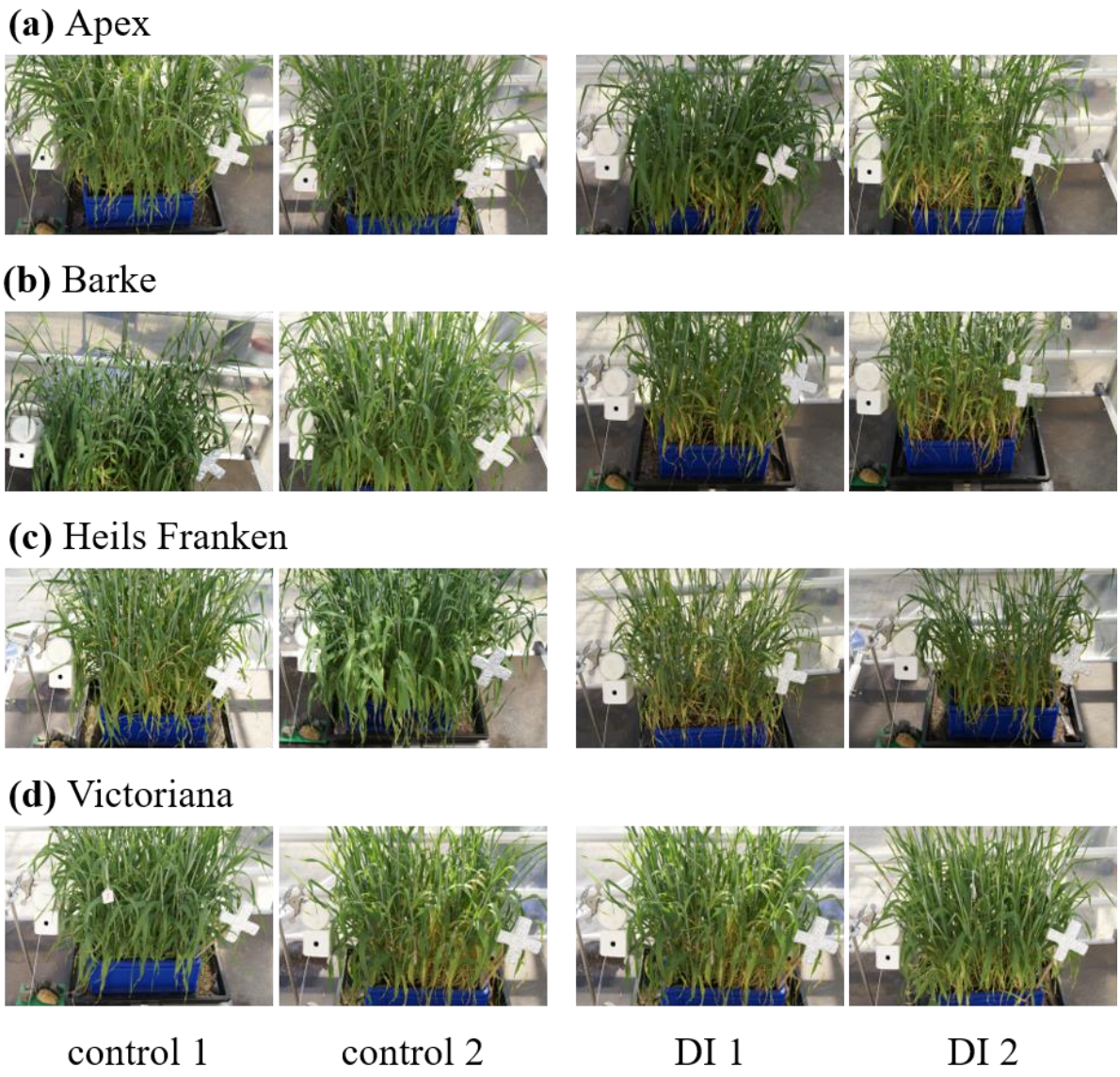

Figure A.6.1: Photos of spring barley canopies in the greenhouse experiment on July 6th, 2015. **(a)** Variety Apex, **(b)** variety Barke, **(c)** variety Heils Franken, and **(d)** variety Victoriana. First two columns on the left side show the control 1 and control 2 measurements. Third and fourth column on the right side show canopies under deficit irrigation (DI), DI 1 and DI 2, respectively.

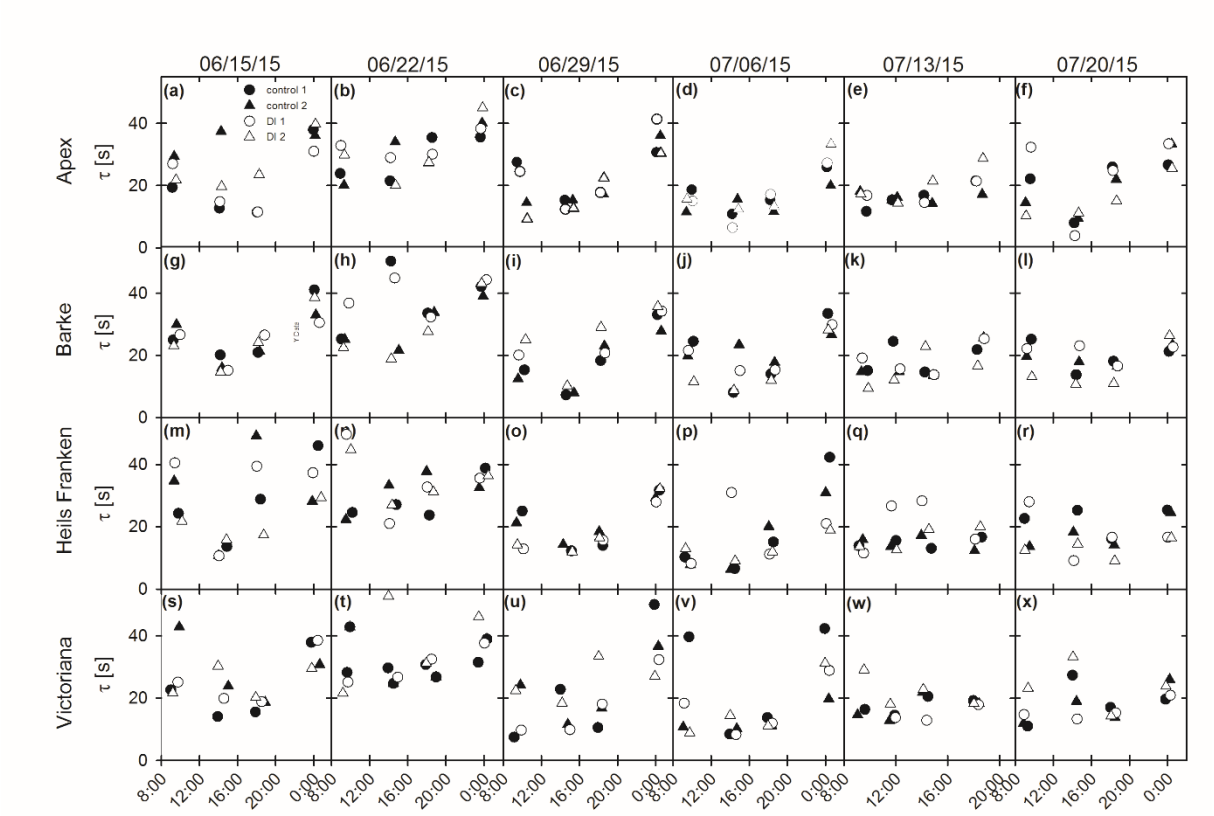

Figure A.6.2: Diurnal measurement of time constant (τ) at each day during the greenhouse experiment. **(a)** to **(f)** show measurements of the variety Apex, **(g)** to **(l)** show measurements of the variety Barke, **(m)** to **(r)** show measurements of the variety Heils Franken, and **(s)** to **(x)** show measurements of the variety Victoriana. Each point represents the median value of one measured plant box. Closed symbols are control treatments and open symbols are deficit irrigation (DI) treatments. Circles refer to replicate 1 and triangles to replicate 2.

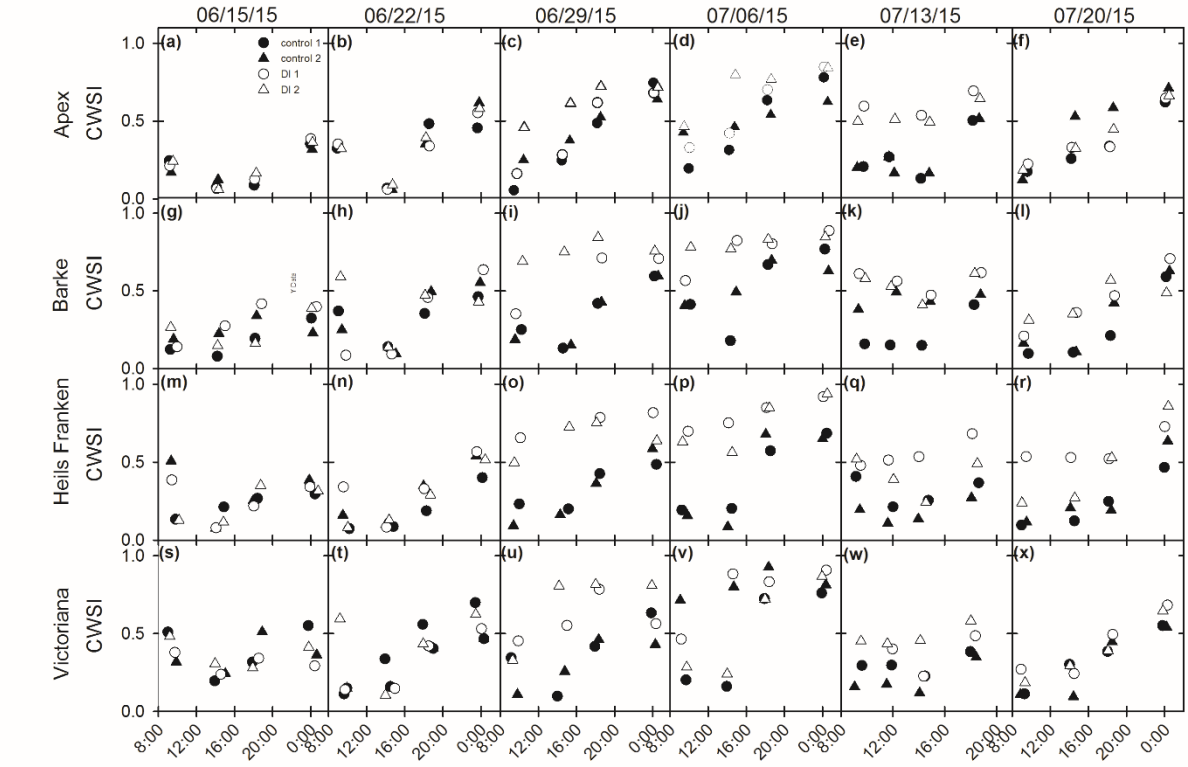

Figure A.6.3: Diurnal measurement of the crop water stress index (CWSI) at each day during the greenhouse experiment. **(a)** to **(f)** show measurements of the variety Apex, **(g)** to **(l)** show measurements of the variety Barke, **(m)** to **(r)** show measurements of the variety Heils Franken, and **(s)** to **(x)** show measurements of the variety Victoriana. Each point represents the median value of one measured plant box. Closed symbols are control treatments and open symbols are deficit irrigation (DI) treatments. Circles refer to replicate 1 and triangles to replicate 2.

Table A.6.1: Pearson correlation analysis for data obtained by diurnal meausrements. Compariosn betwenn the time constant (τ), the crop water stress index (CWSI), the difference between leaf temperature and ir temperature (T_L-T_a), photosynthetic photon flux density (PPFD), and the time of day.

		06/15/15				07/06/15			
		CWSI	T_L-T_a	PPFD	time of day	CWSI	T_L-T_a	PPFD	time of day
all data									
τ	r	0.37	0.55	-0.43	0.31	0.35	0.523	-0.48	0.45
	p-value	0.042	0.0013	0.015	0.086	0.051	0.0026	0.0055	0.0097
CWSI	r		0.54	-0.48	0.31		0.9	-0.71	0.689
	p-value		0.0016	0.0066	0.09		> 0.001	> 0.001	> 0.001
T_L-T_a	r			-0.66	0.058			-0.79	0.64
	p-value			> 0.001	0.76			> 0.001	> 0.001
PPFD	r				-0.41				-0.68
	p-value				0.024				> 0.001
control									
τ	r	0.54	0.6	-0.59	0.4	0.35	0.44	-0.45	0.57
	p-value	0.0013	> 0.001	> 0.001	0.025	0.047	0.012	0.01	> 0.001
CWSI	r		0.65	-0.651	0.33		0.94	-0.44	0.7
	p-value		> 0.001	> 0.001	0.064		> 0.001	0.012	> 0.001
T_L-T_a	r			-0.7	0.06			-0.64	0.69
	p-value			> 0.001	0.76			> 0.001	> 0.001
PPFD	r				-0.44				-0.61
	p-value				0.012				> 0.001
deficit irrigation									
τ	r	0.44	0.57	-0.49	0.35	0.28	0.45	-0.46	0.5
	p-value	> 0.001	> 0.001	> 0.001	0.0054	0.025	> 0.001	> 0.001	> 0.001
CWSI	r		0.59	-0.56	0.32		0.9	-0.504	0.63
	p-value		> 0.001	> 0.001	0.011		> 0.001	> 0.001	> 0.001
T_L-T_a	r			-0.68	0.057			-0.68	0.63
	p-value			> 0.001	0.66			> 0.001	> 0.001
PPFD	r				-0.42				-0.64
	p-value				> 0.001				> 0.001

Table A.6.2: Pearson correlation analysis for data obtained druing the whole experiment. Compariosn between the time constant (τ) measured at night, τ measured at midday, the crop water stress index (CWSI) measured at midday, the canopy water loss rate (WLR) measured at midday, and the daily mean of WLR.

		τ mid-day	CWSI	WLR	WLR daily mean
all data					
τ night	r	0.286	-0.415	-0.05	-0.06
	p-value	0.01	> 0.001	0.65	0.61
τ midday	r		-0.3	-0.37	-0.43
	p-value		0.008	> 0.001	> 0.001
CWSI	r			0.02	0.06
	p-value			0.88	0.59
control					
τ night	r	0.19	-0.4	-0.12	-0.1
	p-value	0.25	0.01	0.47	0.53
τ midday	r		-0.21	-0.52	-0.56
	p-value		0.2	> 0.001	> 0.001
CWSI	r			0.23	0.25
	p-value			0.15	0.13
deficit irrigation					
τ night	r	0.38	-0.45	-0.06	-0.1
	p-value	0.02	0.005	0.74	0.54
τ midday	r		-0.39	-0.28	-0.44
	p-value		0.015	0.089	0.005
CWSI	r			0.23	0.39
	p-value			0.18	0.016

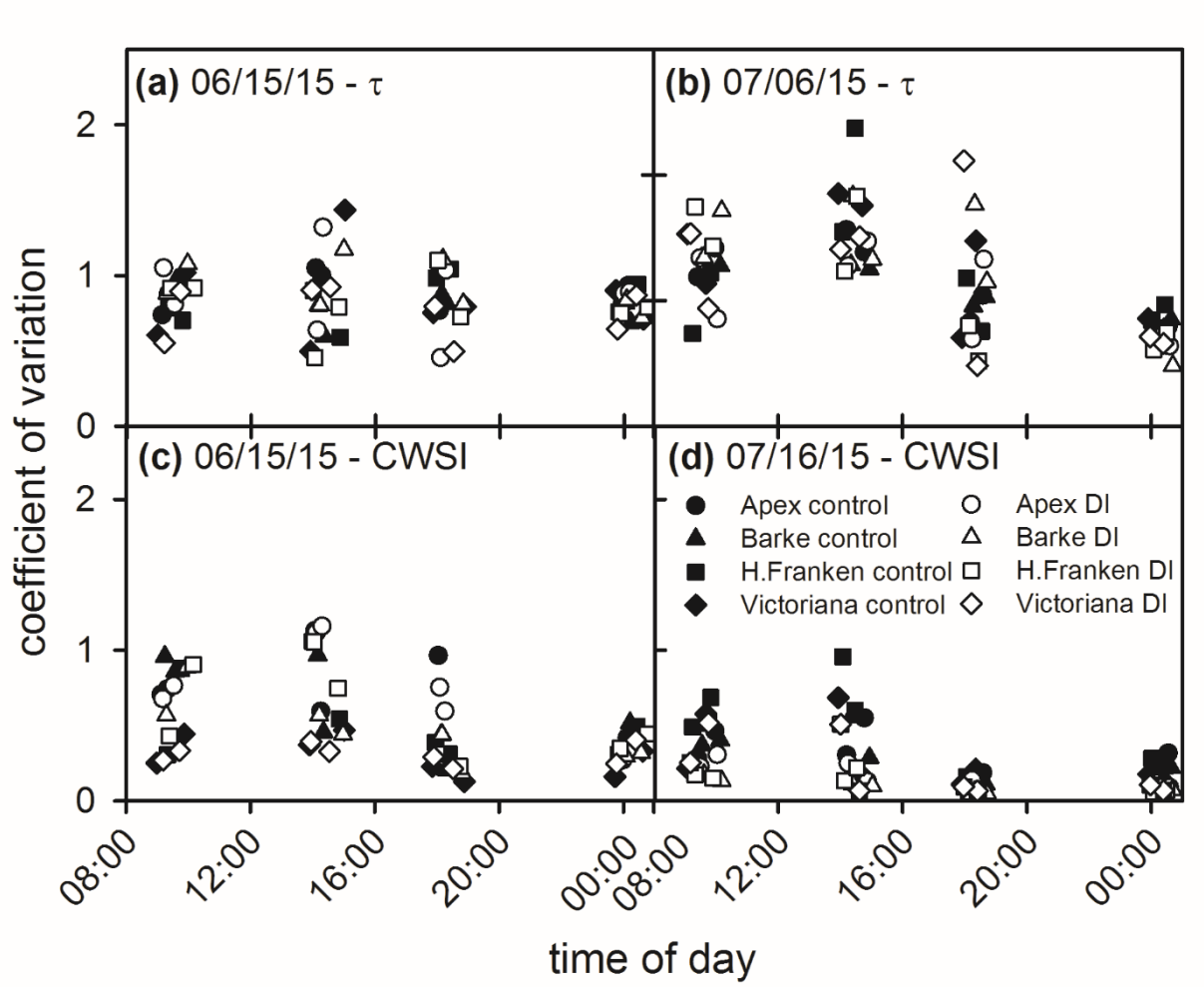

Figure A.6.4: Coefficient of variation of time constant (τ) and crop water stress index (CWSI) images measured on June 15th, 2015 and July 6th, 2015. **(a)** and **(b)** show coefficient of variation for τ, and **(c)** and **(d)** show coefficient or variation for the CWSI. Closed symbols are control treatments and open symbols are deficit irrigation (DI) treatments. Circles refer to the variety Apex, triangles to the variety Barke, squares to the variety Heils Franken (H.Franken), and diamonds refer to the variety Victoriana.

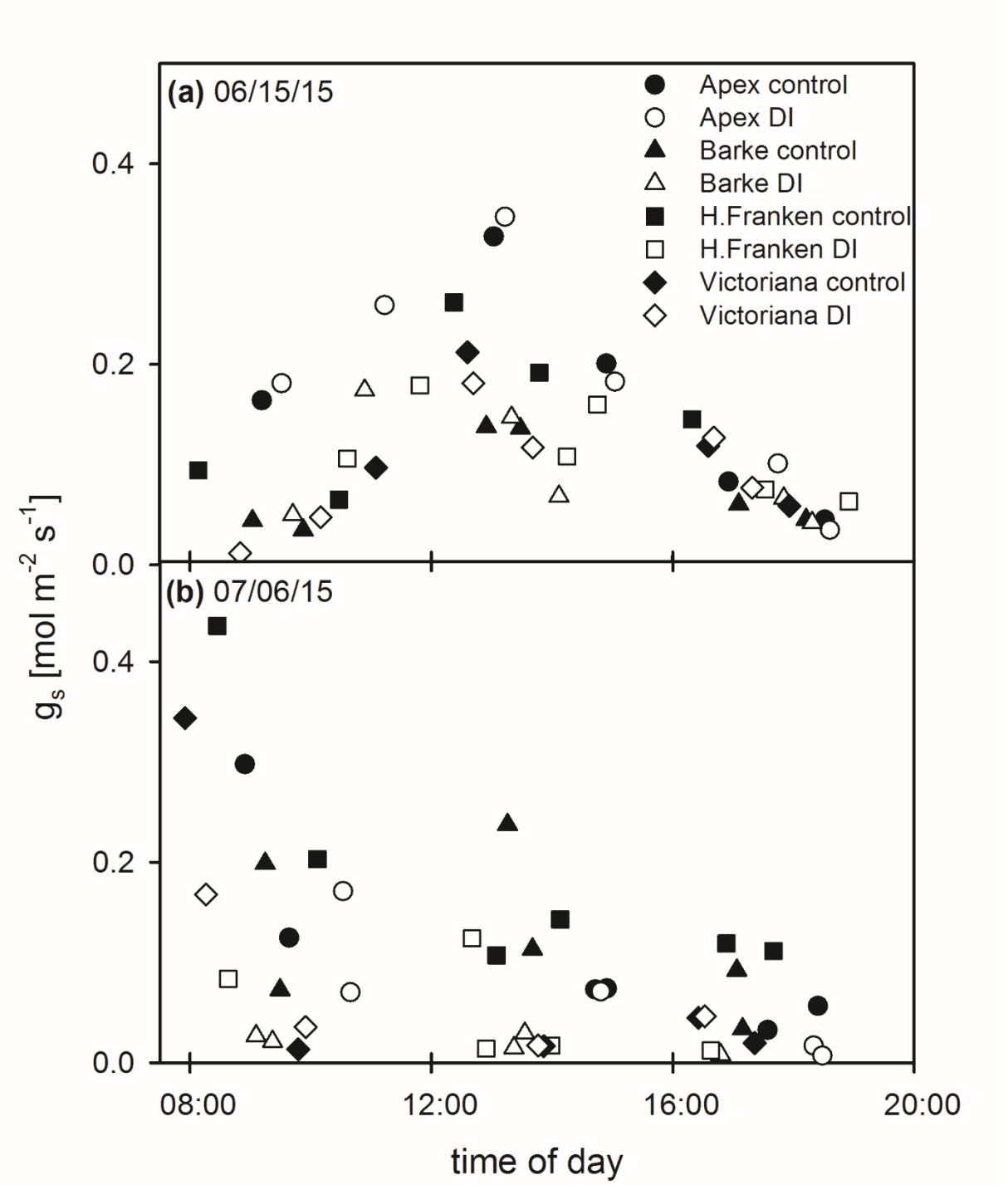

Figure A.6.5: Diurnal course of stomatal conductance (g_s) measured on June 15th, 2015 and July 6th, 2015. **(a)** Measurements on June 15th, 2015, and **(b)** measurements on July 6th, 2015. Closed symbols are control treatments and open symbols are deficit irrigation (DI) treatments. Circles refer to the variety Apex, triangles to the variety Barke, squares to the variety Heils Franken (H.Franken), and diamonds refer to the variety Victoriana.

Acknowledgements

There are a lot of people who somehow contributed to this work or somehow helped me finishing this thesis. I need to thank every single person in my working and private environment. Although I do not name everybody here, I am grateful to every person with whom I worked together and I got to know during my PhD period.

I want to thank Uwe Rascher, my Doktorvater, who gave me the opportunity to work on this interesting and complex topic and pushed me beyond my thought borders by always motivating me and having a friendly ear for nearly everything. Lukas Schreiber, thank you for being willing to take over the part as the second supervisor at the University Bonn. Further, I want to thank Fabio Fiorani and Roland Pieruschka, who were, together with Uwe, my supervisor team at the IBG-2. My supervisor team was an indispensable pillar of my work who contributed a lot with helpful discussions, new ideas, motivation, but also with nice discussions far away from my actual work. I also want to thank my whole working group, the "Shoot functioning", former "Ecosystem Dynamics" group, where I, unfortunately, cannot name every single person. Here, I particularly want to thank Maria Pilar Cendrero, with whom together I performed the very exhausting greenhouse experiment at the Campus Klein-Altendorf, and Mark Müller-Linow who created the MATLAB tool, which saved about decades of data analyses. Thank you everybody in the working group for the pleasant working atmosphere and the helpful input and ideas. Furthermore, I want to thank all the people from the Campus Klein-Altendorf who helped us with the greenhouse experiment by providing the facility, applying plant protection and so on.

Part of this work was performed within the German-Plant-Phenotyping Network (DPPN) which is funded by the German Federal Ministry of Education and Research (project number: 031A053). I also acknowledge the funding of the PhenoCrops project in the context of the Ziel 2-Programm NRW 2007-2013 "Regionale Wettbewerbsfähigkeit und Beschäftigung" by the Ministry for Innovation, Science and Research (MIWF) of the state North-Rhine-Westfalia (NRW) and European Union Funds for regional development (EFRE) (005-1105-0035).

Besides my colleagues and friends at my working place, I want to thank all the people who contributed to my work by supporting me in my private life, where of course much more people should be named. Here I want to thank Julia Henke for showing and helping me to go alternative ways. And last but absolutely not least, I want to thank my parents Beate and Hans Albrecht and my girlfriend Julia Hoffmann, who all supported me a lot and helped me to overcome frustrating situations during my work. I love you!